8-2020

UAV-Assisted Water Quality Monitoring

Cengiz Koparan
Clemson University

UAV-ASSISTED WATER QUALITY MONITORING

A Dissertation
Presented to
the Graduate School of
Clemson University

In Partial Fulfillment
of the Requirements for the Degree
Doctor of Philosophy
Plant and Environmental Science

---

by
Cengiz Koparan
August 2020

Accepted by:
Dr. A. Bulent Koc, Committee Chair
Dr. Calvin B. Sawyer
Dr. Charles V. Privette
Dr. Christopher Post

ABSTRACT

Water quality assessment for the management of water resources requires the collection of water samples for physical, chemical, and biological analysis. It is essential to reduce the cost of water quality monitoring by minimizing the number of grab samples and to reduce the sampling time by rapidly accessing the sampling points. Adaptive, remote, and smart water sampling systems can provide more effective water quality monitoring programs. An adaptive water sampling system with an unmanned aerial vehicle integrated with sensor nodes was developed and tested in this research. Individual phases of this research were; in-situ water quality measurements with a UAV-integrated sensor node; autonomous water sample collection with a UAV-integrated water sampler; and integration of water sampler and sensor node sub-systems for UAV-assisted adaptive water sampling. The UAV-assisted adaptive water sampling system consists of a hexacopter UAV, a triple water sampling cartridge, and a sensor node. The payload capacity and endurance of the UAV were determined using an indoor test station. The UAV was able to hover 10 min while producing 64 N of thrust at 4.61 kg of takeoff weight with no payload attached. The thrust-to-weight ratio of the UAV was measured as 1.41 at 50% throttle level. The adaptive water sampling method depended on computer-based automated decision making. The decision to activate the water sampling cartridge for water sample collection was made based on pH, dissolved oxygen (DO), electrical conductivity (EC), and temperature sensor inputs from the sensor node. The adaptive sampling enabled selective water sample collection only when the water constituent measurements exceeded the assigned allowable limits during indoor tests. Field

experiments were conducted to test the systems to achieve adaptive water sampling from a 1.1 ha fishing pond and a 11 ha portion of a 36 ha lake. Instantaneous decision making for sample collection based on in-situ pH, DO, EC and temperature measurements would eliminate unnecessary water sample collection while providing data with high spatial resolution for assessing water quality in surface waters.

DEDICATION

I dedicate this dissertation to my parents whom by example taught the discipline, perseverance and commitment necessary to complete this degree. Also, to Serkan Okur for his continued encouragement and mentorship during this process. And to Lacie Lagroon for her continued support and guidance.

ACKNOWLEDGMENTS

I would like to thank my advisor Dr. A. Bulent Koc for his mentorship, time, and knowledge that were vital in pursuit of my career goals. I would like to thank my committee members Dr. Charles V. Privette, Dr. Calvin B. Sawyer, and Dr. Christopher Post for their time, motivation, and research guidance. I would like to thank my fellow graduate students Dan David and Denise Garcia for the assistance, support, and friendship. Thank you undergraduate students who participated in the sensor subsystem development, microcontroller integration, code development and field experiments, especially Harrison Eggers, Brendan Macinnis, Curtis Erwin, Arnaldy Medina Cotto, Jonathan Rodriguez, Antonio Negron and Kevin Gibson.

TABLE OF CONTENTS

Table of Contents (Continued) Page

LIST OF TABLES

LIST OF FIGURES

List of Figures (Continued)

Figure Page

List of Figures (Continued)

Figure Page

ORGANIZATION OF DISSERTATION

This dissertation consists of five chapters, including the Introduction (Chapter 1), three consecutive manuscripts (Chapter 2, Chapter 3, and Chapter 4), and Conclusions (Chapter 5). The manuscripts were formatted for publication in scientific journals.

Chapter 2: In Situ Water Quality Measurements Using an Unmanned Aerial Vehicle (UAV) System

Published in MDPI Water Journal

Chapter 3: Autonomous In Situ Measurements of Noncontaminant Water Quality Indicators and Sample Collection with a UAV

Published in MDPI Water Journal

Chapter 4: Adaptive Water Sampling with an Aerial Robot

Targeted Journal: MDPI Drones

CHAPTER ONE

INTRODUCTION

Water is one of the critical resources for human survival and continuous monitoring is essential to preserve its quality. Periodic water sampling and analysis is required to identify changes and trends in water quality over time (Shoda, Sprague, Murphy, & Riskin, 2019). Water quality indicators of lakes and rivers are used to develop management plans to ensure drinking water safety, protect public health, and control pollution and diseases (Moore, Dowell, Bradt, & Verdu, 2014). According to relevant research, 420 billion m^3 of sewage is discharged into rivers and lakes and 550 billion m^3 of freshwater is polluted each year around the world (Ma, Ding, Wei, Zhao, & Huang, 2009). Current water quality monitoring methods poses limitations to characterize spatial and temporal variability of water quality data (Dörnhöfer & Oppelt, 2016).

Water quality indicators can be measured in situ or can be analyzed from grab samples (Chung & Yoo, 2015). These indicators include dissolved oxygen (DO), hydrogen ion export (pH), electrical conductivity (EC), turbidity, temperature, algal chlorophyll, total phosphorus, nitrogen, and suspended solids (Shoda et al., 2019). Among these parameters, DO, EC, pH, and temperature are used as significant factors reflecting the "quantity" features of water quality (Li & Liu, 2019b). Temperature and pH are indicators of biological and chemical activities in water. Water temperature varies according to time of year, time of day, weather conditions, water depth, total dissolved solid, shading, and vegetation (Yang et al., 2018). Aquatic organisms require certain pH range for survival. The majority of aquatic organism require a pH that ranges between 6.5 and 9.0 which provides adequate survival conditions (Li & Liu, 2019c). DO is an indicator of non-compound oxygen present in water and it is the most important parameter in assessing water

quality (Chung & Yoo, 2015). Low DO due to the decomposition of organic material by bacteria and fungi below epilimnion (surface layer) can harm aquatic life and affect water quality (Rucinski, Beletsky, DePinto, Schwab, & Scavia, 2010). EC is a measure of water's capability to pass electrical flow and is related to the concentration of ions in water. These ions are indicators of dissolved salts and inorganic materials such as alkalis, chlorides, sulfides, and carbonate (Crescentini, Bennati, & Tartagni, 2011). A sudden change in EC in a waterbody can indicate pollution that is caused by phosphate and nitrate ions due to agricultural runoff (Li & Liu, 2019c).

Nutrients leaching from farm fields or pasture lands into surface water have the potential to cause algal blooms (Blaas & Kroeze, 2016). The growth of dense algal blooms causes discoloration in a waterbody and can potentially result in damaging fluctuations of dissolved oxygen. Blue-green algae have the genetic potential to produce toxins which are harmful to humans and animals (McGowan, 2016). In addition to above concerns, contaminated drinking water may pose risks to human health because of high levels of microorganisms. *Escherichia coli (E. coli)* is an indicator for fecal contamination and zero E. coli per 100 ml of water was defined as safe level by World Health Organization (Mara & Horan, 2003). The health concerns, requirements and limitations of an effective water quality monitoring increase the need for a remote, easily deployable, adaptive water sampling system that would provide continuous, real time, and reliable water quality data.

Current water quality monitoring in lakes and reservoirs may be done by volunteers who have access to a waterbody (Peters, Zhan, Schwartz, Godoy, & Ballard, 2017). Volunteers collect water samples from shore or a desired location on a waterbody to do water quality analysis. These samples are taken to a laboratory for further analysis because many of the

parameters cannot be easily or cost effectively analyzed in situ. Despite the availability of help from volunteers to monitor water quality, some lakes, retired mining zones, or other waterbodies surrounded by steep and difficult terrain may not be accessible by boats. Because of these, traditional water sampling can be costly, labor-intensive, and the measurements would not be representative of the neighboring waterbodies.

New tools for water quality monitoring such as remote sensing, wireless sensor stations, and automated monitoring devices have been developed (Tyler et al., 2009; Wernersson et al., 2015; Winkelbauer, Fuiko, Krampe, & Winkler, 2014; Winkler, Zessner, Saracevic, & Fleischmann, 2008). Remote sensing has the advantages of making measurements on a larger scale and over a long time period (Schaeffer et al., 2013). This allows the managers to observe the changes in water quality in coastal waters, estuaries, lakes, and reservoirs. Despite the developments in remote sensing, most management decisions are still based on the traditional measurement methods of water sample collection and subsequent laboratory analysis (Gholizadeh, Melesse, & Reddi, 2016). In addition, data from traditional point sampling is not sufficient for identifying spatial or temporal variations of water quality parameters in a large waterbody (Gholizadeh et al., 2016). The integration of remote sensing data with in situ measurements is necessary for making accurate and timely management decisions (Schaeffer et al., 2013).

Wireless sensor stations that are placed at desired locations on waterbodies continuously monitor water quality parameters. A number of these sensor stations are utilized to create Wireless Sensor Networks (WSNs) in waterbodies. Therefore, water pollution in streams, rivers, and coastal areas are monitored with WSNs (Chung & Yoo, 2015; Winkler et al., 2008). These WSNs can collect in situ and continuous real-time water quality data, and transmit it through a

wireless network (Li & Liu, 2019a; Winkelbauer et al., 2014). For example, retrieval of chlorophyll-a concentrations from WSNs are used to monitor the development of phytoplankton blooms in inland and coastal water (Tyler et al., 2009). The WSNs can be expensive to set up and difficult to maintain due to their complexity and nature of sensor technology. Besides, spatial and temporal variability of the data from these networks would be insufficient based on their sparse distribution in a large waterbody.

Autonomous underwater vehicles (AUVs) and autonomous surface vehicles (ASVs) have been used for water quality monitoring in recent years (Kaizu, Iio, Yamada, & Noguchi, 2011; Karimanzira et al., 2014). The major challenge of water quality monitoring with an underwater vehicle is the accurate positioning of the vehicle as the GPS systems either cannot fully function or require additional complex and expensive sub systems (Karimanzira et al., 2014). Because of this limitation, the AUVs have to be equipped with additional navigational systems or acoustic localization systems. The ASV can automatically navigate to predefined sampling points and measure pH, DO, EC, turbidity, temperature, sensor depth, water depth, chlorophyll-a concentration, and nitrates (Kaizu et al., 2011). The disadvantages of automatic sampling with ASVs are the operational difficulties due to swaying from side to side and uncertain engine-control frequencies (Kaizu et al., 2011).

Unlike the above methods, unmanned aerial vehicles (UAVs) can also be used for water quality monitoring. UAVs are commonly used for remote sensing in agriculture for scouting of field crops and livestock monitoring (Freeman & Freeland, 2015). Crop yield assessments, crop height monitoring, crop weed mapping, and biomass monitoring are some of the examples for remote sensing with a multispectral camera integrated UAVs (Bendig et al., 2015; Chang, Jung, Maeda, & Landivar, 2017; Pérez-Ortiz et al., 2016; Schut, Traore, Blaes, & de By, 2018). UAVs

can also acquire air quality data with high spatial and temporal resolution (Villa, Gonzalez, Miljievic, Ristovski, & Morawska, 2016). Recent developments in sensor technology led to the design of compact devices that can measure a variety of air pollutants (Snaddon, Petrokofsky, Jepson, & Willis, 2013). The use of UAVs is not limited with remote sensing or air quality monitoring. UAVs are also used for aerial spraying of herbicides or pesticides, aerial sensing of sound and identifying changes in land structure for city planning (Gallacher, 2017; Koc, 2017). Emergency applications of UAVs include but are not limited to blood delivery, ambulances for cardiac arrest, and disaster relief operations (Rabta, Wankmüller, & Reiner, 2018; Rutkin, 2016; Van de Voorde et al., 2017). Distinct advantages that UAVs provide include the ability to rapidly and remotely travel to locations that are difficult to access and the efficient execution of tasks with relatively reduced costs and time. For example, aerial images that are taken remotely with a UAV can help visualize disturbances in water and provide enhanced spatial water quality monitoring data (Rusnák, Sládek, Kidová, & Lehotský, 2018; Zeng, Richardson, & King, 2017). Aerial surveys with a high-resolution camera attached to a UAV may also be used to monitor topographic changes in watersheds (Cook, 2017). Information gathered from these surveys can provide the specific coordinates of contaminations, which can be included in water quality monitoring plan for further sampling. In addition to water quality monitoring, a water sampling UAV can be used to collect water from pre-determined locations (Ore, Elbaum, Burgin, Zhao, & Detweiler, 2015).

Scope of the research project

The overall purpose of this research was to develop an adaptive, remote, aerial, and autonomous water quality monitoring system. An adaptive water quality data collection with this system will help quick evaluation of the water quality in a lake or pond. The research questions were:

- Is it applicable to evaluate water quality parameters with an unmanned aerial vehicle (UAV) assisted sampling device and sensor node?
- How accurate the in situ water quality measurements would be with UAV-assisted sensor node?
- Can adaptive water sampling method be integrated with the UAV to assess water quality?

There were three objectives to this research. The first objective focused on integrating an open source electronic sensor platform with a UAV to conduct autonomous in situ water quality measurements to compare with manual sensor measurements. The second objective focused on integrating the sensor node and the water sampling cartridges with a UAV for autonomous noncontaminant water quality sampling at two different depths. The goal of this approach was to streamline water sampling by conducting real-time in situ measurements and water sample collection. The third objective focused on the design and prototyping of a triple cartridge water sampler along with the proof of concept for adaptive water sampling.

References

Bendig, J., Yu, K., Aasen, H., Bolten, A., Bennertz, S., Broscheit, J., . . . Bareth, G. (2015). Combining UAV-based plant height from crop surface models, visible, and near infrared vegetation indices for biomass monitoring in barley. *International Journal of Applied Earth Observation and Geoinformation, 39*, 79-87. doi:https://doi.org/10.1016/j.jag.2015.02.012

Blaas, H., & Kroeze, C. (2016). Excessive nitrogen and phosphorus in European rivers: 2000–2050. *Ecological Indicators, 67*, 328-337. doi:https://doi.org/10.1016/j.ecolind.2016.03.004

Chang, A., Jung, J., Maeda, M. M., & Landivar, J. (2017). Crop height monitoring with digital imagery from Unmanned Aerial System (UAS). *Computers and Electronics in Agriculture, 141*, 232-237. doi:https://doi.org/10.1016/j.compag.2017.07.008

Chung, W.-Y., & Yoo, J.-H. (2015). Remote water quality monitoring in wide area. *Sensors and Actuators B: Chemical, 217*, 51-57. doi:http://dx.doi.org/10.1016/j.snb.2015.01.072

Cook, K. L. (2017). An evaluation of the effectiveness of low-cost UAVs and structure from motion for geomorphic change detection. *Geomorphology, 278*, 195-208. doi:https://doi.org/10.1016/j.geomorph.2016.11.009

Crescentini, M., Bennati, M., & Tartagni, M. (2011, 7-10 Aug. 2011). *Integrated and autonomous conductivity-temperature-depth (CTD) sensors for environmental monitoring.* Paper presented at the 2011 IEEE 54th International Midwest Symposium on Circuits and Systems (MWSCAS).

Dörnhöfer, K., & Oppelt, N. (2016). Remote sensing for lake research and monitoring – Recent advances. *Ecological Indicators, 64*, 105-122. doi:https://doi.org/10.1016/j.ecolind.2015.12.009

Freeman, P. K., & Freeland, R. S. (2015). Agricultural UAVs in the U.S.: potential, policy, and hype. *Remote Sensing Applications: Society and Environment, 2*, 35-43. doi:https://doi.org/10.1016/j.rsase.2015.10.002

Gallacher, D. (2017). *Drone Applications for Environmental Management in Urban Spaces: A Review* (Vol. 3).

Gholizadeh, M., Melesse, A., & Reddi, L. (2016). A Comprehensive Review on Water Quality Parameters Estimation Using Remote Sensing Techniques. *Sensors, 16*(8), 1298.

Kaizu, Y., Iio, M., Yamada, H., & Noguchi, N. (2011). Development of unmanned airboat for water-quality mapping. *Biosystems Engineering, 109*(4), 338-347. doi:https://doi.org/10.1016/j.biosystemseng.2011.04.013

Karimanzira, D., Jacobi, M., Pfuetzenreuter, T., Rauschenbach, T., Eichhorn, M., Taubert, R., & Ament, C. (2014). First testing of an AUV mission planning and guidance system for water quality monitoring and fish behavior observation in net cage fish farming. *Information Processing in Agriculture, 1*(2), 131-140. doi:https://doi.org/10.1016/j.inpa.2014.12.001

Koc, C. (2017). *Design and Development of a Low-cost UAV for Pesticide Applications* (Vol. 34).

Li, D., & Liu, S. (2019a). Chapter 2 - Wireless Sensor Networks in Water Quality Monitoring. In D. Li & S. Liu (Eds.), *Water Quality Monitoring and Management* (pp. 55-100): Academic Press.

Li, D., & Liu, S. (2019b). Chapter 4 - Water Quality Evaluation. In D. Li & S. Liu (Eds.), *Water Quality Monitoring and Management* (pp. 113-159): Academic Press.

Li, D., & Liu, S. (2019c). Chapter 8 - Water Quality Detection for Lakes. In D. Li & S. Liu (Eds.), *Water Quality Monitoring and Management* (pp. 221-231): Academic Press.

Ma, J., Ding, Z., Wei, G., Zhao, H., & Huang, T. (2009). Sources of water pollution and evolution of water quality in the Wuwei basin of Shiyang river, Northwest China. *Journal of Environmental Management, 90*(2), 1168-1177. doi:https://doi.org/10.1016/j.jenvman.2008.05.007

Mara, D., & Horan, N. J. (2003). *Handbook of water and wastewater microbiology*: Elsevier.

McGowan, S. (2016). Chapter 2 - Algal Blooms A2 - Shroder, John F. In R. Sivanpillai (Ed.), *Biological and Environmental Hazards, Risks, and Disasters* (pp. 5-43). Boston: Academic Press.

Moore, T. S., Dowell, M. D., Bradt, S., & Verdu, A. R. (2014). An optical water type framework for selecting and blending retrievals from bio-optical algorithms in lakes and coastal waters. *Remote Sensing of Environment, 143*, 97-111. doi:10.1016/j.rse.2013.11.021

Ore, J.-P., Elbaum, S., Burgin, A., Zhao, B., & Detweiler, C. (2015). Autonomous Aerial Water Sampling. In L. Mejias, P. Corke, & J. Roberts (Eds.), *Field and Service Robotics: Results of the 9th International Conference* (pp. 137-151). Cham: Springer International Publishing.

Pérez-Ortiz, M., Peña, J. M., Gutiérrez, P. A., Torres-Sánchez, J., Hervás-Martínez, C., & López-Granados, F. (2016). Selecting patterns and features for between- and within- crop-row weed mapping using UAV-imagery. *Expert Systems with Applications, 47*, 85-94. doi:https://doi.org/10.1016/j.eswa.2015.10.043

Peters, C. B., Zhan, Y., Schwartz, M. W., Godoy, L., & Ballard, H. L. (2017). Trusting land to volunteers: How and why land trusts involve volunteers in ecological monitoring. *Biological Conservation, 208,* 48-54. doi:https://doi.org/10.1016/j.biocon.2016.08.029

Rabta, B., Wankmüller, C., & Reiner, G. (2018). A drone fleet model for last-mile distribution in disaster relief operations. *International Journal of Disaster Risk Reduction, 28,* 107-112. doi:https://doi.org/10.1016/j.ijdrr.2018.02.020

Rucinski, D. K., Beletsky, D., DePinto, J. V., Schwab, D. J., & Scavia, D. (2010). A simple 1-dimensional, climate based dissolved oxygen model for the central basin of Lake Erie. *Journal of Great Lakes Research, 36*(3), 465-476.

Rusnák, M., Sládek, J., Kidová, A., & Lehotský, M. (2018). Template for high-resolution river landscape mapping using UAV technology. *Measurement, 115*, 139-151. doi:https://doi.org/10.1016/j.measurement.2017.10.023

Rutkin, A. (2016). Blood delivered by drone. *New Scientist, 232*(3096), 24. doi:https://doi.org/10.1016/S0262-4079(16)31935-2

Schaeffer, B. A., Schaeffer, K. G., Keith, D., Lunetta, R. S., Conmy, R., & Gould, R. W. (2013). Barriers to adopting satellite remote sensing for water quality management. *International Journal of Remote Sensing, 34*(21), 7534-7544. doi:10.1080/01431161.2013.823524

Schut, A. G. T., Traore, P. C. S., Blaes, X., & de By, R. A. (2018). Assessing yield and fertilizer response in heterogeneous smallholder fields with UAVs and satellites. *Field Crops Research, 221,* 98-107. doi:https://doi.org/10.1016/j.fcr.2018.02.018

Shoda, M. E., Sprague, L. A., Murphy, J. C., & Riskin, M. L. (2019). Water-quality trends in U.S. rivers, 2002 to 2012: Relations to levels of concern. *Science of The Total Environment, 650,* 2314-2324. doi:https://doi.org/10.1016/j.scitotenv.2018.09.377

Snaddon, J., Petrokofsky, G., Jepson, P., & Willis, K. J. (2013). Biodiversity technologies: tools as change agents. *Biology Letters, 9*(1), 20121029. doi:10.1098/rsbl.2012.1029

Tyler, A. N., Hunter, P. D., Carvalho, L., Codd, G. A., Elliott, J. A., Ferguson, C. A., . . . Scott, E. M. (2009). Strategies for monitoring and managing mass populations of toxic cyanobacteria in recreational waters: a multi-interdisciplinary approach. *Environmental Health, 8*(1), S11. doi:10.1186/1476-069x-8-s1-s11

Van de Voorde, P., Gautama, S., Momont, A., Ionescu, C. M., De Paepe, P., & Fraeyman, N. (2017). The drone ambulance [A-UAS]: golden bullet or just a blank? *Resuscitation, 116*, 46-48. doi:https://doi.org/10.1016/j.resuscitation.2017.04.037

Villa, T., Gonzalez, F., Miljievic, B., Ristovski, Z., & Morawska, L. (2016). An Overview of Small Unmanned Aerial Vehicles for Air Quality Measurements: Present Applications and Future Prospectives. *Sensors, 16*(7), 1072.

Wernersson, A.-S., Carere, M., Maggi, C., Tusil, P., Soldan, P., James, A., . . . Kase, R. (2015). The European technical report on aquatic effect-based monitoring tools under the water framework directive. *Environmental Sciences Europe, 27*(1), 7. doi:10.1186/s12302-015-0039-4

Winkelbauer, A., Fuiko, R., Krampe, J., & Winkler, S. (2014). Crucial elements and technical implementation of intelligent monitoring networks. *Water Science and Technology, 70*(12), 1926-1933. doi:10.2166/wst.2014.415

Winkler, S., Zessner, M., Saracevic, E., & Fleischmann, N. (2008). Intelligent monitoring networks – transformation of data into information for water management. *Water Science and Technology, 58*(2), 317-322. doi:10.2166/wst.2008.672

Yang, K., Yu, Z., Luo, Y., Yang, Y., Zhao, L., & Zhou, X. (2018). Spatial and temporal variations in the relationship between lake water surface temperatures and water quality - A case study of Dianchi Lake. *Science of The Total Environment, 624,* 859-871. doi:https://doi.org/10.1016/j.scitotenv.2017.12.119

Zeng, C., Richardson, M., & King, D. J. (2017). The impacts of environmental variables on water reflectance measured using a lightweight unmanned aerial vehicle (UAV)-based spectrometer system. *ISPRS Journal of Photogrammetry and Remote Sensing, 130,* 217-230. doi:https://doi.org/10.1016/j.isprsjprs.2017.06.004

CHAPTER TWO

IN SITU WATER QUALITY MEASUREMENTS USING AN UNMANNED AERIAL VEHICLE (UAV) SYSTEM

Abstract

An unmanned aerial vehicle-assisted water quality measurement system (UAMS) was developed for in situ surface water quality measurement. A custom-built hexacopter was equipped with an open-source electronic sensors platform to measure the temperature, electrical conductivity (EC), dissolved oxygen (DO), and pH of water. Electronic components of the system were coated with a water-resistant film, and the hexacopter was assembled with flotation equipment. The measurements were made at thirteen sampling waypoints within a 1.1 ha agricultural pond. Measurements made by an open source multiprobe meter (OSMM) attached to the unmanned aerial vehicle (UAV) were compared to the measurements made by a commercial multiprobe meter (CMM). Percent differences between the OSMM and CMM measurements for DO, EC, pH, and temperature were 2.1 %, 3.43 %, 3.76 %, and <1.0 %, respectively. The collected water quality data was used to interpret the spatial distribution of measurements in the pond. The UAMS successfully made semiautonomous in situ water quality measurements from predetermined waypoints. Water quality maps showed homogeneous distribution of measured constituents across the pond. The concept presented in this paper can be applied to the monitoring of water quality in larger surface waterbodies.

Introduction

Water is essential for human survival, and its quality should be monitored and protected. The safety of water resources is threatened by external factors such as industrial wastes and

agricultural fertilizers. Water quality monitoring programs have been developed to preserve water quality and eliminate the contamination of water sources. The quality of water in rivers, ponds, and lakes can be evaluated by monitoring dissolved oxygen (DO), pH, temperature, and electrical conductivity (EC), which are the most commonly used indicators of impairment (Xu et al., 2016). Low concentration of dissolved oxygen, undesirable temperature or pH, and inappropriate concentration of salinity lead to poor water quality. Periodic sampling and analysis allow one to characterize water and identify changes or trends in water quality over time. For example, pollutants carried by stormwater may include bacteria, nutrients, litter, sediment, oils, and heavy metals (Thomas, Hurst, Matthiessen, Sheahan, & Williams, 2001). Data from water quality indicators can be used to create maps for the visualization of water quality distribution over a waterbody. Such maps are used by hydrologists to understand circulation in the waterbody and make predictions (Kaizu, Iio, Yamada, & Noguchi, 2011). Through monitoring, information can be gathered to implement specific pollution prevention and remediation programs.

Streams receive point source pollutants from drainage channels, outlets from industrial plants, wastewater treatment facilities, confined animal feeding operations (CAFOs), and runoff from agricultural operations; while nonpoint source pollutant inflow occurs after rainfall or emergency overflow during a short period (Liu, Xu, Zhang, Yu, & Men, 2016). Nonpoint sources, including impervious surfaces such as roadways, rooftops, parking lots, and sidewalks, accumulate pollutants and convey them directly to lakes, rivers, and estuaries (Ma, Egodawatta, McGree, Liu, & Goonetilleke, 2016). Runoff that is heated up on parking lots and roadways leads to warmer-than-normal water entering nearby waterways, thereby increasing the surface water temperature. These sources can be monitored using event-controlled water samplers, automated real-time remote monitoring systems, and grab samples collected by individuals

(Glasgow, Burkholder, Reed, Lewitus, & Kleinman, 2004; Neumann, Liess, & Schulz, 2003; Weiss et al., 2010). In addition to water sampling after a storm event, regular water sampling is necessary to identify the entry points of pollutants into surface water. For example, nutrient leaching from farm fields or pasture land into surface water has the potential to cause algal blooms (Blaas & Kroeze, 2016). The growth of dense algal blooms causes discoloration in water bodies and can potentially result in damaging fluctuations of dissolved oxygen. Among algal blooms, blue-green algae have the genetic potential to produce toxins which are harmful to humans and animals (McGowan, 2016; van der Merwe, 2015). Traditionally, to detect harmful changes in the waterbodies, agencies responsible for water quality monitoring collect water samples periodically and analyze them in the laboratory. These methods are costly, labor-intensive, and the measurements are not representative of the neighboring waterbodies (Schaeffer et al., 2013). Therefore, watershed managers face the challenge of integrating new tools for water quality monitoring, such as effect-based tools (e.g., biomarkers and bioassays) (Wernersson et al., 2015), automated monitoring devices (Winkelbauer, Fuiko, Krampe, & Winkler, 2014; Winkler, Zessner, Saracevic, & Fleischmann, 2008), and remote sensing (Tyler et al., 2009). Remote sensing has the advantages of making measurements on a larger scale and over a long time period (Schaeffer et al., 2013). This allows the managers to observe the changes in water quality in coastal waters, estuaries, lakes, and reservoirs over time (Schaeffer et al., 2013). Despite the developments in remote sensing, most management decisions are still based on the traditional measurement methods of water sample collection and subsequent laboratory analysis (Gholizadeh, Melesse, & Reddi, 2016). In addition, data from traditional point sampling is not sufficient for identifying spatial or temporal variations in water quality, nor for forecasting for large waterbodies (Gholizadeh et al., 2016). The integration of satellite remote sensing data with

in situ measurements is necessary for making accurate and timely management decisions (Schaeffer et al., 2013).

Autonomous underwater vehicles (AUVs) and autonomous surface vehicles (ASVs) have been developed for water quality monitoring in order to address this issue (Blaas & Kroeze, 2016; Karimanzira et al., 2014). The autonomous vehicles that are operated in water are effective and able to conduct continuous water quality monitoring. These vehicles also have limitations and challenges. The major challenge of water quality monitoring with an underwater vehicle is the accurate positioning of the vehicle, as the Global Positioning System (GPS) cannot be used accurately when the vehicle is underwater. Because of this limitation, the AUVs must be equipped with additional navigational devices or acoustic localization systems. The ASV can automatically navigate to predefined sampling points and measure pH, DO, EC, turbidity, temperature, sensor depth, water depth, chlorophyll *a* concentration, and nitrates (Blaas & Kroeze, 2016). One of the limitations of ASVs is the difficulties in operation caused by swaying from side to side and uncertain engine-control frequencies. The ASVs and AUVs provide high spatiotemporal resolution of data and adaptive sampling due to their ability to do continuous sampling (Dunbabin, Grinham, & Udy, 2009). A disadvantage is the collection of biased data due to dirty and continuously used sensor equipment.

Despite the availability of assistance from volunteers for monitoring water quality, some lakes, retired mining zones, or other waterbodies surrounded by steep and difficult terrain may not be accessible by boats (Peters, Zhan, Schwartz, Godoy, & Ballard, 2017). In addition, lakes with cyanobacteria (blue-green algae) blooms may pose risks to humans during collection of water samples (Glasgow et al., 2004; Partyka, Bond, Chase, & Atwill, 2017). While AUVs, ASVs, and fixed monitoring stations are available for in situ water quality monitoring, advanced

remote and autonomous in situ water sampling systems are underdeveloped (Ravalli, Rossi, & Marrazza, 2017). The developments in unmanned aerial vehicle (UAV) technology provide new opportunities to collect water samples and to conduct in situ water quality measurements. Compared with traditional water quality monitoring methods, UAVs are relatively inexpensive, and they can be used for water quality monitoring in waterbodies that are inaccessible with boats or dangerous to field personnel.

In this study, we developed a multiprobe meter and integrated it within a hexacopter UAV for autonomous in situ water quality measurements and verified the functionality and accuracy of the system with laboratory and field tests.

Materials and Methods

Design, Control, and Navigation

The primary purpose of using a UAV-assisted measurement system (UAMS) was the navigation of the UAV to the predetermined sampling points to measure the DO, EC, pH, and temperature of the water. The developed system consists of a hexacopter UAV and an open source multiprobe meter (OSMM). We designed and built the hexacopter, developed the OSMM using off-the-market sensors and electronic components, and designed the 3D-printed cases. The design considerations for the UAV included the abilities to complete the flight mission within the allowed battery power limits, to overcome wind conditions and gusts, and to minimize crash risks that may occur due to environmental conditions or an electronic component failure; and a size large enough to carry the payload (OSMM). A hexacopter UAV was chosen to enable the carrying of relatively large payloads and overcoming wind conditions. All electronic circuits in the system were waterproofed by using a corrosion prevention spray (Corrosion-X 90102,

Corrosion Technologies, Dallas, TX, USA). Flotation attachments were placed under each motor and mainframe to minimize air drag, and to increase stability during landing and takeoff. The initial hexacopter frame that was built had a hull length of 550 mm. After preliminary testing of the hexacopter with flotation attachments and the OSMM payload, the UAV was not providing a stable buoyancy in water. Therefore, the arms of the frame were lengthened with 8 mm extension plates, and this provided a more stable buoyancy in water. Thus, the total hull length of the hexacopter was 566 mm (Figure 2.1). The weight of the aircraft (hexacopter) was 2333 g, including the weights of the UAV frame, main battery, Electronic Speed Controllers (ESCs), motors, propellers, Pixhawk controller, GPS sensor, buzzer, safety switch, and flotation equipment. The payload had a weight of 750 g, including the weights of the OSMM components: a second battery, an Arduino board, probes, probe cables, and the protective cases for the probes and the microcontroller. The gross weight of the UAMS was 3083 g, including the weight of the aircraft and the payload.

Two batteries were used in the UAMS: one for the UAV and one for the OSMM. The main battery used to power the UAV was a 14.8 V Lithium Polymer (LiPo) battery with a 25 C discharge rate and 5000 mAh capacity (Venom, Rathdrum, ID, USA). The second battery was a 7.4 V LiPo battery with an 8 C discharge rate and 2200 mAh capacity (Venom, Rathdrum, ID, USA). The second battery was used with a battery eliminator circuit (BEC) to regulate the voltage to the microcontrollers' power specifications used for the OSMM. Using a separate battery for the OSMM allowed the operator to dismount the OSMM for standalone measurements (if needed) without the UAV being on the shore or on the boat.

(**a**) (**b**)

Figure 2.1 The unmanned aerial vehicle-assisted measurement system (UAMS): (**a**) prior to a flight mission; (**b**) floating on a water surface while making measurements.

The OSMM was integrated with the frame of the UAV and located on top. The electronic components of the OSMM were placed into a waterproof case to prevent water damage. The case was positioned as to maintain the center of gravity of the hexacopter. Probes were connected to the case with a BNC (Bayonet Neill-Concelman) connector, and extension cords were tied together to provide uniformity. Extension cords were 60 cm long, which determined the depth of water quality measurements. Water sampling depth may be adjusted by using longer extension cords. A custom-designed probe housing was 3D-printed and assembled to provide safeguard around the probes, to prevent the probes from getting damaged during takeoff and landing (Figure 2.2).

Figure 2.2 Custom-designed probe housing was 3D-printed with polylactic acid (PLA) material.

Control of the UAV can be accomplished either manually or autonomously. Manual control of the hexacopter was accomplished with a radio controller (RC) (Turnigy 9X, Hextronik, ChengDu, Donguan, China). Autonomous control of the hexacopter was accomplished with a Pixhawk autopilot (Pixhawk, 3DR Robotics, Berkeley, CA, USA). The Pixhawk is accompanied with a GPS receiver (3DR, Berkeley, CA, USA) and radio telemetry (3DR, Berkeley, CA, USA) for autonomous control and ground communication. The Pixhawk controller contains an MPU6000 main accelerometer and gyro, ST Micro 16-bit gyroscope, ST Micro 14-bit accelerometer/compass (magnetometer) (3DR, Berkeley, CA, USA), and MEAS barometer sensors (3DR, Berkeley, CA, USA). Mission Planner software was used to specify flight boundary, waypoints, autonomous navigation details, and to configure integrated sensors/actuators (Ardupilot, 2017a).

Stabilized control of a UAV is essential when flying over water surfaces. Multiple considerations must be evaluated when choosing electronic parts for these vehicles (Gupta, Jha, & Gupta, 2014). Electronic parts were chosen depending on desired payload, flight time, and compatibility. Thrust-to-weight ratio must be justified in UAV design for a stable flight. Higher thrust-producing UAVs can be designed with larger components, but this would increase costs.

The major limiting factor for the UAV that we designed in-house was the cost of the motors, frames, propellers, ESCs, and battery. In this study, we used a UAV that we built for collecting water samples (Koparan & Bulent Koc, 2016). In the design, the payload capacity was assumed to be 400 g, which was the weight of a thief water sampler holding 130 mL of water (Koparan & Bulent Koc, 2016). Previous indoor flight experiments showed that the UAV can fly autonomously and continuously for 6 min while carrying a payload of 400 g (Koparan & Bulent Koc, 2016). These limitations were considered during OSMM construction and integration with the UAV. During the experiments, the UAMS landed on the water surface at each measurement point. Therefore, during the measurements, the main battery of the motors did not consume power, enhancing its endurance.

Accuracy Assessment

The commercial multiprobe meter (CMM) contained a portable Sension 156 meter (Hach, CO) for measuring pH and EC, and a portable HQ10 meter (Hach, Loveland, CO, USA) with DO and temperature probes. The OSMM was a combination of a water sensor node (Atlas Scientific, New York, NY, USA) and an open-source electronic platform (Arduino Mega 2560, Ivrea, Italy) (Figure 2.3). The water sensor node consisted of EC, DO, pH, and temperature circuits (Atlas Scientific, New York, NY, USA), and was integrated with a microcontroller (Atmel ATmega2560, San Jose, CA, USA). The circuit was integrated with a tentacle shield (Atlas Scientific, NY, USA). The sensor readings were gathered with an Inter-Integrated Circuit (I^2C) protocol, and data was recorded in a Secure Digital Card (SD card) inserted on the shield (SunFounder, Shenzhen City, Guangdong Province, China). The advantage of an I^2C over a serial peripheral interface (SPI) is that the I^2C bus uses only two wires for multiple devices, either as a slave or a master (Lynch, Marchuk, & Elwin, 2016). Both the CMM and OSMM

probes were calibrated in the laboratory following the manufacturers' (Atlas Scientific, NY, and Hach, CO, USA) calibration procedures.

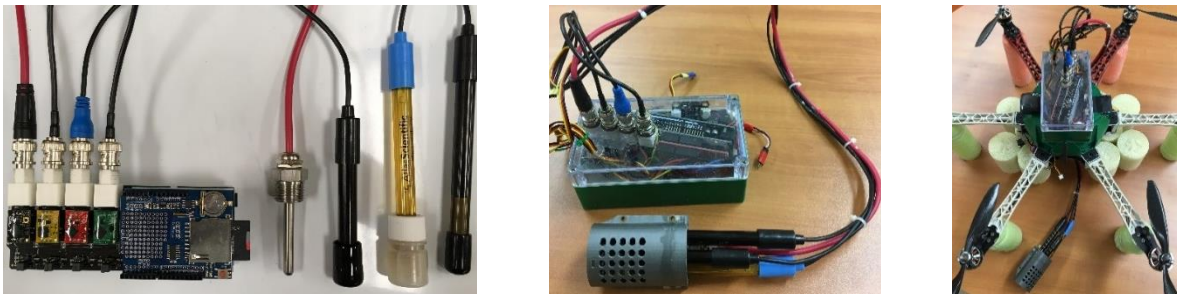

(**a**) (**b**) (**c**)

Figure 2.3 (**a**) The open source multiprobe meter (OSMM) components; (**b**) placed in a waterproof case; (**c**) placed on top of the unmanned aerial vehicle (UAV).

Preliminary experiments were conducted to determine whether water quality measurements were consistent between the OSMM and the commercial multiprobe meter (CMM), before integrating the OSMM with the UAV. Both the OSMM and CMM were brought to the sampling points by kayak. To minimize the risk of the electronics of the OSMM and CMM probes getting in contact with water, water samples were collected at the predetermined sampling locations and measurements were made on the kayak. The UAMS was designed to take measurements at a depth of 60 cm. Because of this, water samples were collected with a custom-designed 3D-printed thief style sampler at a depth of 60 cm (Koparan & Koc, 2016). The measurements for each water quality parameter were made at the same time from two different beakers. Water samples in the beakers were manually stirred with the probe during DO measurements.

Water samples were collected from thirteen locations to verify consistency between OSMM and CMM measurements. At each location, three replicates of water samples were collected, and

the average of the measurements was used in analysis. Measurements of DO, EC, pH, and temperature were made with the OSMM and CMM at each location. Of primary interest was the accuracy of the measurements made with the OSMM. A paired *t*-test analysis was conducted in Microsoft Excel (Excel 2016, Microsoft, Redmond, WA, USA) to evaluate statistical differences between the measurements of DO, EC, pH, and temperature made by the OSMM and CMM, respectively. Percent errors of each water quality parameter were calculated to determine how close the OSMM measurements were to the CMM measurements.

In Situ Data Collection with UAMS

The UAMS was launched from the shore and ascended to the flight altitude of 10 m (Figure 2.4). Once the UAMS had reached the waypoint in the flight mission, it descended and landed on the water. The OSMM recorded the measurements, then lifted off to the 10-m flight altitude and navigated to the next waypoint in the flight mission. A relay command was assigned to the first relay channel of the Pixhawk's auxiliary output port, to activate the data recording in OSMM. The OSMM was activated by the Pixhawk for 60 s at the sampling location. This was the time necessary for the sensors to provide stabilized measurements. The Mission Planner navigation command order that was used to collect water at each measurement location is shown in Table 2.1. The "waypoint" command with 60 s delay and without latitude and longitude coordinates provided the necessary time for UAMS to take measurements (Ardupilot, 2017b). During the measurements, the probes were placed in the water, and there was no stirring for the DO measurements except the mixing during the entry of the probes in water.

Fifteen continuous readings were made at each waypoint. The average of these measurements was taken as the water quality data for the given sampling point. Subsequently, the OSMM was switched off and the UAMS navigated to the next waypoint. The navigation path

was divided into sections which included two, three, or four waypoints, depending on the distance to the launch location and available battery power.

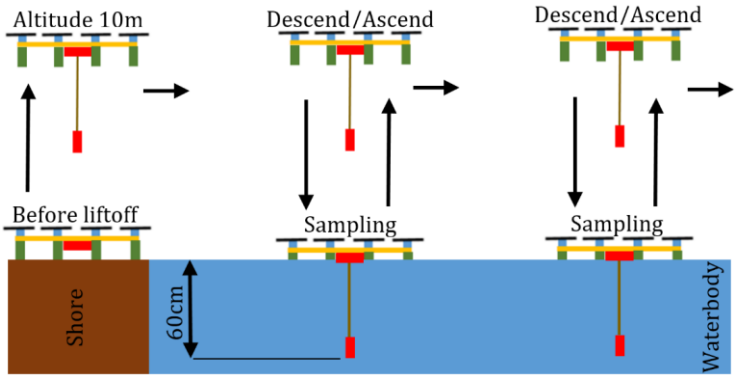

Figure 2.4 Applied method of water quality measurement using the UAMS.

Table 2.1 Autonomous navigation commands used for the UAMS mission flight.

UAMS Position	Command	UAMS's Response	Delay (s)	Latitude	Longitude	Altitude (m)
Home	Takeoff	Take off	0	34.656951	−82.820333	10
Home	Waypoint	Navigate to WP1	0	34.656996	−82.820065	10
WP1	Land	Land at WP1	0	34.656996	−82.820065	0
WP1	Do_Set_Relay	Data recording	0	34.656996	−82.820065	0
WP1	Waypoint	Float for 60s	60	-	-	0
WP1	Takeoff	Take off	0	34.656996	−82.820065	10
WP1	Waypoint	Navigate to WP2	0	34.656884	−82.819681	10
WP2	Land	Land at WP2	0	34.656884	−82.819681	0
WP2	Do_Set_Relay	Data recording	0	34.656884	−82.819681	0
WP2	Waypoint	Float for 60s	60	-	-	0
WP2	Takeoff	Take off	0	34.656884	−82.819681	10
WP2	Waypoint	Navigate to WP3	0	34.656909	−82.819256	10

Note: These command orders were repeated for all the waypoints.

The UAMS was designed for fully autonomous operation. In autonomous mode, the UAMS navigates to the predefined waypoint, lands on the water surface, triggers the OSMM measurements, lifts off, and navigates to the next waypoint. In addition to this, a remote-control

option of the UAMS for water quality measurements was added to the system. For this purpose, a manual switch on the radio controller (RC) was designated to turn the OSMM measurements on and off remotely. The OSMM starts to record the measurements when the OSMM switch on the RC is turned on, and stops when the OSMM switch is turned off by the operator. The remote-control option of the UAMS allows the operator to conduct water quality measurements independently from autonomous UAMS control. The UAMS can be piloted manually via the RC to collect water quality data from random locations. The remote-control option allowed flexibility when the flight path was blocked by trees or when the wind speed was not suitable for safe flight.

The collected water quality data was used to create maps for visualization of water quality distribution. The data was processed in ArcMap (Esri, Redlands, CA, USA) and interpolated using the Inverse Distance Weighted Interpolation (IDW) method (Ahmad, Aziz, Rehman, & Saifullah, 2015). Vector data in Geographic Information System (GIS) was interpolated to develop raster maps to simulate data values for intermediate locations.

Experiment Site

Both the accuracy assessment experiments of OSMM, and in situ data collection were made at Lamaster Pond at Clemson, SC. The area of the pond was 1.1 ha. The total number of measurement points on the pond and the duration of a flight mission were limited by battery power availability, and the difficulty of autonomous operation at the narrow section of the pond. Thirteen waypoints were selected randomly, with respect to the representation of the entire pond. Water depth measurements were made manually with a kayak and a marked rope at each location. The UAMS launch location and sampling waypoints are represented by circles on the map (Figure 2.5). The Lamaster Pond was selected as the experiment site because of its size and

ease of access. The number of sampling points and their locations were selected randomly, for more stringent testing of the in situ measurement method.

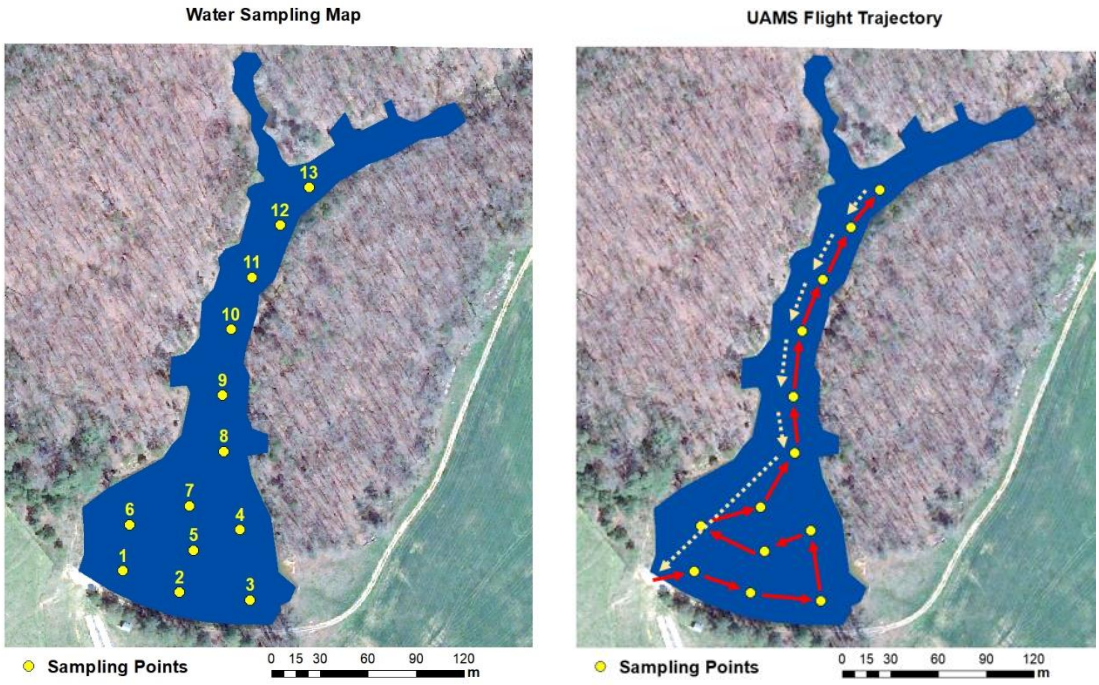

(**a**) **(b)**

Figure 2.5 Satellite images from Google (maps.google.com). (**a**) UAMS sampling waypoints; (**b**) Complete flight mission trajectory at Lamaster Pond, Clemson, SC. The dashed arrows on (**b**) indicate the flight path from the last waypoint to the home location.

The flight mission was divided into three sections. The first mission flight included sampling points 1, 2, 3, 4, 5, and 6. The second mission flight included sampling points 7, 8, 9, and 10. The third mission flight included sampling points 11, 12, and 13. The first and second flight missions were launched from the home location, but the third flight mission was launched from the water surface near waypoint 11. The total direct flight lengths were 256 m for the first

flight, 396 m for the second, and 166 m for the third. Batteries were replaced before each flight mission. If the batteries used had had enough capacity to provide longer endurance, water sampling from all thirteen points could have been achieved in one mission flight with a total flight length of 765 m. The flight altitude was set to 10 m to minimize crash damage risks and optimize battery usage. In order to maximize battery usage, the UAMS was landed at each waypoint and the motors were shut down during in situ measurements.

Results

Accuracy Assessment Results

Both the OSMM and CMM probes were calibrated in the laboratory following the manufacturers' guidelines. At each measurement location, 15 measurements were made with the OSMM, providing a total of 195 data points. The CMM measurements were replicated three times at each location, providing 39 data points. A paired *t*-test was conducted to compare the differences between the OSMM and CMM measurements for each water quality parameter. In the paired *t*-test, we hypothesized that differences in the measurements made by the OSMM and CMM for each parameter, respectively, would not be statistically significant at an alpha level of 0.05.

The paired *t*-test statistics indicated that the temperature measurements made by the OSMM were significantly higher than those made by the CMM ($t(12) = 9.7$, $p < 0.001$). The paired *t*-test statistics also indicated that EC measurements made by the OSMM were significantly lower than the corresponding CMM measurements ($t(12) = 6.1$, $p < 0.001$). The percent error of the EC and temperature measurements made by the OSMM as compared with those of the CMM were 23.99% and 9.55%, respectively; whereas the differences in pH and DO between measurements

made by the OSMM and CMM were not statistically significant. The average difference in DO measurements made by the OSMM and CMM was not significantly high ($t(12) = 1.34$, $p = 0.1$). There was not a significant difference in the average pH values between the OSMM and CMM measurements ($t(12) = 1.76$, $p = 0.05$). The accuracy of the DO and pH measurements made by the OSMM, relative to those made by the CMM, was 97.92% and 96.24%, respectively. Table 2.2 shows the summary statistics for water quality parameters obtained by the OSMM and CMM.

Table 2.2 Descriptive statistics for water quality parameters obtained by the OSMM and CMM.

Quality Parameter	OSMM			CMM			Difference (%)	*t* value (DF)	*p* value
	N	Mean	SD	N	Mean	SD			
Temp. (°C)	195	27.15	0.93	39	24.79	0.58	2.33	9.7 (12)	0.0001***
EC (µS/cm)	195	49.2	9.69	39	64.73	4.57	3.43	6.1 (12)	0.0001***
pH	195	8.43	0.86	39	8.12	0.36	3.76	1.76 (12)	0.05
DO (mg/L)	195	9.05	0.27	39	8.87	0.49	2.08	1.34 (12)	0.1

Notes: N: Number, SD: Standard deviation, DF: Degrees of freedom, Significance levels *** = $p < 0.001$

Although EC and temperature measurements were statistically different, they followed a similar pattern, as shown in Figure 2.6. The average difference in EC measurements (17.75 µS/cm) between those of the CMM and OSMM was added to the OSMM measurements as a correction factor. Similarly, the average difference in temperature measurements (−2.33 °C) between those of the OSMM and CMM was added to the OSMM measurements as a correction factor. These differences would be a result of the type of instruments made by different

companies causing instrument error. The Hach EC probe is supplied with a meter that measures temperature with a thermistor for automatic compensation, whereas the Atlas Scientific temperature probe is a RTD (Resistance Temperature Detector). The EC measurements are corrected for sample temperature. The differences in the method of temperature measurement may be the reason for the differences in the EC measurements between the OSMM and CMM.

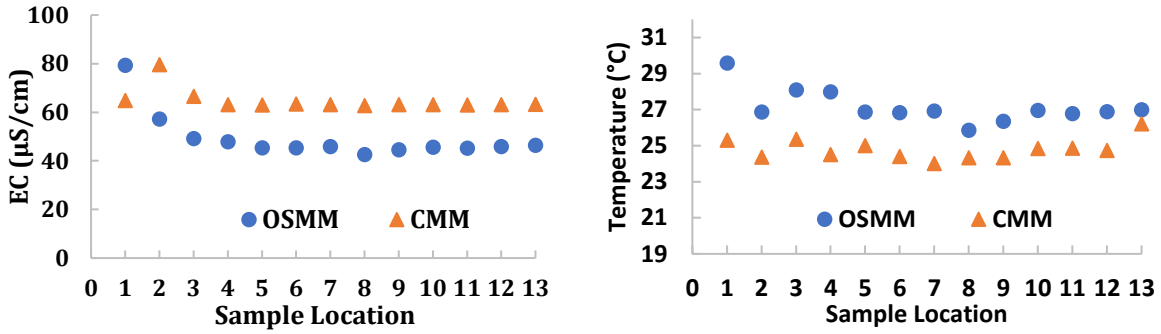

(**a**) (**b**)

Figure 2.6 (**a**) Electrical conductivity (EC) and (**b**) temperature measurements, as made by the OSMM and CMM.

After applying the correction factors, the paired *t*-test statistics were conducted again for EC and temperature data. The results of the descriptive statistics is shown in Table 2.3. The paired *t*-test indicated that there was not a significant difference in the averages of EC measurements between the OSMM and the CMM ($t(12) = 0.87$, $p = 0.2$). The average corrected temperature values of the OSMM were not significantly different from the CMM values ($t(12) = 0.13$, $p = 0.45$). After applying the correction factors, the accuracies of the EC and temperature measurements made by the OSMM increased to 96.5% and 99.87%, respectively.

Table 2.3 Descriptive statistics for water quality parameters obtained by the OSMM and CMM, after applying correction factors to the EC and temperature measurements.

Quality Parameter	OSMM			CMM			Difference (%)	t value (DF)	*p* value
	N	Mean	SD	N	Mean	SD			
Temp. (°C)	195	24.82	0.93	39	24.79	0.58	0.13	0.13 (12)	0.45
EC (µS/cm)	195	66.95	9.69	39	64.73	4.57	3.43	0.87 (12)	0.2
pH	195	8.43	0.86	39	8.12	0.36	3.76	1.76 (12)	0.05
DO (mg/L)	195	9.05	0.27	39	8.87	0.49	2.08	1.34 (12)	0.1

Notes: N: Number, SD: Standard deviation, DF: Degrees of freedom

In Situ Water Quality Measurements using the UAMS

The UAMS was tested in multiple preliminary field experiments to evaluate its performance, measurement accuracy, and suitability with the proposed in situ water quality measurement method, in a variety of wind conditions and operational scenarios. All the preliminary tests and data collection experiments were conducted at Lamaster Pond in Clemson, SC. The autonomous navigation and control of the UAMS was interrupted occasionally to determine the best control method for in situ measurements. It is important to note that once the autonomous mode of the flight mission was interrupted by the operator in case of an emergency, the operator took over the control of the UAMS with the RC. The operator landed the UAMS on the water surface and manually activated the OSMM measurements. During this process, the previous sampled waypoints were removed from the flight mission using the control station, and a new flight mission was transmitted to the UAMS for autonomous navigation via radio telemetry. The operator activated the new flight mission remotely, and the UAMS continued

sampling for the remaining waypoints autonomously. This process was repeated whenever the flight mission was interrupted by the operator.

The water quality parameters in Lamaster Pond were measured using the UAMS following the procedure described in Section 2.3. The data recorded on the OSMM SD card was retrieved and processed to develop surface maps for each measured parameter. Figures 2.7 and 2.8 show the manual depth measurements and the spatially interpolated data retrieved from the UAMS. The water depth at the measured locations varied between 1.22 and 4.57 m. The depth at the southeast of the pond was the deepest, whereas the north side of the pond had the shallowest depth measurements. The temperature measurements varied between 14.02 and 16.42 °C. The shallower sections of the pond had slightly higher temperatures than the deeper sections (Figure 2.8a). The data maps show an inverse relationship between pH and water depth (Figure 2.8b). As shown by the map, the pH values tended to be lower where the depth was increased. The highest pH measurements were recorded at the north side of the pond, where the water depth was lower than in the other locations. The maps indicate an inverse relationship between DO and EC values (Figure 2.8c, d). In addition, the DO values decreased with increasing temperature. The variation of EC values was not high across the pond, but it tended to be higher at the southwest part of the pond. Maps provided graphical representation of the distribution of water quality parameters in the pond. These maps were useful in terms of interpreting the spatial distribution of water quality data.

Traditional in situ water quality measurement and water collection for laboratory analyses is still the preferred method used to make management decisions (Schaeffer et al., 2013). While these measurements provide accurate results, they do not give a spatial or temporal view of water quality over the waterbody (Ritchie, Zimba, & Everitt, 2003). Remote sensing

techniques are being used to develop regression models between the band ratios and water quality parameters (Su & Chou, 2015). To develop accurate regression models, the remote sensing data must be verified with labor-intensive and time-consuming field experiments. UAMS-type measurement systems can be used for collecting field data and for verification of remote sensing data.

While satellite remote sensing can cover large areas, the satellite remote sensing devices scan earth surfaces systematically, and there would be a delay between passes over a given area of earth; thus, the resolution of the satellite images may not be high enough for developing regression models between the band ratios and water quality parameters (Su & Chou, 2015). Furthermore, prolonged weather conditions such as cloudiness would hinder the quality of satellite imaging. In those conditions, UAVs can be mounted with imaging sensors to collect high-resolution aerial images of relatively small waterbodies (Su & Chou, 2015). High-resolution aerial imagery would be useful for identifying hydromorphological features such as riffles, side bars, and submerged vegetation along the rivers (Rivas Casado, Ballesteros Gonzalez, Wright, & Bellamy, 2016). Aerial images with resolutions of less than 5 cm can only be accomplished with UAV-mounted imaging devices (Rivas Casado et al., 2016).

In this study, we selected the measurement locations in a pattern to collect data from which to develop surface maps for each measured parameter. For larger waterbodies, optical and thermal sensors on UAVs, satellites, or manned aircrafts can be used as guidelines for determining the water quality measurement or water collection sampling locations (Ritchie et al., 2003). Depending on the variation in aerial imagery, the number of measurement points and their locations can be determined for in situ measurements or sample collections. UAMS-type systems can also be used for water collection after natural disasters such as hurricanes and flooding

(Koparan & Bulent Koc, 2016; Ore, Elbaum, Burgin, & Detweiler, 2015). Field personnel may not be able to collect water samples or conduct water quality measurements immediately after a disaster. In those cases, UAMS-type systems can be deployed for water sampling and water quality assessment.

Stationary sensors or sensors placed on ASVs and AUVs are often used for prolonged durations in water without being cleaned. The OSMM probes can be cleaned and maintained after every mission flight; this would eliminate problems caused by dirty and continuously used sensor equipment.

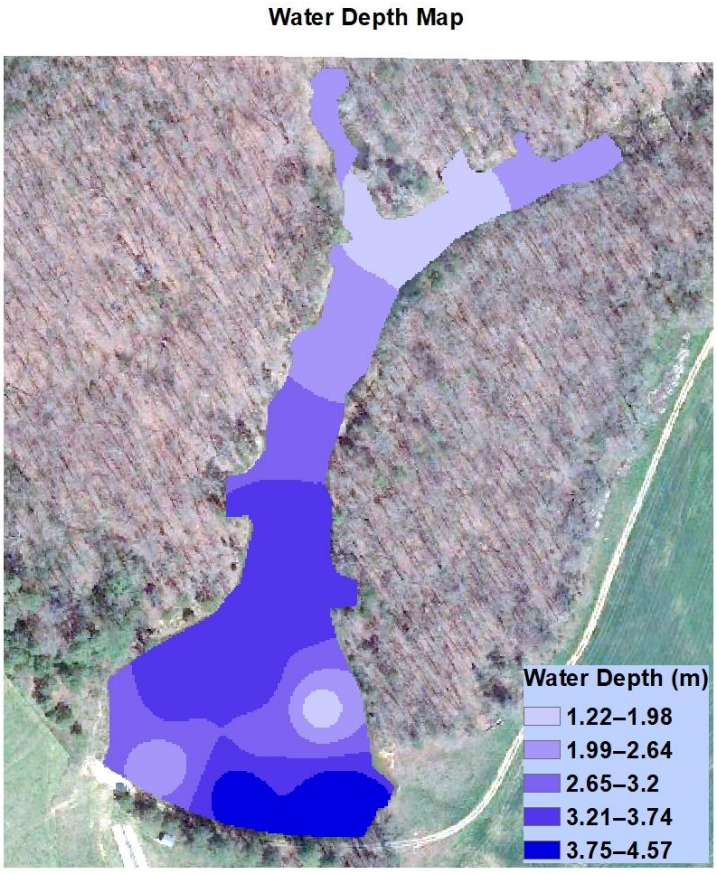

Figure 2.7 Spatially interpolated data from manual depth measurements.

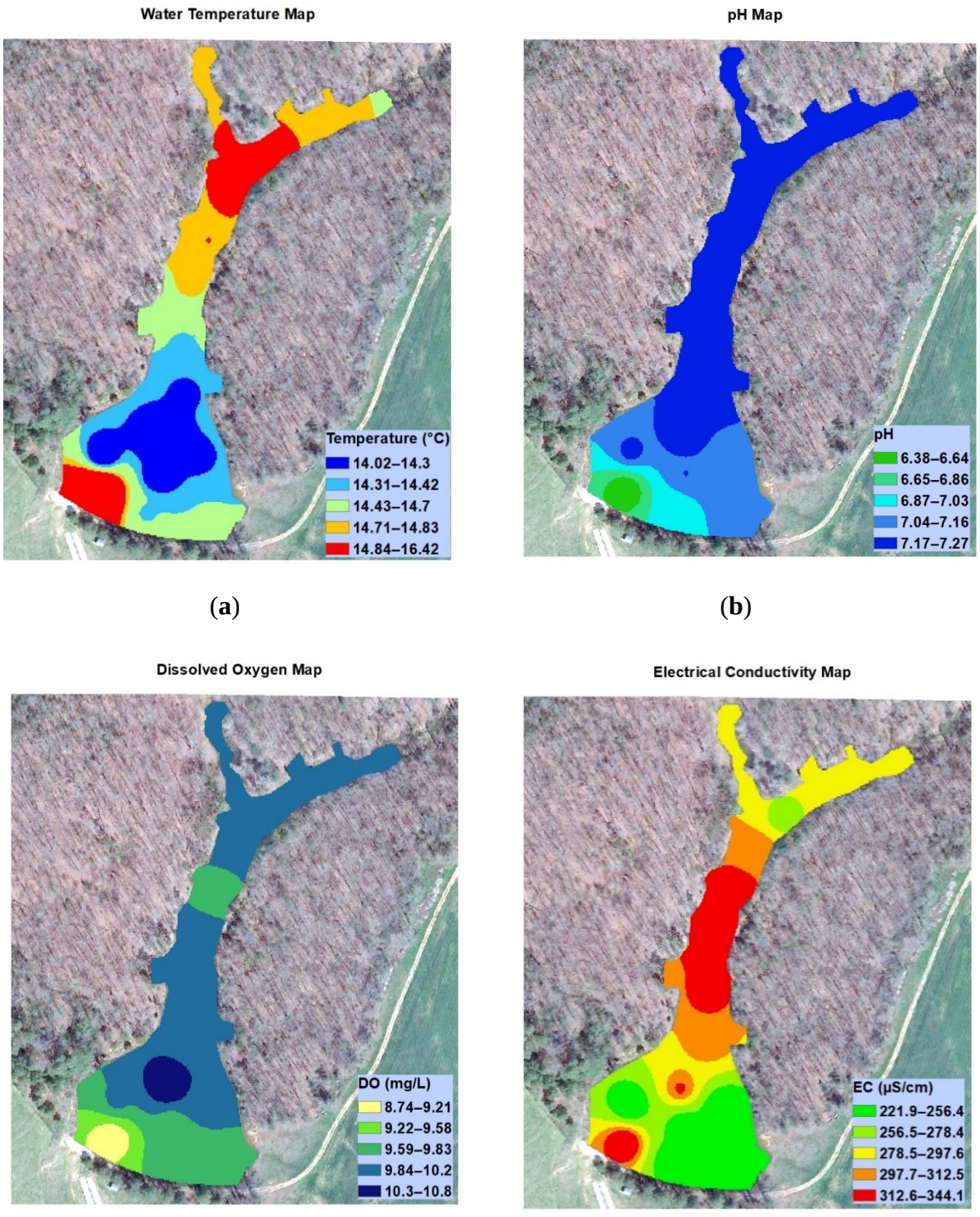

Figure 2.8 Spatially interpolated data from the UAMS: Water quality maps showing (**a**) water temperature, (**b**) pH, (**c**) dissolved oxygen, and (**d**) electrical conductivity.

Conclusions

A UAV-assisted in situ water quality measurement system (UAMS) was developed and tested. The backbone of the UAMS was the custom-built hexacopter that carried the open source multiprobe meter (OSMM). Flotation equipment mounted under the hexacopter allowed the UAV to land on the water surface at the waypoints in the flight mission. Landing and lifting off from water surface avoided requiring the hexacopter to hover during the in situ measurements with the OSMM. This option greatly increased the endurance of the UAMS and the possible number of sampling points in each flight mission. Landing on the water surface during sampling reduced the complexity of the UAMS, by eliminating the need to use additional sensors for safe hovering for taking measurements at a precise depth. The developed prototype UAMS was waterproof, lightweight, and fully functional for collecting georeferenced temperature, electrical conductivity (EC), dissolved oxygen (DO), and pH data from a 1.1 ha agricultural pond.

The developed prototype UAMS can be used to collect field data for the development of algorithms for water quality assessment with satellite remote sensing. UAMSs can also be used for conducting field measurements at inaccessible or dangerous waterbodies. Another important contribution of the UAMS would be in rapid water quality measurements after natural disasters such as flooding and hurricane events. The major limiting factor for the UAMS is flight duration. Advancements in battery technology and optimal UAV designs can increase the endurance of the UAMS. Future research activities will focus on the development of a new UAMS for smart water sampling, based on the OSMM measurements.

References

Ahmad, H. R., Aziz, T., Rehman, Z. R., & Saifullah. (2015). Chapter 15 - Spatial Mapping of Metal-Contaminated Soils A2 - Hakeem, Khalid Rehman. In M. Sabir, M. Öztürk, & A. R. Mermut (Eds.), *Soil Remediation and Plants* (pp. 415-431). San Diego: Academic Press.

Ardupilot. (2017a). Installing Mission Planner. Retrieved from http://ardupilot.org/planner/docs/common-install-mission-planner.html

Ardupilot. (2017b, December 10). MAVLink Mission Command Messages. Retrieved from http://ardupilot.org/planner/docs/common-mavlink-mission-command-messages-mav_cmd.html

Blaas, H., & Kroeze, C. (2016). Excessive nitrogen and phosphorus in European rivers: 2000–2050. *Ecological Indicators, 67,* 328-337. doi:https://doi.org/10.1016/j.ecolind.2016.03.004

Dunbabin, M., Grinham, A., & Udy, J. (2009). *An autonomous surface vehicle for water quality monitoring.* Paper presented at the Proceedings of the 2009 Australasian Conference on Robotics and Automation, ACRA 2009.

Gholizadeh, M., Melesse, A., & Reddi, L. (2016). A Comprehensive Review on Water Quality Parameters Estimation Using Remote Sensing Techniques. *Sensors, 16*(8), 1298.

Glasgow, H. B., Burkholder, J. M., Reed, R. E., Lewitus, A. J., & Kleinman, J. E. (2004). Real-time remote monitoring of water quality: a review of current applications, and advancements in sensor, telemetry, and computing technologies. *Journal of Experimental Marine Biology and Ecology, 300*(1), 409-448. doi:https://doi.org/10.1016/j.jembe.2004.02.022

Gupta, A. K., Jha, V., & Gupta, V. K. (2014). Design and Development of Remote Controlled Autonomous Synchronic Hexaroter Aerial (ASHA) Robot. *Procedia Technology, 14*, 51-58. doi:https://doi.org/10.1016/j.protcy.2014.08.008

Kaizu, Y., Iio, M., Yamada, H., & Noguchi, N. (2011). Development of unmanned airboat for water-quality mapping. *Biosystems Engineering, 109*(4), 338-347. doi:https://doi.org/10.1016/j.biosystemseng.2011.04.013

Karimanzira, D., Jacobi, M., Pfuetzenreuter, T., Rauschenbach, T., Eichhorn, M., Taubert, R., & Ament, C. (2014). First testing of an AUV mission planning and guidance system for water quality monitoring and fish behavior observation in net cage fish farming. *Information Processing in Agriculture, 1*(2), 131-140. doi:https://doi.org/10.1016/j.inpa.2014.12.001

Koparan, C., & Bulent Koc, A. (2016). *Unmanned Aerial Vehicle (UAV) assisted water sampling*. Paper presented at the 2016 ASABE Annual International Meeting, St. Joseph, MI. http://elibrary.asabe.org/abstract.asp?aid=47024&t=5

Koparan, C., & Koc, A. B. (2016). *Unmanned Aerial Vehicle (UAV) assisted water sampling.* Paper presented at the 2016 ASABE Annual International Meeting.

Liu, R., Xu, F., Zhang, P., Yu, W., & Men, C. (2016). Identifying non-point source critical source areas based on multi-factors at a basin scale with SWAT. *Journal of Hydrology, 533*, 379-388. doi:https://doi.org/10.1016/j.jhydrol.2015.12.024

Lynch, K. M., Marchuk, N., & Elwin, M. L. (2016). Chapter 13 - I2C Communication. In *Embedded Computing and Mechatronics with the PIC32* (pp. 191-211). Oxford: Newnes.

Ma, Y., Egodawatta, P., McGree, J., Liu, A., & Goonetilleke, A. (2016). Human health risk assessment of heavy metals in urban stormwater. . *Science of The Total Environment 2016, 557–558, 764-772.*

McGowan, S. (2016). Chapter 2 - Algal Blooms A2 - Shroder, John F. In R. Sivanpillai (Ed.), *Biological and Environmental Hazards, Risks, and Disasters* (pp. 5-43). Boston: Academic Press.

Neumann, M., Liess, M., & Schulz, R. (2003). A qualitative sampling method for monitoring water quality in temporary channels or point sources and its application to pesticide contamination. *Chemosphere, 51*(6), 509-513.

Ore, J.-P., Elbaum, S., Burgin, A., & Detweiler, C. (2015). Autonomous Aerial Water Sampling. *Journal of Field Robotics, 32*(8), 1095-1113. doi:10.1002/rob.21591

Partyka, M. L., Bond, R. F., Chase, J. A., & Atwill, E. R. (2017). Monitoring bacterial indicators of water quality in a tidally influenced delta: A Sisyphean pursuit. *Science of The Total Environment, 578*, 346-356. doi:https://doi.org/10.1016/j.scitotenv.2016.10.179

Peters, C. B., Zhan, Y., Schwartz, M. W., Godoy, L., & Ballard, H. L. (2017). Trusting land to volunteers: How and why land trusts involve volunteers in ecological monitoring. *Biological Conservation, 208*, 48-54. doi:https://doi.org/10.1016/j.biocon.2016.08.029

Ravalli, A., Rossi, C., & Marrazza, G. (2017). Bio-inspired fish robot based on chemical sensors. *Sensors and Actuators B: Chemical, 239*(Supplement C), 325-329. doi:https://doi.org/10.1016/j.snb.2016.08.030

Ritchie, J. C., Zimba, P. V., & Everitt, J. H. (2003). Remote Sensing Techniques to Assess Water Quality. *Photogrammetric Engineering & Remote Sensing, 69*(6), 695-704. doi:10.14358/PERS.69.6.695

Rivas Casado, M., Ballesteros Gonzalez, R., Wright, R., & Bellamy, P. (2016). Quantifying the Effect of Aerial Imagery Resolution in Automated Hydromorphological River Characterisation. *Remote Sensing, 8*(8), 650.

Schaeffer, B. A., Schaeffer, K. G., Keith, D., Lunetta, R. S., Conmy, R., & Gould, R. W. (2013). Barriers to adopting satellite remote sensing for water quality management. *International Journal of Remote Sensing, 34*(21), 7534-7544. doi:10.1080/01431161.2013.823524

Su, T.-C., & Chou, H.-T. (2015). Application of Multispectral Sensors Carried on Unmanned Aerial Vehicle (UAV) to Trophic State Mapping of Small Reservoirs: A Case Study of Tain-Pu Reservoir in Kinmen, Taiwan. *Remote Sensing, 7*(8), 10078.

Thomas, K. V., Hurst, M. R., Matthiessen, P., Sheahan, D., & Williams, R. J. (2001). Toxicity characterisation of organic contaminants in stormwaters from an agricultural headwater stream in South East England. *Water Research, 35*(10), 2411-2416. doi:https://doi.org/10.1016/S0043-1354(00)00535-2

Tyler, A. N., Hunter, P. D., Carvalho, L., Codd, G. A., Elliott, J. A., Ferguson, C. A., . . . Scott, E. M. (2009). Strategies for monitoring and managing mass populations of toxic cyanobacteria in recreational waters: a multi-interdisciplinary approach. *Environmental Health, 8*(1), S11. doi:10.1186/1476-069x-8-s1-s11

van der Merwe, D. (2015). Chapter 31 - Cyanobacterial (Blue-Green Algae) Toxins A2 - Gupta, Ramesh C. In *Handbook of Toxicology of Chemical Warfare Agents (Second Edition)* (pp. 421-429). Boston: Academic Press.

Weiss, P. T., Erickson, A. J., Gulliver, J. S., Hozalski, R. M., Mohseni, O., & Herb, W. R. (2010). Stormwater Treatment: Assessment and Maintenance. University of Minnesota, St. Anthony Falls Labratory. Minneapolis, MN.

Wernersson, A.-S., Carere, M., Maggi, C., Tusil, P., Soldan, P., James, A., . . . Kase, R. (2015). The European technical report on aquatic effect-based monitoring tools under the water framework directive. *Environmental Sciences Europe, 27*(1), 7. doi:10.1186/s12302-015-0039-4

Winkelbauer, A., Fuiko, R., Krampe, J., & Winkler, S. (2014). Crucial elements and technical implementation of intelligent monitoring networks. *Water Science and Technology, 70*(12), 1926-1933. doi:10.2166/wst.2014.415

Winkler, S., Zessner, M., Saracevic, E., & Fleischmann, N. (2008). Intelligent monitoring networks – transformation of data into information for water management. *Water Science and Technology, 58*(2), 317-322. doi:10.2166/wst.2008.672

Xu, Z., Dong, Q., Otieno, B., Liu, Y., Williams, I., Cai, D., . . . Li, B. (2016). Real-time in situ sensing of multiple water quality related parameters using micro-electrode array (MEA) fabricated by inkjet-printing technology (IPT). *Sensors and Actuators B: Chemical, 237*, 1108-1119. doi:https://doi.org/10.1016/j.snb.2016.09.040

CHAPTER THREE

AUTONOMOUS IN SITU MEASUREMENTS OF NONCONTAMINANT WATER QUALITY INDICATORS AND SAMPLE COLLECTION WITH A UAV

Abstract

Water sampling location, depth, and scheduling are important management parameters for a water quality monitoring program. It is essential to reduce cost by minimizing the number of grab samples while accurately reflecting the comprehensive condition of water quality. Autonomous water sampling systems can provide remotely obtained water quality data for rapid management decisions. An autonomous water sampling system with an unmanned aerial vehicle integrated sensor node was developed and tested in this research. The UAV-assisted autonomous water sampling system (UASS) consists of a hexacopter UAV, a water sampling cartridge (WSC), and a sensor node to measure the noncontaminant water quality indicators of pH, dissolved oxygen (DO), electrical conductivity (EC) and temperature. Payload capacity and endurance of the UAV were determined using an indoor test station. The UAV was able to produce 106 N of thrust for 10 min with 6.3 kg of total takeoff weight. The thrust-to-weight ratio of the UAV was 2.5 at 50% throttle setting. The decision for activating the water sampling cartridge and sensor node was made autonomously from an onboard microcontroller. Water sampling and in situ measurements were conducted at 6 pre-defined locations at sampling depths of 0.5 m and 2 m over a 1.1 ha agricultural pond. The UASS successfully activated the WSC when the vehicle reached the sampling locations. Instantaneous decision making for sample collection based on in situ measurements would eliminate unnecessary sample collection while providing data to assess water quality. The UASS would reduce water quality assessment

duration and help monitoring personnel and researchers to conduct frequent observations with lower operational costs.

Introduction

Effective water quality monitoring is critical for water resource programs due to increased human population growth and industry pressure that can degrade water quality in coastal and inland waters (Lewitus et al., 2003; Tyler et al., 2009). Increased risks of water degradation and human interaction with inland waters such as capture fisheries and other activities bring additional need for periodic water sampling methods to ensure public health (Garg et al., 2017; Null, Mouzon, & Elmore, 2017; Shoda, Sprague, Murphy, & Riskin, 2019). Periodic sampling and analysis allow one to characterize water and identify changes or trends in water quality over time.

Water quality detection in waterbodies can be performed by monitoring contaminant and noncontaminant indicators. Contaminant indicators reflect the status of water pollution while noncontaminant indicators reflect the comprehensive conditions of water quality (Li & Liu, 2019b). Contaminant indicators include chemical oxygen demand, total phosphorus, total nitrogen, chlorophyll-a, and turbidity (Pearse, 1984). Some contaminant indicators can be measured in situ but the most accurate results are obtained only with laboratory analyses (Schaeffer et al., 2013; Xu & Boyd, 2016). Regular monitoring of dispersed suspended solids such as silt, clay, algae, organic matter, and other particles also play important roles in water quality monitoring (Anderson, 2005). However, bacterial studies require laboratory evaluation of samples and the number of grab samples that are needed could reach large numbers (Stauber, Miller, Cantrell, & Kroell, 2014). Dissolved oxygen (DO), electrical conductivity (EC), pH, and temperature are the noncontaminant water quality indicators that are measured and evaluated in

situ (Chung & Yoo, 2015). Measured changes in these indicators can be used to address the presence of pollution (Li & Liu, 2019a) and subsequent evaluation can be used to make management decisions about sampling events for pollution monitoring.

Water quality indicators that are measured at different locations may vary (Khalid, Hamzah, & Saat, 2009; Kim, Seo, & Choi, 2017; Yang et al., 2018). Water sample collection and in situ measurements at a precise depth is a challenging task using existing methods. Current water quality monitoring methods are grab sampling from the shore or with a boat off-shore, fixed sensor stations, and autonomous vehicles that operates underwater, on or above the water surface (Eichhorn et al., 2018; Esakki et al., 2018; Glasgow, Burkholder, Reed, Lewitus, & Kleinman, 2004; Kaizu, Iio, Yamada, & Noguchi, 2011; Mayer & Ali, 2017; Ore & Detweiler, 2018). Water sampling depth and location cannot be adjusted with the fixed sensor stations because they are placed at certain depths, or systems that have depth adjustment mechanisms could increase equipment costs (Winkelbauer, Fuiko, Krampe, & Winkler, 2014). Underwater, surface, and aerial autonomous vehicles can collect water samples at various depths, but these systems pose operational and technical challenges (Eichhorn et al., 2018; Kaizu et al., 2011; Liu, Noguchi, & Yusa, 2014; Ore, Elbaum, Burgin, & Detweiler, 2015). Water levels in water treatment facilities vary due to seasonal changes. Water sampling from lowered water reservoirs might pose challenges because access to a sampling point with a boat, kayak, autonomous surface and underwater vehicles may be difficult.

Sensors used to measure water quality have other limitations that include operational temperature and fouled measurements. When these sensors are used outside of manufacturers' specified operational temperature, measurements may result in error (Tai, Li, Wei, Ma, & Ding, 2011). If temperature conditions are at extreme levels when such sensors are continually used, it

could damage the sensor. Sediments that built-up around stationary sensors may cause measurement fouling. In these situations, data would not be reliable, time would be wasted, and costs of water sampling operations would be increased due to replacement of the sensor array and repeated sampling.

To address several of these monitoring challenges, a water sampler with a single cartridge was designed and integrated with a UAV for autonomous water sampling (Koparan, Koc, Privette, Sawyer, & Sharp, 2018a). System operation and field experiments were conducted to evaluate its performance. Water collection was made while the UAV was hovering during field experiments. Hovering altitude and sampling depth analyses were conducted to determine precise water collection depths. The single cartridge water sampler was designed and consistently able to collect a volume of 130 ml. The average water sampling depth ranged between 0.56 – 0.79 m because the UAV was hovering during collection. Wind speeds of less than 24 km/h were recommended for safe autonomous flight of the system. The evaluated system proved water sampling with a UAV-assisted mechanism can be achieved while the UAV was flying near a waterbody. Further field tests showed that landing the UAV on the water surface could be optimized for safety and battery consumption reasons.

A sensor array that can measure DO, EC, temperature, and pH was integrated with a UAV and field tests were conducted to evaluate system performance (Koparan, Koc, Privette, & Sawyer, 2018b). In situ water quality measurement experiments were conducted in a 1.1 ha agricultural pond in Clemson, SC. An accuracy assessment was made for the sensor array and measurements were compared with commercially available reference sensors. The UAV and sensor node were autonomously controlled, and interventions were made with a remote controller when necessary. Interventions were required for safety when wind speed suddenly

changed. The UAV was equipped with floatation attachments to facilitate water landing and to increase flight time, thus reducing battery usage. In situ measurement depth was fixed at 0.6 m for all sampling locations after landing on the water surface. Spatially interpolated data from the sensor node mounted UAV were represented in water quality maps to visualize the distribution of the noncontaminant water quality indicators. The resulting system can be used to collect field data for development of algorithms for water quality assessment with satellite remote sensing. The final autonomous configuration can also be used for conducting field measurements at inaccessible or dangerous waterbodies.

Previous research conducted by Koparan et al (2018a and 2018b) collected water samples and conducted in situ measurements with separate missions. As the major noncontaminant water quality indicators of DO, pH, EC and temperature would potentially indicate impairment, collecting water samples based on in situ measurements may eliminate unnecessary sampling, increase flight duration, and reduce operational costs. Therefore, the objective of this research was to integrate a water quality sensor node and a water sampler on a multirotor UAV for autonomous water quality assessment. To accomplish this objective, a triple cartridge water sampler was designed, a multirotor UAV was built, and operation of the system was tested in field conditions.

Materials and Methods

Water sampler design

The single cartridge water sample collection mechanism previously designed posed challenges during field experiments (Koparan et al., 2018a). The mechanism used a metal weight of 200 g as a triggering apparatus. The metal weight was released from the UAV and sent through a tether while the sampler dangled at the bottom end. The sampler was triggered once

the metal weight made contact with the sampler in the water. This design concept was not 100 % functional because the velocity and water entry angle of the metal weight affected the impact force on the sampler's triggering mechanism. In addition, sampling depth could not be adjusted precisely. Outdoor experimentation resulted in an unacceptable triggering success rate. In addition, more samples were needed for replicate sampling purposes that required more than one cartridge. Eliminating the metal weight would reduce the resulting payload by 200g and more cartridges could be added. To eliminate challenges of the previous design exposed during field testing, a new water collection mechanism with a triple cartridge that was triggered by a waterproofed servo motor was devised and fabricated (Appendix A).

The water sampling cartridge (WSC) consists of a metal geared waterproof servo actuator (Savox SW-0230MG, Salt Lake City, Utah, US), triple cartridges, caps, frame, gear rack and pinon gear, and hooks (Figure 3.1). Cap components were 3D printed with selective laser sintering (SLS) technique from polymer plastic material. Cartridges, frame and hooks were 3D printed with fused deposition modeling (FDM) technique from polylactic acid material (PLA). Parts that were printed with PLA material were less flexible than parts printed with polymer plastic material. Cap components were printed out of polymer plastic to provide a better seal and ensure water did not leak from the cartridges. The empty weight of the new triple cartridge with servo mechanism was 0.4 kg.

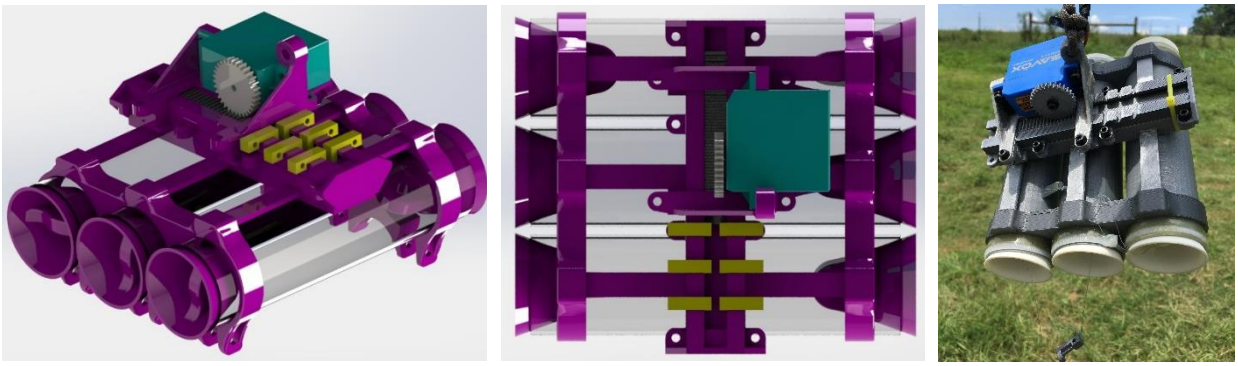

(a) **(b)** **(c)**

Figure 3.1 Water sampling cartridge and its components. **(a)** The green component is the servo, the yellow components are hooks, transparent components are cartridges, and purple components are the frame and caps, **(b)** the gray components are pinon gear and gear rack, **(c)** fabricated sampler.

The servo actuator was used to pull or push the gear rack by rotating the pinon gear at a given angle. The degree of rotation was adjusted by the flight controller depending on distance between the hooks. At each given rotation, a single hook was pushed away by the gear rack, allowing single cartridge activation. The two caps at both ends of the cartridges were connected with latex tubing. This component allowed the caps to pull the open ends of the cartridges towards each other when the hooks were released, thus storing water sample.

Sensor node integration and system configuration

The sensor node consisted of probes and a microcontroller platform (Figure 3.2) and was capable of obtaining measurements for DO, pH, EC, and temperature (Koparan et al., 2018b). The microcontroller platform was placed in a sealed waterproof box on top of the UAV to isolate it from exposure to moisture during water landings. Probes were placed in a 3D printed case and connected to the tentacle shield with a 3 m long cable. The cable connection was made at the top

of the box using *BNC* (*Bayonet Neill–Concelman*) quick connectors. The probes were dangled through the bottom center of the UAV. Total weight of the sensor node including extension cables, 3D printed probe case, and the sealed waterproof box was 1.0 kg.

The sensor node consisted of EC, DO, pH, and temperature circuits (Atlas Scientific, New York, Water 2018, 10, 264 5 of 14 NY, USA), and was integrated with a microcontroller (Atmel ATmega2560, San Jose, CA, USA). Circuits were integrated with a tentacle shield (Atlas Scientific, NY, USA). Sensor readings were taken with an Inter-Integrated Circuit (I2C) protocol, and data were recorded on a Secure Digital (SD) card inserted in the shield (SunFounder, Shenzhen City, Guangdong Province, China). The sensor node was calibrated in the laboratory following the manufacturer's specifications.

(a) **(b)** **(c)**

Figure 3.2 Sensor node; **(a)** microcontroller platform mounted on top of the UAV, **(b)** probes dangled from the UAV, and **(c)** probes located above the water sampling cartridges (WSC).

Calibration of the sensor node was made with Arduino Integrated Development Environment (IDE) interface. The IDE was used to debug and upload the program, enter the calibration commands, and retrieve the measurements during calibration. The calibration buffer

values for each sensor were entered using the serial monitor in IDE while the probes were in buffer solutions. Each sensor was identified and recalled with specific I2C addresses for calibration and data retrieval. The I2C addresses for DO, pH, EC and temperature were 97, 99, 100 and 102, respectively.

The sensor node activation for in situ measurement of water quality parameters was made by the flight controller after autonomous UAV navigation to the sampling points. Sensor node activation was programmed to be made without operator input at each sampling location during field experiments. The activation signal source was the auxiliary signal output port on the flight controller. The sensor node and WSC system configuration is shown in Figure 3.3.

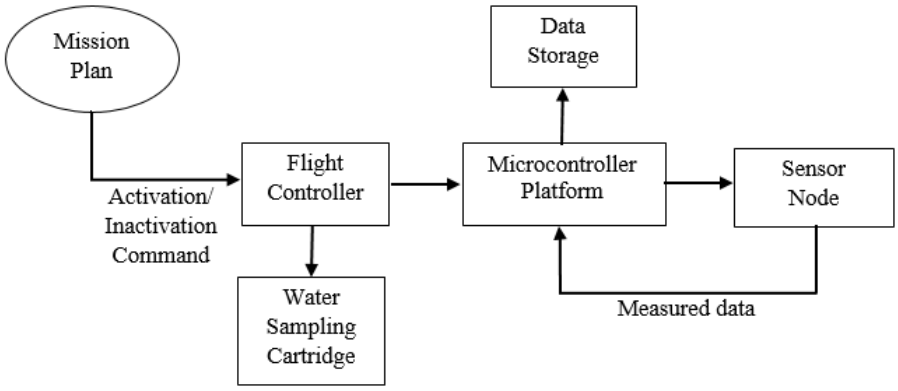

Figure 3.3 System configuration with flight controller, microcontroller, sensor node and water sampling cartridge (WSC).

UAV characteristics and weight distribution

To carry the sensor node and triple cartridge mechanism, a multirotor UAV was built and tested (Figure 3.4). The UAV was used as a platform to transport the sensor node and WSC payload to a pre-defined water sampling location. The flight controller was used to initiate water sampling and in situ measurement events. The UAV can carry the WSC, sensor nodes, and water samples long enough to accomplish an autonomous mission flight. Therefore, the UAV produces

enough thrust to carry the payload to a desired predefined location and accomplish an autonomous water sampling mission.

Primary components of the UAV included a frame, motors, propellers, electronic speed controllers, a flight controller (Pixhawk, 3DR, Robotics, Berkeley, CA, USA), a GPS receiver (Ublox, 3DR, Berkeley, CA, USA), a telemetry radio transmitter (3DR radio, 3DR, 3DR, Berkeley, CA, USA), and a power supply. Six 400 KV motors were selected because of their capacity to resist water and dust with high performance rates (T-Motors U5, Nanchang, Jiangxi, P.R. China). Carbon fiber propellers with 40 cm length were chosen based on manufacturer's specifications for selected motors (T-Motors, Nanchang, Jiangxi, P.R. China). A custom made hexacopter frame with 800 mm hull length was chosen (RCT800, Powerhobby, Mahwah, NJ, US). The hull length of the frame was wide enough to provide enough space for each propeller and center base where electronic components and payload were integrated. The battery size was large enough to provide the greatest power output as possible, and light enough to provide better thrust-to-weight ratio of the UAV. A 22.2 V battery was selected based on the motors' manufacturer recommendation. The maximum continuous current that a single motor requires from the battery is 30 A. The total continuous current that was required from the battery by six motors was 180 A. The total theoretical power requirement of motors was calculated as 3,996 W. Therefore, the battery with 8,000 mAh current capacity with 25C discharge rate at 22.2 V can produce 4,440 W of electrical power (Tattu, Dublin, CA, US). A battery with 10,000 mAh current capacity with 25C discharge at 22.2V was also tested to determine which battery provides the best thrust-to-weight ratio. An ESC with 40 A continuous current capacity was selected as manufacturer's recommendation for safe power distribution (Air 40A, T-Motor, Nanchang, Jiangxi, P.R. China).

(a) **(b)**

Figure 3.4 (a) The multirotor UAV that was built as a carrier platform for the **(b)** sensor node and the water sampling cartridge (WSC) with a closed cell floatation section for depth adjustment.

One essential flight characteristic is thrust-to-weight ratio. Thrust-to-weight ratio determines how long a UAV can fly and how much payload it can carry (Panagiotou, Fotiadis-Karras, & Yakinthos, 2018). For a UAV to safely hover at 50% throttle settings, it must produce thrust that is at least twice the downward force due to weight. A UAV performance test station was designed and built to measure thrust and endurance (Appendix B and C). Test results indicated the newly configured UAV met required minimum thrust-to-weight ratio for hover (Bravo-Mosquera, Botero-Bolivar, Acevedo-Giraldo, & Cerón-Muñoz, 2017) under prescribed conditions. The weight of the UAV and payload were measured prior to thrust and endurance tests (Table 3.1). The measurements were made in the test station with and without payload mounted on the UAV. Takeoff weight was 4.3 kg without the payload, and 6.4 kg with the payload when the battery with 8,000 mAh capacity was used. Takeoff weight was 4.8 kg without the payload when the battery with 10,000 mAh capacity was used. Working principles, data

acquisition system, test procedure, and construction details of the UAV test station were explained in detail in a previously published study (Koparan et al., 2018a).

Table 3.1 Weight distribution of UAV and payload.

Component	**Weight (kg)**
Sensor Node	0.75
Extension Cord	0.25
Water Sampling Cartridge	0.4
Water Samples	0.4
Floatation attachment	0.3
UAV	4.3
Takeoff weight	***6.4***

Thrust and endurance data were measured at 50 % throttle setting with batteries that have 8000 mAh and 10,000 mAh capacities. Two repeated measurements were made for each battery and results were compared to find which battery provided better thrust-to-weight ratio. Subsequently, thrust and endurance measurements were made at 50%, 60%, and 70% throttle settings with the battery that provided the highest thrust-to-weight ratio. The tests with higher throttle levels were conducted to evaluate how endurance and thrust changes, since windy conditions may affect these performance parameters.

Floatation attachment

A floatation attachment was required to facilitate water landing to make in-situ measurements and collect water samples. The floatation attachment had to be placed under the UAV frame to ensure UASS stability and position above the water surface. The floatation attachment had to be durable enough to be used as landing gear as well as absorb impact during potentially rough or crash landings. Cylindrical foam swimming aids were chosen as floatation

attachment because of their lightweight, flexibility, ease of replacement, low cost, and ability to absorb impact. The volume of the floatation attachment, which was required to keep the UASS above water surface, was determined by calculating the buoyancy force (Higgins & Detweiler, 2016) using Equation 1;

$$F_b = V_s \times \rho_w \times g \quad (1)$$

where F_b = Buoyancy force (N)

V_s = Submerged volume (m^3)

ρ_w = Density of water (kg/m^3)

g = Acceleration due to gravity (m/s^2).

For an object to float, the buoyancy force must be greater than the gravitational force created by the object due to its weight (Bormashenko, 2016). When the weight of the UAV, density of water, and the acceleration due to gravity was determined, the minimum volume of floatation attachment required to keep the UAV above water could be estimated. The total takeoff weight of the UAV was 6.4 kg which created 63N of downward force. Therefore, using Equation 1, minimum total submerged volume of the floatation attachment was calculated as 0.0064 m^3. The floatation attachments were cut out of 7 cm diameter and 30 cm long foam sections and placed under each motor vertically away from the center base of the UAV. Remaining floatation attachments were cut out of 7 cm diameter and 20 cm long foams and placed under each arm where they are connected to the center base of the UAV. Placement of floatation attachment had to be far enough away from the center to keep the UAV horizontally stable on water surface. Vertical placement of the floatation attachment was intended to

minimize drag, provide free downward airflow to maximize the lifting force created by the propellers, and provide an open space under the UAV to position the WSC and sensor node at the bottom center.

Study site and data collection procedure

Field tests were conducted at the LaMaster agricultural pond at Clemson University, Clemson SC. Total surface area of the pond was 1.1 ha. The pond is wider near the experiment site and narrower from the center towards the far end. Because the UAV system did not have enough endurance capacity and for safety precautions, the narrow area of the pond was avoided during sample and data collection. The launch location marked with "H", the sampling locations marked with yellow dots, and the autonomous flight trajectory of the UAV marked with dotted and straight lines are shown in Figure 3.5.

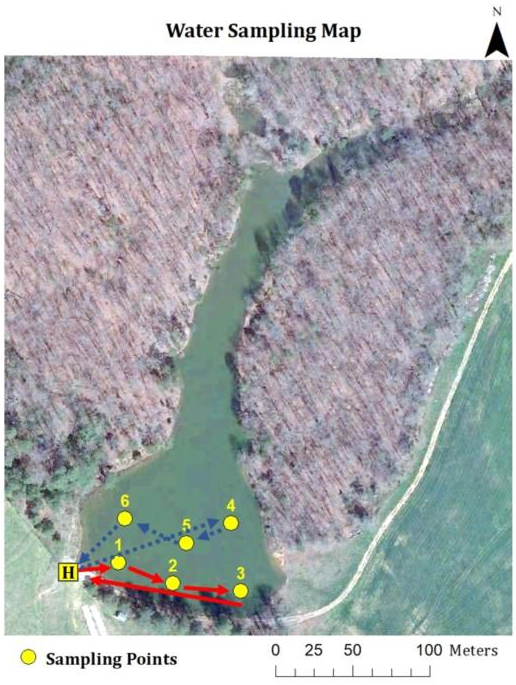

Figure 3.5 Water sampling locations and autonomous flight trajectory in LaMaster Pond.

There were six sampling locations chosen for field experiments. A single autonomous flight mission was limited to collect water samples and make in situ measurements from three locations at a time. This limitation on number of locations was due to the number of cartridges on the mechanism. The solid red lines and the dotted blue lines represent individual autonomous flight trajectories. Water sample collections and in situ measurements were made from 0.5 m and 3.0 m depths at each location by using the same flight trajectory. Four autonomous mission flights were conducted to accomplish designated sampling tasks from these locations. Two of the autonomous flights were made for water sampling at the depth of 0.5 m and the other two were made at the depth of 3 m. Sampling depth adjustment was made by changing the position of a float section mounted on the extension cables. The float section stayed at the water surface while the sensor node and WSC submerged to desired depths. Continuous 12 measurements were made and recorded at each sampling location. Data were stored on the SD card for analysis. Quantitative analyses of measurements were made with paired *t*-test to evaluate statistical differences in DO, EC, pH, and temperature.

Results

UAV flight characteristics of endurance and thrust were evaluated to confirm capability of carrying the payload for a given time to accomplish an autonomous water sampling and measurement mission. Battery capacity was the limiting factor for available flight time, therefore lab tests were conducted prior to field experiments. Lab test results confirmed the UAV was capable of carrying the necessary experimental payload. In situ measurement and water collection trials were made with field experiments. Autonomous activation of sensor node and WSC for in situ measurements and water collection was successful. Autonomous water sampling experiments required auto landing and takeoff from water surface. The floatation attachment had

to keep the UAV above water surface while allowing easy landing and takeoff. The number of successful water collection attempts were recorded to provide information about WSC.

Thrust measurements indicated the UAV could produce 64 N of upward force with 4.3 kg of operating empty weight, which does not include anticipated payload. This result was achieved when 8,000 mAh battery was used. The downward force acting on the UAV due to weight was 42 N. The UAV produced 106 N of thrust for takeoff and pull up the sensor node and sampling cartridges at the sampling locations. The thrust-to-weight ratio of the UAV was 2.5 (Figure 3.6). Because power output of the motors and available thrust are not linear, a 20% safety factor for thrust-to-weight ratio was considered. The thrust-to-weight ratio was greater than minimum thrust-to-weight requirement of 2.2 that included the safety factor. Lab tests for endurance and thrust measurements showed that the UAV was capable of carrying the payload and had 10 min of endurance. The endurance of the UAV was 12 min and the thrust-to-weight ratio was 2.3 when the 10,000 mAh battery was used. The battery with higher capacity provided longer endurance but the thrust-to-weight ratio was correspondingly lower. The difference in thrust-to-weight ratio was due to the additional weight of 0.5 kg that the larger battery added on the UAV. In order to provide safe flights for water sampling experiments, battery with 8,000 mAh capacity was chosen.

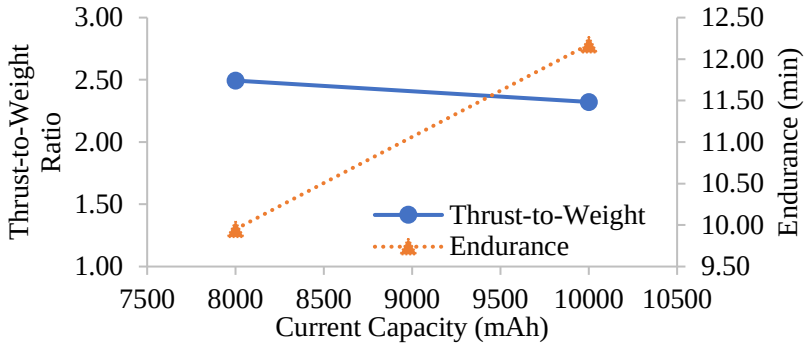

Figure 3.6 Thrust-to-weight ratio and endurance of the UAV with 8,000 mAh and 10,000 mAh batteries.

Tests with payload and the 8,000 mAh battery showed that endurance was shorter than the tests conducted without payload (Figure 3.7). The UAV produced more thrust by pulling greater current from the battery to compensate for the 2.1 kg payload. This compensation was the reason for shorter endurance. The UAV produced 127 N of thrust and the endurance was 8.7 min. When the throttle setting was increased to 60%, the thrust and endurance were measured as 129 N and 7.7 min. The thrust and endurance measurements at 70% throttle were 139 N and 7.3 min. The thrust was higher at 70% throttle as endurance was the lowest. These results indicate that if the flight conditions change with the wind speed fluctuation or gusts, endurance will be reduced, because the UAV consumes more battery power to increase the thrust to overcome the wind. The endurance in field experiments would be lower than the field tests. Therefore, the duration of water sampling missions and UAV travel distance can be planned in a way that the UAV system can travel to the sampling locations and return the launch location safely.

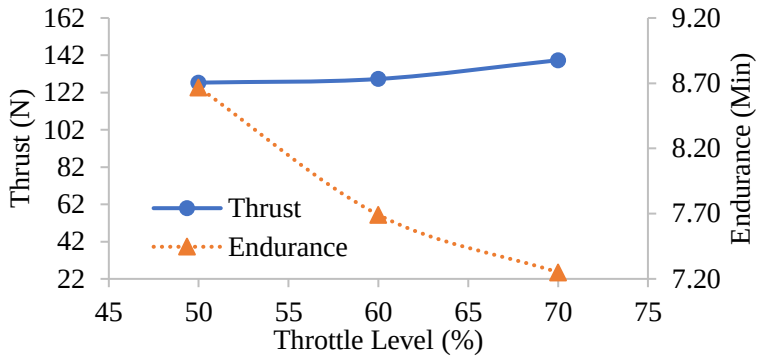

Figure 3.7 Thrust and endurance measurements of the UAV with 8,000 mAh battery at 50%, 60%, and 70% throttle settings.

Autonomous in situ measurements and water sampling flights were successfully achieved without remote pilot intervention. Mission flight commands such as takeoff, navigate, land, activate the sensor node, and activate the WSC were performed without error. At each sampling point, the UAV landed on water, waited for 60 seconds, conducted the in situ measurements, collected 130 ml of water sample, and lifted off to navigate autonomously to the next waypoint on the flight path. In situ water quality measurements made at the same depths in different locations showed similar trend (Figure 3.8). At 0.5 m depth, measured values ranged between 8 mg/L and 10 mg/L for DO, 31 °C and 33 °C for temperature, 52 µS/cm and 60 µS/cm for EC, 5.5 and 5.6 for pH . At 3 m depth, measured values ranged between 4 mg/L and 7 mg/L for DO, 22 °C and 27 °C for temperature, 50 µS/cm and 88 µS/cm for EC, 5.3 and 5.5 for pH .

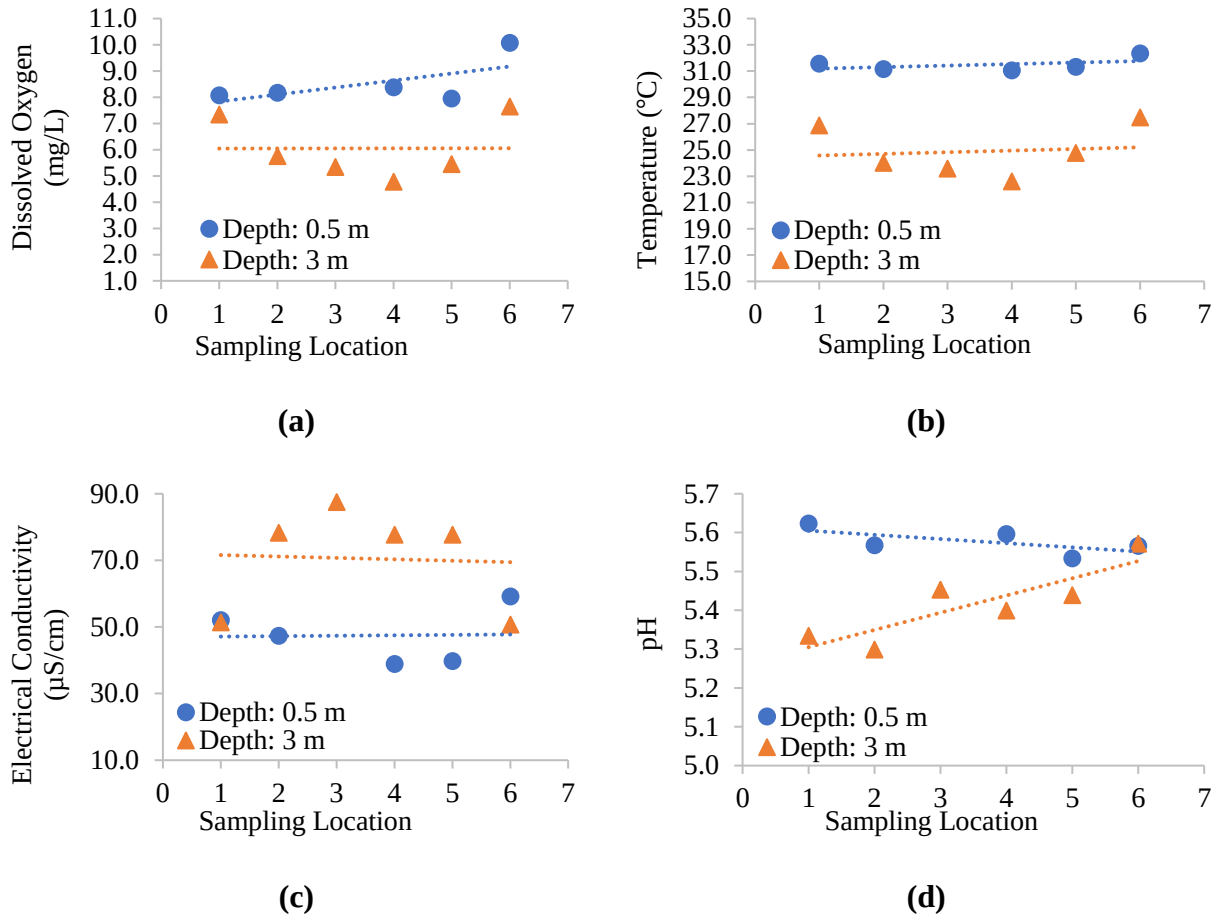

Figure 3.8 UAV-assisted in situ measurements of noncontaminant water quality indicators at 0.5 m and 3 m depths in six sampling locations; **(a)** dissolved oxygen, **(b)** temperature, **(c)** electrical conductivity, and **(d)** pH.

The measurements of DO, temperature, and pH were higher at the depth of 0.5 m than the depth of 3 m. EC measurements were higher at the depth of 3 m than the depth of 0.5 m while the measurements at the sampling locations 1 and 6 showed opposite trend. The reason for variations at sampling locations of 1 and 6 were due to the actual depth of the sensor node in the water. The water depth at the sampling location 1 was measured as 2.1 m. This indicates that the sensor node did not reach the sampling depth of 3 m and submerged all the way to the bottom of the water at the sampling location 1. At sampling location 6, the sensor node did not fully deploy

due to the presence of submerged aquatic vegetation. Therefore, the measurements at the sampling locations 1 and 6 do not represent depth-specific conditions. The average of sampling locations 2, 3, 4, and 5 were calculated and they represent depth specific conditions. Average measurements of EC, pH, DO, and temperature at the depth of 0.5 m were 60 µS/cm, 5.5, 8.1 mg/L, and 30 °C while the measurements at the depth of 3 m were 108 µS/cm, 5.3, 5.34 mg/L, and 20 °C respectively.

Data collected from locations 1 and 6 were not depth specific, while data from location 3 at 0.5 m was not acquired due to operator error. As a result, only data from locations 2, 4, and 5 were used in paired *t*-test analysis. At these locations, 12 continuous measurements were made with the sensor node, providing 48 data points at the depth of 0.5 m, and 48 data points at the depth of 3 m. In the paired *t*-test, it was hypothesized that the differences in the DO, EC, pH, and temperature measurements made at the depths of 0.5 m and 3 m would be statistically different at an alpha level of 0.05.

Paired *t*-test analysis indicated there was no significant difference between the pH measurements that were made at the depths of 0.5 m and 3 m ($t(2) = -3.56$, $p = 0.0705$). The pH in water column did not change with depth. However, results indicated there were significant differences between the DO, EC, and temperature measurements made at the depths of 0.5 m and 3 m. DO measurements at 3 m depth were 21% lower than DO measurements at 0.5 m ($t(2) = -7.46$, $p = 0.0175$). Mean difference between EC measurements at 0.5 m and 3 m were the highest at 29.9% ($t(2) = 14.33$, $p = 0.0048$). Temperature measurements were significantly lower at 3 m than temperature at 0.5 m ($t(2) = -13.30$, $p = 0.0056$).

Table 3.2 Descriptive statistics of water quality parameters obtained by UASS at 0.5 m and 3 m.

Quality Parameters	Depth at 0.5 m			Depth at 3 m			Difference (%)	*t* Value (DF)	*p* Value
	N	Mean	SD	N	Mean	SD			
DO (mg/L)	48	8.17	0.21	48	5.33	0.50	21	-7.46 (2)	0.0175***
pH	48	5.57	0.03	48	5.38	0.07	1.7	-3.56 (2)	0.0705
EC (µS/cm)	48	42.01	4.66	48	77.87	0.33	29.9	14.33 (2)	0.0048***
Temperature (◦C)	48	31.18	0.14	48	23.80	1.1	13.4	-13.30 (2)	0.0056***

Notes: N: Number, SD: Standard deviation, DF: Degrees of freedom, Significance level*** = $p < 0.001$

The WSC was activated during mission flights and 130 ml of water samples at each cartridge were successfully stored in the cartridges until the UAV returned to the launch location. The number of successful activation and collection trials were recorded as successful sampling, and the number of failed attempts were recorded as unsuccessful sampling. Sampling events with WSC at each trial were recorded as successful. Therefore, the success rate of the WSC was 100%. Landing and takeoff from water surface with the mounted floatation attachments was successful. Autonomous navigation of the UAV during landing and takeoff from water surface was swift and did not pose any challenges. Anecdotally, autonomous control of the system appeared to be more stable than manual control with a radio controller for both navigating to the sampling points and takeoff/landing from water surface.

Conclusion

The objective of integrating a sensor node for the measurement of noncontaminant water quality indicators and a water sampler was successfully achieved. A unique triple cartridge water collection mechanism and a sensor node were designed and integrated with a multirotor UAV. Field tests demonstrated the system was able to navigate autonomously to predefined locations and perform measurement and water collection tasks instantaneously. While the number of sampling locations was limited to three per mission flight due to the number of cartridges on the

sampling mechanism, the system was capable of navigating to all the six locations with one autonomous flight. The sizing of floatation attachment allowed the system to land and takeoff from the water surface successfully. The thrust-to-weight ratio of the UAV was 2.5 and it was within safe operation limits.

In situ noncontaminant water quality indicators measured with the system were dissolved oxygen, pH, electrical conductivity and temperature. As deployed, the system provided rapid water sampling and in situ measurement capability that facilitated analysis at two depths of 0.5 meter and 3 meter. Differences in measured parameter values by depth was visible, but further data collection and field experimentation is required for better assessment. A sensor that could measure the depth of the sensor node could be integrated with the system to measure the actual depth of the pond at each sampling location.

Instantaneous water sample collection and in situ measurements allowed acquiring water quality information in the exact space/time in a water body while providing discreet samples for lab analysis. Precise timing and accuracy would provide better data comparison between in situ measurements and lab analysis results from collected samples. The water sampling mechanism consisted of three cartridges, which enabled triple sample collection at the same point or one sample collection at three different points in water. Using a waterproof servo proved to be a better design upgrade for the water sampling approach. Integration of sensor node and WSC with the flight controller enabled fully autonomous UAV-assisted water quality evaluation. Battery selection was important due to its effect on thrust-to-weight ratio of the UAV. The instantaneous activation capability of the sensor node and WSC could be utilized with a computer program for adaptive water sampling. The adaptive water sampling then could be achieved by measuring the

noncontaminant water quality indicators and matching the measurements with the allowable water quality limits.

References

Anderson, C. W. (2005). *Chapter A6. Section 6.7. Turbidity* (09-A6.7). Retrieved from http://pubs.er.usgs.gov/publication/twri09A6.7

Bormashenko, E. (2016). Surface tension supported floating of heavy objects: Why elongated bodies float better? *Journal of Colloid and Interface Science, 463*, 8-12. doi:https://doi.org/10.1016/j.jcis.2015.10.031

Bravo-Mosquera, P. D., Botero-Bolivar, L., Acevedo-Giraldo, D., & Cerón-Muñoz, H. D. (2017). Aerodynamic design analysis of a UAV for superficial research of volcanic environments. *Aerospace Science and Technology, 70*, 600-614. doi:https://doi.org/10.1016/j.ast.2017.09.005

Chung, W.-Y., & Yoo, J.-H. (2015). Remote water quality monitoring in wide area. *Sensors and Actuators B: Chemical, 217*, 51-57. doi:http://dx.doi.org/10.1016/j.snb.2015.01.072

Eichhorn, M., Ament, C., Jacobi, M., Pfuetzenreuter, T., Karimanzira, D., Bley, K., . . . Wehde, H. (2018). Modular AUV System with Integrated Real-Time Water Quality Analysis. *Sensors, 18*(6), 1837.

Esakki, B., Ganesan, S., Mathiyazhagan, S., Ramasubramanian, K., Gnanasekaran, B., Son, B., . . . Choi, J. S. (2018). Design of Amphibious Vehicle for Unmanned Mission in Water Quality Monitoring Using Internet of Things. *Sensors, 18*(10), 3318.

Garg, V., Senthil Kumar, A., Aggarwal, S. P., Kumar, V., Dhote, P. R., Thakur, P. K., . . . Rastogi, G. (2017). Spectral similarity approach for mapping turbidity of an inland waterbody. *Journal of Hydrology, 550*, 527-537. doi:https://doi.org/10.1016/j.jhydrol.2017.05.039

Glasgow, H. B., Burkholder, J. M., Reed, R. E., Lewitus, A. J., & Kleinman, J. E. (2004). Real-time remote monitoring of water quality: a review of current applications, and advancements in sensor, telemetry, and computing technologies. *Journal of Experimental Marine Biology and Ecology, 300*(1), 409-448. doi:https://doi.org/10.1016/j.jembe.2004.02.022

Higgins, J., & Detweiler, C. (2016, 9-14 Oct. 2016). *The waterbug sub-surface sampler: Design, control and analysis.* Paper presented at the 2016 IEEE/RSJ International Conference on Intelligent Robots and Systems (IROS).

Kaizu, Y., Iio, M., Yamada, H., & Noguchi, N. (2011). Development of unmanned airboat for water-quality mapping. *Biosystems Engineering, 109*(4), 338-347. doi:https://doi.org/10.1016/j.biosystemseng.2011.04.013

Khalid, S. D. R., Hamzah, Z., & Saat, A. (2009). *In-Situ Measurement of Selected Water Quality Parameters in Ringlet's Lake, Cameron Highlands*.

Kim, S. E., Seo, I. W., & Choi, S. Y. (2017). Assessment of water quality variation of a monitoring network using exploratory factor analysis and empirical orthogonal function. *Environmental Modelling & Software, 94*(Supplement C), 21-35. doi:https://doi.org/10.1016/j.envsoft.2017.03.035

Koparan, C., Koc, A. B., Privette, C., & Sawyer, C. (2018b). In Situ Water Quality Measurements Using an Unmanned Aerial Vehicle (UAV) System. *Water, 10*(3), 264.

Koparan, C., Koc, A. B., Privette, C., Sawyer, C., & Sharp, J. (2018a). Evaluation of a UAV-Assisted Autonomous Water Sampling. *Water, 10*(5), 655.

Lewitus, A. J., Schmidt, L. B., Mason, L. J., Kempton, J. W., Wilde, S. B., Wolny, J. L., . . . Ringwood, A. H. (2003). Harmful Algal Blooms in South Carolina Residential and Golf

Course Ponds. *Population and Environment, 24*(5), 387-413. doi:10.1023/a:1023642908116

Li, D., & Liu, S. (2019a). Chapter 7 - Detection of River Water Quality. In D. Li & S. Liu (Eds.), *Water Quality Monitoring and Management* (pp. 211-220): Academic Press.

Li, D., & Liu, S. (2019b). Chapter 8 - Water Quality Detection for Lakes. In D. Li & S. Liu (Eds.), *Water Quality Monitoring and Management* (pp. 221-231): Academic Press.

Liu, Y., Noguchi, N., & Yusa, T. (2014). Development of an Unmanned Surface Vehicle Platform for Autonomous Navigation in Paddy Field. *IFAC Proceedings Volumes, 47*(3), 11553-11558. doi:https://doi.org/10.3182/20140824-6-ZA-1003.00616

Mayer, C. C., & Ali, K. A. (2017). Field Spectroscopy as a Tool for Enhancing Water Quality Monitoring in the ACE Basin, SC. *Journal of South Carolina Water Resources, 4*(1). doi:https://tigerprints.clemson.edu/jscwr/vol4/iss1/5

Null, S. E., Mouzon, N. R., & Elmore, L. R. (2017). Dissolved oxygen, stream temperature, and fish habitat response to environmental water purchases. *Journal of Environmental Management, 197*, 559-570. doi:https://doi.org/10.1016/j.jenvman.2017.04.016

Ore, J.-P., & Detweiler, C. (2018). *Sensing water properties at precise depths from the air.* Paper presented at the Field and Service Robotics.

Ore, J.-P., Elbaum, S., Burgin, A., & Detweiler, C. (2015). Autonomous Aerial Water Sampling. *Journal of Field Robotics, 32*(8), 1095-1113. doi:10.1002/rob.21591

Panagiotou, P., Fotiadis-Karras, S., & Yakinthos, K. (2018). Conceptual design of a Blended Wing Body MALE UAV. *Aerospace Science and Technology, 73*, 32-47. doi:https://doi.org/10.1016/j.ast.2017.11.032

Pearse, J. (1984). Phytoplankton-nutrient relationships in South Carolina reservoirs: Implications for management strategies. *Lake and Reservoir Management, 1*(1), 193-197.

Schaeffer, B. A., Schaeffer, K. G., Keith, D., Lunetta, R. S., Conmy, R., & Gould, R. W. (2013). Barriers to adopting satellite remote sensing for water quality management. *International Journal of Remote Sensing, 34*(21), 7534-7544. doi:10.1080/01431161.2013.823524

Shoda, M. E., Sprague, L. A., Murphy, J. C., & Riskin, M. L. (2019). Water-quality trends in U.S. rivers, 2002 to 2012: Relations to levels of concern. *Science of The Total Environment, 650*, 2314-2324. doi:https://doi.org/10.1016/j.scitotenv.2018.09.377

Stauber, C., Miller, C., Cantrell, B., & Kroell, K. (2014). Evaluation of the compartment bag test for the detection of Escherichia coli in water. *Journal of Microbiological Methods, 99*(Supplement C), 66-70. doi:https://doi.org/10.1016/j.mimet.2014.02.008

Tai, H., Li, D., Wei, Y., Ma, D., & Ding, Q. (2011). *A Simple Temperature Compensation Method for Turbidity Sensor*, Berlin, Heidelberg.

Tyler, A. N., Hunter, P. D., Carvalho, L., Codd, G. A., Elliott, J. A., Ferguson, C. A., . . . Scott, E. M. (2009). Strategies for monitoring and managing mass populations of toxic cyanobacteria in recreational waters: a multi-interdisciplinary approach. *Environmental Health, 8*(1), S11. doi:10.1186/1476-069x-8-s1-s11

Winkelbauer, A., Fuiko, R., Krampe, J., & Winkler, S. (2014). Crucial elements and technical implementation of intelligent monitoring networks. *Water Science and Technology, 70*(12), 1926-1933. doi:10.2166/wst.2014.415

Xu, Z., & Boyd, C. E. (2016). Reducing the monitoring parameters of fish pond water quality. *Aquaculture, 465*, 359-366. doi:https://doi.org/10.1016/j.aquaculture.2016.09.031

Yang, K., Yu, Z., Luo, Y., Yang, Y., Zhao, L., & Zhou, X. (2018). Spatial and temporal variations in the relationship between lake water surface temperatures and water quality - A case study of Dianchi Lake. *Science of The Total Environment, 624,* 859-871. doi:https://doi.org/10.1016/j.scitotenv.2017.12.119

CHAPTER FOUR

ADAPTIVE WATER SAMPLING WITH AN AERIAL ROBOT

Abstract

Water quality monitoring and predicting the changes in water characteristics require the collection of water samples in a timely manner. Water sample collection based on in situ measurable water quality indicators can increase the efficiency and precision of data collection while reducing the cost of laboratory analyses. The objective of this research was to develop an adaptive water sampling device for an aerial robot and demonstrate the accuracy of its functions in laboratory and field conditions. The prototype device consisted of a sensor node with dissolved oxygen, pH, electrical conductivity, temperature, turbidity, and depth sensors, a microcontroller, and a sampler with three cartridges. Activation of water capturing cartridges was based on in situ measurements from the sensor node. The activation mechanism of the prototype device was tested with standard solutions in the laboratory and with autonomous water sampling flights over the 11 ha section of a lake. A total of 7 sampling locations were selected based on a grid system. Each cartridge collected 130 mL of water samples at a 3.5 m depth. Mean water quality parameters were measured as 8.47 mg/L of dissolved oxygen, 5.34 of pH, 7 µS/cm of electrical conductivity, 18 °C of temperature, and 37 FNU of turbidity. The dissolved oxygen was within allowable limits that were pre-set in the self-activation computer program while the pH, electrical conductivity, and temperature were outside of allowable limits that were specified by Environmental Protection Agency (EPA). Therefore, the activation mechanism of the device was triggered, and water samples were collected from all the sampling locations

successfully. The adaptive water sampling with a UAV-assisted water sampling device was proved to be a successful method for water quality evaluation.

Introduction

Monitoring water quality is important to determine the impact of contaminants from agriculture, stormwater, wastewater, and residential houses. According to The United Nations World Water Development Report, 80% of wastewater in the world is released to the rivers, lakes, and oceans without adequate treatment (World Water Assesment Programme, 2017). More than 3.4 million people die from water-related diseases every year (Berman, 2009). Polio, malaria, cholera, and diarrhea are some of the major waterborne diseases responsible for causing health threats (Hawthorne, 2018). World Health Organization (WHO) issues guidelines for water quality to ensure the safety of drinking water to protect public health in developed and developing countries (2018). United States Centers for Disease Control and Prevention (CDC) reports that 780 million people do not have access to clean water sources worldwide (2016).

Determining the impacts of climate change and environmental pollution on ecologically sensitive, large, and remote waterbodies is difficult because of the complex dynamics of water quality monitoring, high costs, and extensive analyses of diverse data sets (Li & Liu, 2019b; Pearse, 1984; Shoda, Sprague, Murphy, & Riskin, 2019; Stauber, Miller, Cantrell, & Kroell, 2014; Yang et al., 2018). Therefore, innovative approaches for water quality monitoring are necessary to enhance water quality evaluation and to prevent waterborne diseases and deaths.

Water quality monitoring involves analyses and evaluation of water properties in freshwater sources to ensure that the water source provides safe water for drinking, irrigation, and livestock production. Quantitative and qualitative assessment of water quality parameters include dissolved oxygen (DO), pH, electrical conductivity (EC), salinity, temperature, turbidity,

water depth, algal chlorophyll content, total phosphorus, nitrogen, and suspended solids (Zhang, Thomas, & Mitsch, 2017; Zhuang et al., 2016). Low concentration of DO, temperature, salinity and pH in addition to increased levels of nitrogen, total phosphorus, turbidity and algal chlorophyll indicate poor water quality which affect the rate of biological and chemical activities in water (Chung & Yoo, 2015; Thomas, Hurst, Matthiessen, Sheahan, & Williams, 2001; Xu et al., 2016). In situ or on site measurements of these parameters can be used for the rapid evaluation of water quality. If the measured parameters are not within the allowed limits, water samples can be collected for further laboratory analysis.

Water sample collection from lakes and ponds are often based on manual sampling from shore or with a boat mostly by volunteers (Peters, Zhan, Schwartz, Godoy, & Ballard, 2017). Manual water sampling from difficult to access lakes, retired mining zones, or water bodies that are surrounded by steep and difficult terrain may be dangerous. In addition, lakes with cyanobacteria blooms increases health risks to humans during water sampling (Lewitus et al., 2003).

Water quality monitoring stations and wireless sensor networks are installed in water bodies to monitor water quality (Chung & Yoo, 2015). These stations continuously assess water quality by making in situ measurements over a long period (Winkelbauer, Fuiko, Krampe, & Winkler, 2014; Winkler, Zessner, Saracevic, & Fleischmann, 2008). The continuously measured water quality parameters are transmitted to a monitoring center or a web server to enable data storage and online access (Adu-Manu, Tapparello, Heinzelman, Katsriku, & Abdulai, 2017). However, water quality stations may provide unreliable data due to continuously used sensors requiring regular maintenance (Bin Omar & Bin MatJafri, 2009; Pule, Yahya, & Chuma, 2017). Because the sensor stations are at fixed locations, they provide water quality data with relatively

low spatial resolutions. All of these methods are time-consuming, spatially limited, costly, or difficult to deploy at multiple locations. In addition to fixed water quality monitoring stations and networks, remotely controlled watercrafts that can either operate on the water surface or underwater have been developed (Dunbabin & Grinham, 2010; Eichhorn et al., 2018; Kaizu, Iio, Yamada, & Noguchi, 2011; Kozyra et al., 2017; Liu, Noguchi, & Yusa, 2014; Melo, Mota, Albuquerque, & Alexandria, 2019; Valada et al., 2014). These watercrafts are controlled either manually by a remote controller or with integrated autonomous guidance systems. The water quality maps are created with spatially interpolated water quality data for visualization (Nagchaudhuri et al., 2016).

Recent studies investigated the use of remote sensing on water quality monitoring (Becker et al., 2019; Friedrichs, Busch, Van der Woerd, & Zielinski, 2017; Leeuw, Boss, & Wright, 2013; Mayer & Ali, 2017; Zeng, Richardson, & King, 2017). Among remote sensing platforms, Unmanned Aerial Vehicles (UAV) are being investigated in use of disaster relief operations, topo-bathymetric monitoring, and algal bloom monitoring of the surface waters (Erena, Atenza, García-Galiano, Domínguez, & Bernabé, 2019; Kislik, Dronova, & Kelly, 2018; Rabta, Wankmüller, & Reiner, 2018). Remote sensing can detect important visual changes in the environment but detecting pollutions and change in water quality parameters might be challenging (Anweiler & Piwowarski, 2017; Erena et al., 2019; Schaeffer et al., 2013). In addition to remote sensing, in situ water quality measurement with UAV integrated sensor systems was tested for water quality monitoring (Esakki et al., 2018; Koparan, Koc, Privette, & Sawyer, 2018; Ore & Detweiler, 2018a; Rodrigues et al., 2015). However, monitoring surface water environments require physical water samples that are taken at specific depths for intended water quality analysis (Ore & Detweiler, 2018b; Saiki et al., 2019). The physical water samples

are required for accuracy evaluation of water quality predictions that were driven based on remote sensing (Schaeffer et al., 2013).

UAVs provide unique opportunities for remote water sample collection from surface waters. UAVs can remotely access to a waterbody for physical water sample collection to better understand the distribution and extent of contaminants (Becker et al., 2019; Dörnhöfer & Oppelt, 2016; Koparan, Koc, Privette, Sawyer, & Sharp, 2018). The UAV-mounted water samplers can be submerged to a specific depth with additional subsystems to analyze depth-specific water quality parameters (Higgins & Detweiler, 2016). An example application of a UAV-mounted water sampler is the sample collection from mines and pit lakes, and isolated multiple waterbodies (Banerjee, Raval, Maslin, & Timms, 2018; Castendyk et al.; Ore, Elbaum, Burgin, & Detweiler, 2015). Using a UAV for water sampling is generally limited by the payload and endurance capacity to carry water samples from desired locations to the shore (Lally, O'Connor, Jensen, & Graham, 2019). In addition, these systems were designed to collect water samples from a waterbody without making in situ measurements of water quality parameters. Unnecessary water sampling could be eliminated to reduce water sample analysis costs by using an adaptive water sampler that measures the major water quality parameters before sample collection (Ankor, Tyler, & Hughes, 2019; Glasgow, Burkholder, Reed, Lewitus, & Kleinman, 2004; Py et al., 2007). The adaptive water samplers continuously monitor changes in water quality parameters and capture water samples when the conditions were satisfied (Kellner, Ettenauer, Zuser, Posnicek, & Brandl, 2016). The decision to collect water samples can be based on the allowable limits of water quality parameters or the limits of selected water quality parameters of interest (Li & Liu, 2019c). Current adaptive water sampling systems are not compatible with UAV systems with limited payload and endurance capacity. Therefore, there is

a need for a light-weight, robust, and UAV compatible adaptive water sampling systems. In order to address above challenges and to contribute to the current research, two separate in situ water quality measurement (Koparan, Koc, Privette, & Sawyer, 2018) and water sampling systems (Koparan, Koc, Privette, Sawyer, et al., 2018) were integrated with a single UAV and tested in a 1.1 ha agricultural pond (Koparan, Koc, Privette, & Sawyer, 2019).

The objective of this research was to develop, test, and integrate a UAV compatible adaptive water sampling system for water quality evaluation of surface waters. The developed adaptive water sampling system reported in Koparan et al. (2019) was further improved by integrating turbidity and depth sensors while including self-activation in a mission flight.

Materials and methods

UAV and sensor components for adaptive water sampling

A custom-designed UAV was used for adaptive water sampling experiments (Koparan et al., 2019). Details regarding the payload capacity, endurance, and the autonomous water sampling performance of UAV were previously reported in (Koparan et al., 2019). The adaptive water sampling approach utilizes water sampling cartridges and sensor array called the Water Sampling Device (WSD). The sensor node measurements were used for self-activation of the cartridges to collect water samples. The adaptive water sampling approach was intended to collect water samples when the measurements exceed allowable water quality limits, as well as record the in situ measurements for on site rapid water quality evaluation. A turbidity sensor and pressure sensor were integrated with the sensor node on WSD (Appendix D).

Turbidity sensor integration with the sensor node and accuracy assessment

The turbidity sensor was an attenuation type sensor that measures the loss of light between a light source and a detector that are placed at 180 degree. (DFRobot, Pudong,

Shanghai, China). The turbidity sensor detects suspended particles in water by measuring the light transmittance and scattering rate which varies depending on the concentration of total suspended solids (TSS) (Bin Omar & Bin MatJafri, 2009). Because these sensors work on the attenuation light principle, ambient light may affect the turbidity measurements (Li & Liu, 2019a). Turbidity units can be reported as Formazin Nephelometric Units (FNU), Nephelometric Turbidity Unit (NTU), or Formazin Attenuation Unit (FAU). While these units may vary based on the instruments used, they have no standardized value and they are qualitative measurements (Lawler, 2016). The turbidity measurements that were made with light attenuation based turbidity sensors are not considered valid for explaining the actual turbidity levels in waters by most agencies. However, attenuation type sensors can be utilized to evaluate water clarity and monitor change in turbidity over time in surface waters (Li & Liu, 2019a). Turbid water does not necessarily indicate an issue related to water quality but a change in turbidity may indicate the development of algal blooms or a change in suspended sediments in a lake.

A case was designed and 3D printed for the turbidity sensor in order to minimize ambient light interference. This case included two chambers and water passage channels that allowed water entry to where the sensor could measure turbidity while blocking the ambient light (Figure 4.1). An accuracy assessment was made in lab conditions to evaluate if the sensor provided reliable turbidity measurements when the sensor was housed in the case.

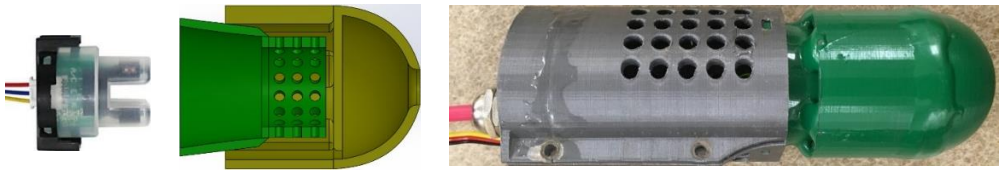

(a) **(b)** **(c)**

Figure 4.1 (a) Turbidity sensor, **(b)** cut-away view of the case design, and **(c)** 3D printed final assembly of the probe case for DO, pH, EC, temperature, and turbidity probes.

Calibration and accuracy assessments of the turbidity sensor was made using a formazin standard solutions at 25 °C (Lawler, 2016). The standard solutions had 62.5, 250, 1000, and 2000 FNU. These solutions were chosen for calibration because they mimic the typical minimum and maximum turbidity levels in lakes (Li & Liu, 2019c). First, the sensor voltage values (0-5 V) were mapped to FNU turbidity levels in order to determine sensor's response to a turbid solution. Second, a calibration equation was developed between the known turbidity and voltage response from the sensor measurements. Finally, the developed calibration equation was used in the microcontroller program to determine the turbidity of water samples.

The turbidity sensor measurements were correlated with standard turbidity solutions to determine the measurement accuracy. Thirty continuous measurements were made in each standard turbidity solution and the data was retrieved from Arduino Integrated Development Environment (IDE). The average of the repeated 30 measurements were recorded as single trial. There were 24 trials in total because 6 repeated random turbidity measurements were made in the same standard solution to minimize operator errors. Last, the random measurements were compared with the standard turbidity values. Paired-t test analysis was conducted to determine if there is a significant difference between the turbidity sensor measurements and the standard solutions using the 0.05 level of significance.

Depth sensor integration with the sensor node and accuracy assessment

A previous work with the sensor node revealed the need for depth specific in-situ water quality parameters (Koparan et al., 2019). A pressure sensor integration with the sensor node was made to provide accurate water quality parameter measurement at a specific water depth. The pressure sensor measures the water pressure and the microcontroller converts it into depth measurements. The conversion is made based on the principle that the water pressure increases by 1 atm with each 10 m of depth. The maximum measurement range of the pressure sensor was 10 m with a water depth resolution of 0.16 mm (Bar02, Blue Robotics, Torrance, CA, USA).

The pressure sensor and voltage converter circuit were placed in a 3D printed case and sealed with epoxy and painted for waterproofing (Figure 4.2). The pressure sensor was integrated with a microcontroller unit (Arduino, Atmel ATmega328P, San Jose, CA, USA). The microcontroller platform was placed on top of the UAV in a water-sealed box and the pressure sensor was suspended with a 3.5 m long tether.

(a) **(b)** **(c)**

Figure 4.2 The pressure sensor components; **(a)** pressure sensor and voltage converter, **(b)** perspective view of waterproof case in SolidWorks, and **(c)** 3D printed and sealed pressure sensor.

Accuracy assessment of depth sensor was made using a 2 m tall clear tube filled with tap water. The depth sensor was lowered to random depths in the tube and depth measurements of the sensor were compared with the manual depth measurements. A correlation equation was developed from 19 depth measurements from the depth sensor and the actual depth. The pressure sensor was integrated with the sensor node as shown in Figure 4.3.

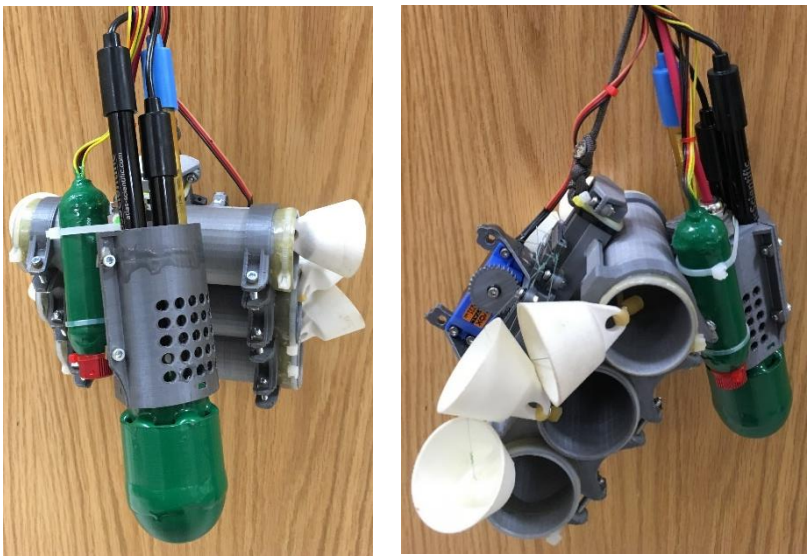

(a) **(b)**

Figure 4.3 Water Sampling Device (WSD) and its components; **(a)** front view with pressure sensor, turbidity sensor, and probes, **(b)** side view with open cartridges and servo mechanism.

Evaluation of sensor node stabilization time

Sensors on the node required certain equilibrium time when placed in water for accurate measurements. The equilibrium time is critical for the autonomous adaptive water sampling, because this timeframe determined how long the UAV stayed at each sampling location. Equilibrium time directly affected the battery usage of the UAV. The mission plan and self-activation program depended on equilibrium time information for decision making. Equilibrium

time evaluation of DO, pH, EC, temperature and turbidity were made in 500 mL of tap water at room temperature (21 °C). The sensor node was fully submerged in the sample water. Commercially available multi parameter sensors (Sension 156 and HQ10, Hach, Loveland, CO, USA) were used along with the sensor node to determine how long it took for sensor node to reach equilibrium. Sensor calibrations for both sensor node and the commercial sensors were made according to the manufacturers' specifications. Three repeated measurements were made with the commercial sensor to determine actual water quality parameters as reference measurements. Turbidity reference measurement was made with a turbidimeter (2100AN, Hach, Loveland, CO, USA). Continuous measurements were made with the sensor node for 5 min at 4 s intervals. The measurement intervals of 4 s was necessary in order to acquire measurements from all the sensors as specified by the manufacturers' specifications. The equilibrium time of each sensor was recorded and examined.

Water Sampling Device self-activation and test procedure

The activation of the WSD was made based on the sensor node measurements. The decision for self-activation of WSD was made by the Micro Controller Unit (MCU) when the allowable limits of noncontaminant water quality indicators exceeded the limits (Appendix E and F). The allowable limits of selected water quality parameters were 6-12 mg/L for DO, 6.5-9.5 for pH, 100-2000 for EC, and 20-35 °C for temperature for lakes (Bhatnagar & Devi, 2013; Kumar & Puri, 2012; Stone & Thomforde). These allowable limits were introduced in the self-activation computer program and the WSD was set to initiate water collection when the sensor node measurements exceeded the programmed limits. Indoor measurements in the lab and outdoor

experiments at the experiment site were conducted to test the performance of the self-activation mechanism of the WSD.

The indoor experiments were conducted for self-activation tests by placing the measurement probes in reference solutions and observing if the WSD was activated by the MCU or not. The probes for each sensor were randomly placed in individual reference solutions. These solutions ranged from below allowable limits to above allowable limits for each parameter to create different test conditions. Self-activation was tested at each solution and the WSD was reset after each trial. The probes were placed in tap water while one of the probes were placed in a standard solution during the trials. This provided within-the-limit measurements from other sensors to ensure that self-activation was achieved or not achieved based on the sensor that was in the standard solution. The self-activation trials for pH were conducted using pH standard solutions of 4, 7, and 10. The pH probe was placed in each solution randomly and self-activations were observed. It was expected that the WSD would be self-activated when the probe was placed in pH solutions of 4 and 10, since these values were outside of the allowable pH limits set in the computer program. It was expected that the WSD would not be self-activated when the probe was placed in pH solution of 7, since it was within the allowable limits. The self-activations while the probe was in the pH solutions of 4 and 10, and no self-activations while the probe was in the pH solution of 7 was recorded as successful trials. The trials with the self-activation decisions (i.e. triggering the sample collection when pH was 7 or not triggering the self-activation when pH solution was 4 or 10) were recorded as unsuccessful trials. The self-activation trials for EC were conducted using EC calibration solutions of 84 µS/cm and 1413 µS/cm. The EC value of 84 µS/cm was used as a parameter that was outside the allowable limits, and EC value of 1413 µS/cm was used as a parameter that was within the allowable limits. The

self-activation trials for DO were conducted using zero oxygen solution and tap water. The DO level of tap water was confirmed with a commercial DO meter. The zero oxygen solution was used as a parameter that was outside the allowable limits as low DO, and tap water was used as a parameter that was within the allowable limits. The self-activation trials for temperature were conducted in pre-heated tap water. The tap water of 500 mL placed in a beaker and it was pre-heated to 50 ℃ and probes were placed in it to acquire temperature measurements while the water was cooling. The beaker was placed in an ice bucket for cooling sample down to 4 ℃. Reference temperature measurements were made with a commercial temperature probe to confirm sensor node measurements. The temperature measurements below 25 ℃ and above 35 ℃ were used as parameters that were outside the allowable limits, and temperature measurements within 25 ℃ and 35 ℃ were used as parameters that were within the allowable limits.

Experiment Site

Lake Issaqueena is a man-made lake located in Pickens County, South Carolina. The US Environmental Protection Agency (EPA) classifies this lake as located in the Inner Southern Piedmont region. The lake basin is long and narrow with relatively steep shorelines. The lake covered approximately 36 ha while the total watershed is 3639 ha with a length of 13 km. The mean summer temperature is 21.9 ℃ while average winter temperature is 4 ℃. (Pilgrim, Mikhailova, Post, & Hains, 2014). The widest section of the lake is approximately 400 m from shore to shore.

The South Carolina Department of Health and Environmental Control (SCDHEC) monitors water quality in Lake Issaqueena watershed with two stations. One of the stations was located on the Six Mile Creek (SV-205) which is the main surface water input for the Lake

Issaqueena. The other monitoring station was located in the Lake Issaqueena (SV-360) however, the water quality monitoring at these stations ended in December 2005 due to compliance with water quality standards (SCDHEC, 2018). Lake Issaqueena was selected for adaptive water sampling experiments because experimental results could be compared with the historical data. In addition, new data sets could be produced for water quality evaluation at this station while testing the performance of the adaptive water sampling system. Lake Issaqueena is easily accessible and provides safe UAV flight conditions due to no boat access from the neighboring Keowee River. The UAV integrated WSD and the launch location were shown in Figure 4.4.

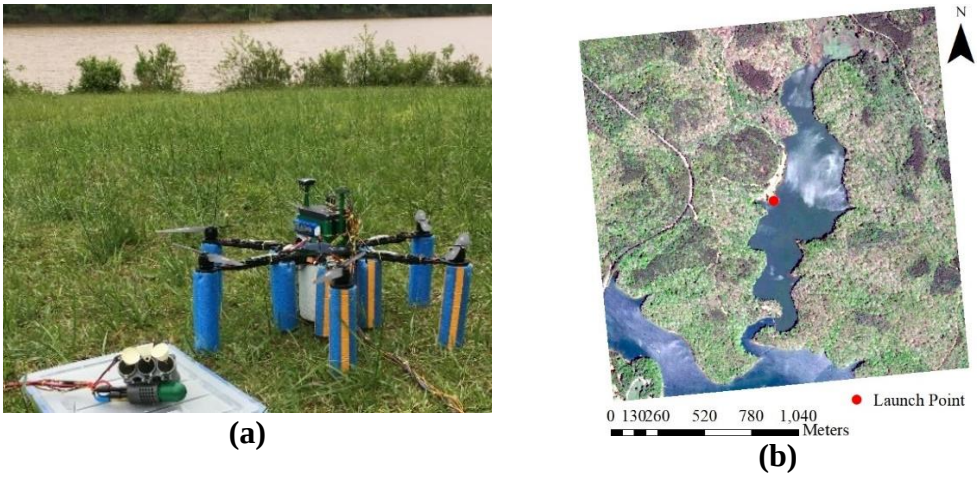

(a) **(b)**

Figure 4.4 (a) UAV integrated WSD and **(b)** the launch location in Lake Issaqueena.

Adaptive sampling experiments were conducted at seven preselected locations on Lake Issaqueena. The locations were randomly selected at the center portion of the lake because the available battery power and endurance of the UAV limited the number of access points and maximum distance to be traveled (Koparan et al., 2019). Seven grid points were selected to enable maximum area coverage on the lake while testing the UAV for its maximum travel

distance for safe flight. The sampling points were approximately 80 m apart from each other on the north east to south west row and approximately 90 m apart from each other on the north west to south east row. The distance between launch point that was marked as 0 and the first sampling point was 73 m as it was the shortest flight distance. The distance between launch point and the seventh sampling point was 290 m as it was the longest flight distance. The launch location was chosen at this point because this location had large open area that is free of trees and provided flat surface for safe takeoff and landing. This location was the only available section at the lake to serve as a secure ground station. Because of this, the adaptive sampling trials were limited within the boundary that was shown in Figure 4.5.

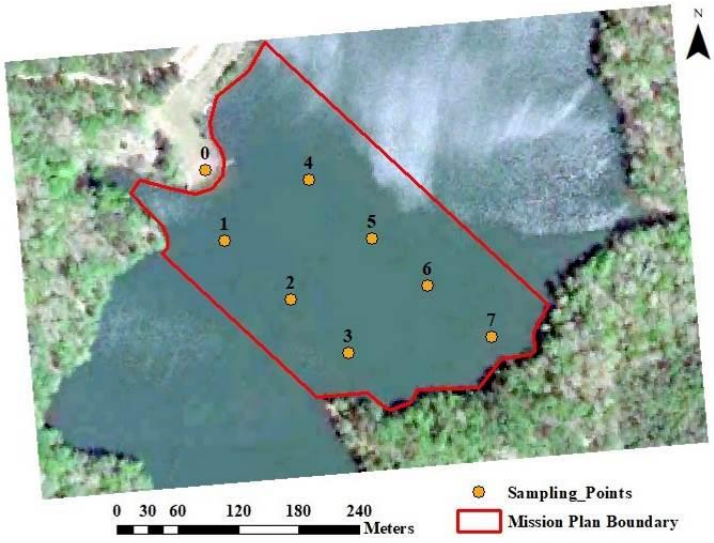

Figure 4.5 Experiment site and water sampling points with mission plan boundary at the lake Issaqueena.

Adaptive Water Sampling Data Collection

The experiment for adaptive water sampling was conducted on May 9, 2019, at 3 pm Eastern Time. UAV-assisted autonomous adaptive water sampling trials were conducted to test if

the WSD would work at all times and collect 130 mL of water samples at each cartridge. The WSD was integrated with the UAV and was sent to predefined sampling locations with autonomous mission flights. The same mission plan boundary was chosen, and it was divided into individual mission plans due to long flight distances and battery limitations of the UAV. The locations 1, 2 and 3 were included in the first mission plan, locations 4, 5, and 6 were included in the second mission plan, and location 7 was included in the third mission plan. The adaptive water sampling depth was chosen as 3.5 m. Observations were made to ensure that UAV can land and take off with the WSD payload with captured water samples (Figure 4.6).

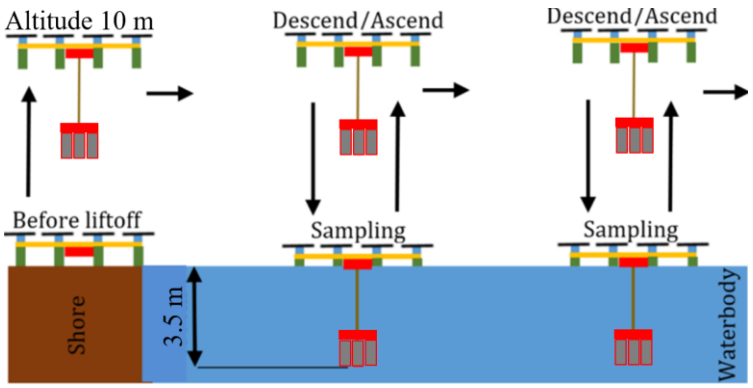

Figure 4.6 UAV flight pattern of adaptive water sampling method.

The WSD was designed as a subsystem that was integrated with the UAV. The initialization signal for adaptive sampling was acquired from the flight controller (Pixhawk, 3DR Robotics, Berkeley, CA, USA). The flight controller initiated the WSD as soon as the UAV reached the predefined sampling locations and landed on water surface. The MCU inside the WSD initiated the sensor node measurements and made water quality evaluation based on the allowable limits. Next, the WSD made decisions to either collect water samples when the measured parameters exceeded the allowable limits, or did not collect water samples when the

measured parameters remained within the allowable limits. The WSD self-activation decision is illustrated in Figure 4.7. The UAV returned to launch location after each self-activation trial for visual confirmation. If the self-activation was successful, the water samples were stored and marked by the location. Three replicate water samples were collected at each sampling location utilizing three cartridges in sequence. The collected water samples with the WSD were transported to the lab in plastic containers for turbidity analysis to compare the in situ turbidity sensor measurements with turbidimeter measurements.

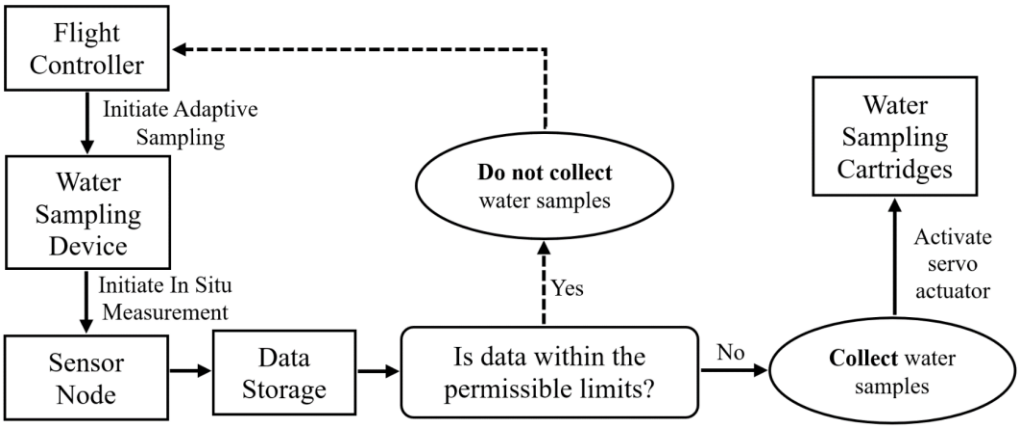

Figure 4.7 The Water Sampling Device (WSD) self-activation flow chart.

The collected water quality data was used to create maps for visualization of water quality distribution. The data was processed in ArcMap (Esri, Redlands, CA, USA) and interpolated using the Inverse Distance Weighted Interpolation (IDW) method (Ahmad, Aziz, Rehman, & Saifullah, 2015). Vector data in Geographic Information System (GIS) was interpolated to develop raster maps to simulate data values for intermediate locations.

Results and Discussions

Depth and Turbidity Sensors Accuracy Evaluation

The depth measurements that were made indoor with the pressure sensor were identical when compared to the actual sensor depth (Figure 4.8). The 3D printed case for the pressure sensor prevented water from leaking and protected the circuits.

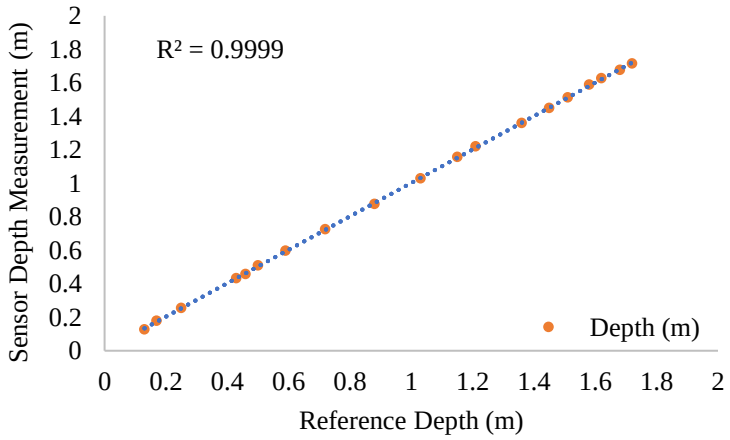

Figure 4.8 Correlation of depth measurements and actual sensor depth in test tube.

The accuracy assessment of turbidity by comparison with standard turbidity solutions showed that the turbidity sensor was reliable and could be used for outdoor experiments. The turbidity sensor measurements were 96% accurate when compared with the standard turbidity solutions of 62.5, 250, 1000, and 2000 FNU (Figure 4.9). The paired t-test showed that the mean difference between the turbidity sensor measurements and the standard solutions were not significant ($t(23) = 0.89$, $p = 0.38$). The mean difference was found to be 31 FNU. The mean turbidity measurements that were made in standard solutions by the sensor node were 859 FNU while the mean turbidity standard solution values were 828 FNU. The percent difference of the two mean turbidity values were 4%.

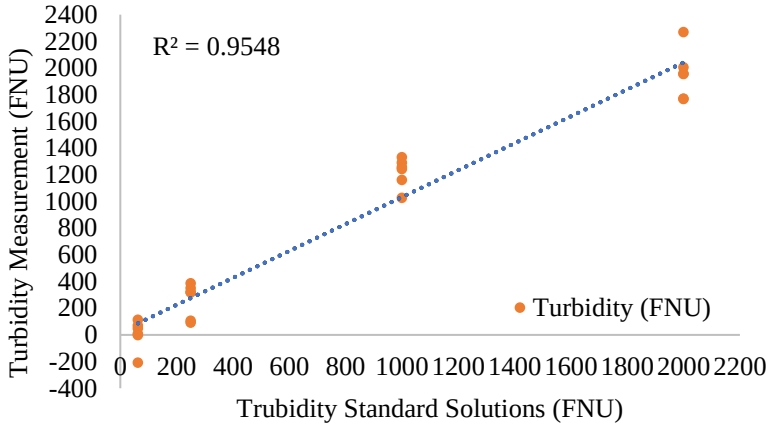

Figure 4.9 Comparison of turbidity measurements obtained from turbidity sensor and turbidity standard solutions.

Evaluation of sensor node equilibrium time

Preliminary experiments that were conducted to evaluate the equilibrium time of the sensor node revealed that the DO sensor took more time to reach equilibrium in comparison with other sensors (Figure 4.10). The turbidity sensor took the shortest time to reach equilibrium as 8 s while DO took 120 s. The DO values were always relatively higher than the actual DO values when the DO probe first entered the water samples. A sudden drop in the first 40 s and a steady decrease in DO values were typically observed. The equilibrium time for pH, EC, and temperature were 44 s, 28 s, and 40 s, respectively. The equilibrium time evaluation results showed that the sensor node had to be kept active for 120 s at each sampling location in order to make accurate measurements. The equilibrium time of 120 s was entered as a delay time in the mission plan. Once the UAV reached a sampling location, it waited for 120 s in idle mode to let the sensor node make measurements.

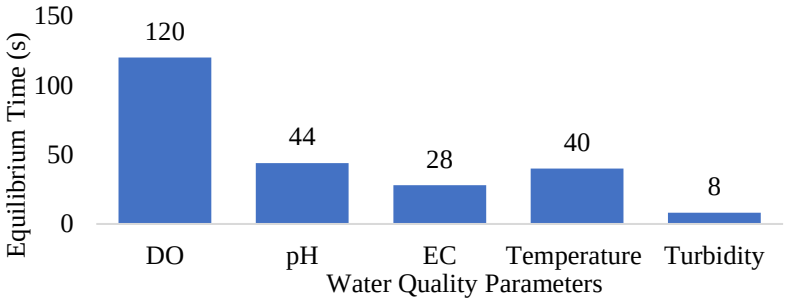

Figure 4.10 Sensor node equilibrium times for each probe.

Self-activation trials and adaptive water sampling

The WSD responded to sensor node measurements with 96 % success rate during self-activation trials with known standard solutions. The total number of successful self-activations trials were recorded as 84 out of 88. The total number of unsuccessful self-activation trials were recorded as four. The unsuccessful self-activations were random and independent from sensor type (Table 4.1). Repeated use of the WSD caused servo to jitter and resetting the WSD after each trial solved the issue. The WSD was activated for water collection 4 s after the self-activation signal was sent by the MCU. The 4 s timeframe appeared to be a processing delay, since sensor node required 4 seconds to acquire measurement from individual sensors. This processing delay of 4 s was introduced in the mission plan to provide WSD enough time for water collection before takeoff.

Table 4.1 WSD self-activation results based on standard solutions.

Parameter	Lower Limit	Higher Limit	Successful Self Activation	Failed Self Activation	Success rate (%)
DO	6 mg/L	12 mg/L	21	1	96
pH	6.5	9.5	20	2	91
EC	100 µS/cm	2000 µS/cm	21	1	96
Temperature	20 ℃	35 ℃	22	0	100
Total	N/A	N/A	84	4	96

Water Quality Evaluation of Lake Issaqueena and Adaptive Water Sampling

The turbidity measurements that were made with the sensor node from Lake Issaqueena and the turbidity measurements from the water samples showed a similar trend by location (Figure 4.11). The turbidity measurements were relatively close to each other when the range of turbidity levels in lakes were considered. However, mean difference in turbidity measurements between sensor node and the turbidimeter appeared to be significant ($t(6) = -5.17$, $p = 0.002$). The mean differences in turbidity measurements were 9 FNU while the percent difference was 22 %. Mean turbidity measurements made by the sensor node was 37 FNU while mean turbidity measurements made by the turbidimeter was 46 FNU.

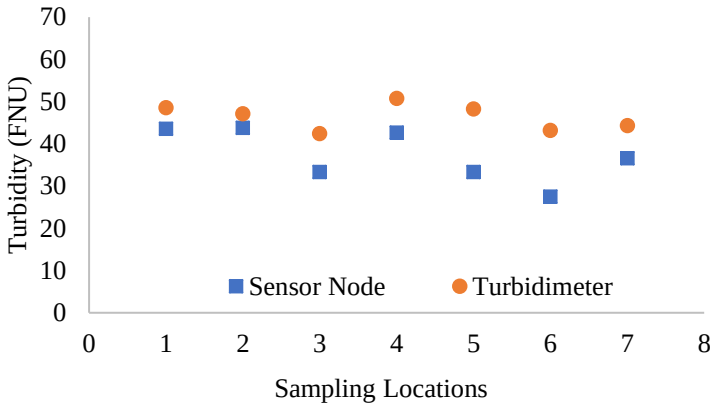

Figure 4.11 Comparison of the turbidity measurements of sampling locations in Lake Issaquena with the sensor node and the turbidimeter.

Turbidity units have no inherent value and they are qualitative measurements (Lawler, 2016). Turbidity measurements of these experiments were presented as water quality indicators based on clarity or transparency. The main factor that affected water transparency in the Lake Issaqueena was suspended sediments that was likely carried into the lake from the creek (Li & Liu, 2019a). The turbidity maps that were created with both sensor node and turbidimeter measurements indicated high turbidity levels at the north west section of the sampling area in Lake Issaqueena (Figure 12). The increase in the turbidity at that section of the lake could be due to transport sediment carried by the stream after the rain event (Garg et al., 2017). The turbidimeter measurements confirmed the high turbidity levels that were measured with the sensor node at the north west section of the lake. The difference in turbidity measurements between sensor node and the turbidimeter was due to the ambient light that affected the turbidity measurements with attenuation type sensor. However, the mean difference in the turbidity measurements was relatively small when compared to the natural range of turbidity in lakes. The overall turbidity in Lake Issaqueena ranged between 42 FNU and 52 FNU based on turbidimeter

results. The turbidity difference between the two shores of the lake was 9 FNU. Change in turbidity can indicate development of algal bloom or a steady increase in suspended sediment on the lake.

The adaptive water sampling experiments from the Lake Issaquena was successful at all locations. The UAV autonomously navigated to each sampling location initiated WSD for in situ measurements and stayed on water surface for 120 s until the sensors reached equilibrium. The in situ measurements indicated that the average pH, EC, and temperature measurements were below allowable limits (Table 4.2). The WSD was self-activated and captured three repeated 130 mL of water samples at all seven locations. The UAV successfully took off from the sampling locations and returned to launch location with the collected water samples.

Table 4.2 Water quality in situ measurements with the WSD and self-activation status by sampling locations.

Sample Location	In Situ Measurements with WSD				Parameters Outside the Allowable Limits	Self-Activation of Cartridges
	DO (mg/L)	pH	EC (µS/cm)	Temp (°C)		
1	8.18	5.08	7.52	18.21	pH, EC, Temperature	Successful
2	8.39	4.98	6.51	18.81	pH, EC, Temperature	Successful
3	8.55	5.59	6.96	18.49	pH, EC, Temperature	Successful
4	8.57	5.15	6.8	16.06	pH, EC, Temperature	Successful
5	8.27	5.37	6.49	18.26	pH, EC, Temperature	Successful
6	8.68	5.92	6.82	16.08	pH, EC, Temperature	Successful
7	8.64	5.28	6.77	17.31	pH, EC, Temperature	Successful
Avg.	8.47	5.34	7	18	N/A	N/A

The lowest DO was 8.18 mg/L at sampling location one while the highest DO was 8.68 mg/L at sampling location six. The lowest pH was 4.98 at sampling location two while the highest pH was 5.92 at sampling location six. The average DO was 8.47 mg/L and the average pH was 5.34. The DO and pH were lower at the north west section within the boundary in the

lake. Although the DO and pH did not change by larger numbers by location, their distribution was illustrated in maps with IDW interpolation (Figure 4.12). The maps illustrated the location where the stream water entered the waterbody and how the pH and DO changed.

The EC and water temperature were shown where the lowest and the highest values can be seen. Inverse Distance Weighting interpolation from In Situ measurements did not show the small increments in the EC and temperature maps. The lowest EC was 6.49 µS/cm at the sampling location five, while the highest EC was 7.52 µS/cm, at the sampling location one. The lowest water temperature was 16 °C at the sampling location four, while the highest water temperature was at 18.81 °C at the sampling location two. The average EC was found as 7 µS/cm and the average water temperature was found as 18 °C. The EC map showed that the EC was the highest where the stream makes entry to the waterbody. There was no clear pattern between stream water entry and its effect on water temperature, but the water temperature was higher at South West section of the area.

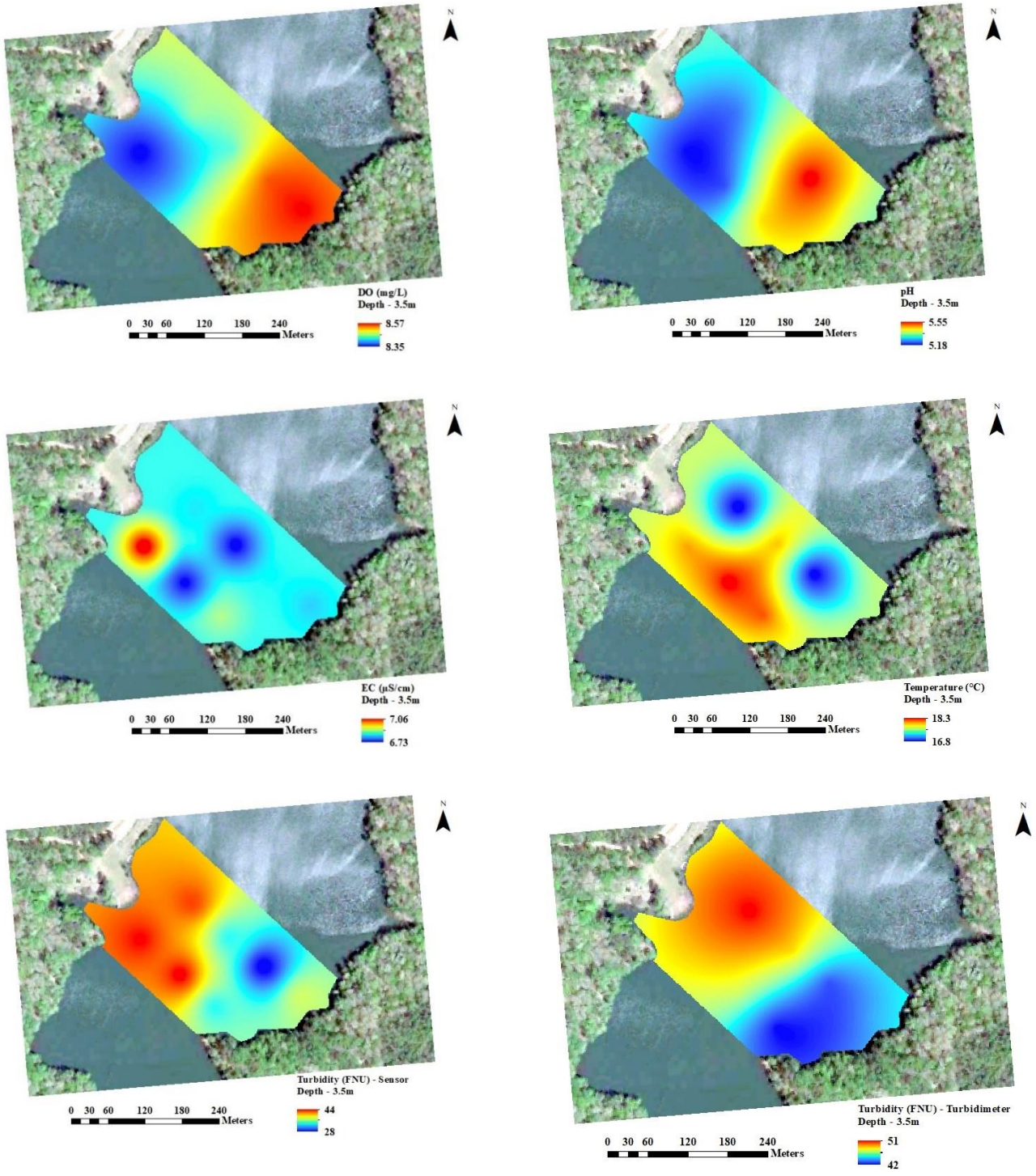

Figure 4.12 Water quality maps that were created from adaptive water sampling experiment data.

Conclusion

Adaptive water sampling with UAV-integrated WSD proved to be an effective water quality evaluation method. The system made in situ measurements of DO, pH, EC, temperature, and turbidity with a precise sampling depth of 3.5 m and made the decision to collect water samples for lab analysis. Self-decision making to collect actual water samples based on in situ sensor node measurement were dependent on allowable limits of water quality parameters. The allowable limits of water quality parameters can be re-adjusted in the computer program for other types of waterbodies, research interests, different climate conditions, and seasons. The size of the waterbody, sampling location distance from the launch location, and the surroundings of the launch location are important parameters to consider adaptive water sampling with this type of aerial system.

A UAV of this size can accomplish safe water sampling at a maximum distance of 290 m. It is not recommended to operate the system for water sampling from a distance greater than 290 m because the UAV exceeds the line-of-sight and it becomes difficult to observe whether the UAV landed on water surface or it continues to fly. Piloting the UAV of this size at an approximate distance of 150 m to 290 m requires a hand-free binocular to ensure landing and takeoff is achieved using the autopilot. Water quality parameters can be measured, and water samples can be collected for quick evaluations with this system within this distance in less than an hour. Rapid water sampling from various locations of a large water body provides valuable information about the type and the location of changes in the specific water quality parameters. Location-specific water quality information can help limnologist to identify a specific problem and develop appropriate management programs to prevent further potential contaminations. High-resolution water quality data can be acquired from difficult to access water bodies and from

water bodies where no water quality monitoring stations exist. The UAV assisted adaptive water sampling system enables remote water quality monitoring without the need of entering a waterbody with a watercraft.

References

Adu-Manu, K. S., Tapparello, C., Heinzelman, W., Katsriku, F. A., & Abdulai, J.-D. (2017). Water Quality Monitoring Using Wireless Sensor Networks: Current Trends and Future Research Directions. *ACM Trans. Sen. Netw., 13*(1), 1-41. doi:10.1145/3005719

Ahmad, H. R., Aziz, T., Rehman, Z. R., & Saifullah. (2015). Chapter 15 - Spatial Mapping of Metal-Contaminated Soils A2 - Hakeem, Khalid Rehman. In M. Sabir, M. Öztürk, & A. R. Mermut (Eds.), *Soil Remediation and Plants* (pp. 415-431). San Diego: Academic Press.

Ankor, M. J., Tyler, J. J., & Hughes, C. E. (2019). Development of an autonomous, monthly and daily, rainfall sampler for isotope research. *Journal of Hydrology, 575*, 31-41. doi:https://doi.org/10.1016/j.jhydrol.2019.04.074

Anweiler, S., & Piwowarski, D. (2017). Multicopter platform prototype for environmental monitoring. *Journal of Cleaner Production, 155*, 204-211. doi:https://doi.org/10.1016/j.jclepro.2016.10.132

Banerjee, B. P., Raval, S., Maslin, T. J., & Timms, W. (2018). Development of a UAV-mounted system for remotely collecting mine water samples. *International Journal of Mining, Reclamation and Environment*, 1-12. doi:10.1080/17480930.2018.1549526

Becker, R. H., Sayers, M., Dehm, D., Shuchman, R., Quintero, K., Bosse, K., & Sawtell, R. (2019). Unmanned aerial system based spectroradiometer for monitoring harmful algal blooms: A new paradigm in water quality monitoring. *Journal of Great Lakes Research, 45*(3), 444-453. doi:https://doi.org/10.1016/j.jglr.2019.03.006

Berman, J. (2009). WHO: Waterborne disease is world's leading killer. Retrieved from https://www.voanews.com/archive/who-waterborne-disease-worlds-leading-killer

Bhatnagar, A., & Devi, P. (2013). Water quality guidelines for the management of pond fish culture. *International Journal of Environmental Sciences, 3*(6), 1980.

Bin Omar, A., & Bin MatJafri, M. (2009). Turbidimeter design and analysis: a review on optical fiber sensors for the measurement of water turbidity. *Sensors, 9*(10), 8311-8335.

Castendyk, D., Hill, B., Filiatreault, P., Straight, B., Alangari, A., Cote, P., & Leishman, W. Experiences with Autonomous Sampling of Pit Lakes in North America using Drone Aircraft and Drone Boats.

Chung, W.-Y., & Yoo, J.-H. (2015). Remote water quality monitoring in wide area. *Sensors and Actuators B: Chemical, 217*, 51-57. doi:http://dx.doi.org/10.1016/j.snb.2015.01.072

Dörnhöfer, K., & Oppelt, N. (2016). Remote sensing for lake research and monitoring – Recent advances. *Ecological Indicators, 64*, 105-122. doi:https://doi.org/10.1016/j.ecolind.2015.12.009

Dunbabin, M., & Grinham, A. (2010, 3-7 May 2010). *Experimental evaluation of an Autonomous Surface Vehicle for water quality and greenhouse gas emission monitoring.* Paper presented at the 2010 IEEE International Conference on Robotics and Automation.

Eichhorn, M., Ament, C., Jacobi, M., Pfuetzenreuter, T., Karimanzira, D., Bley, K., . . . Wehde, H. (2018). Modular AUV System with Integrated Real-Time Water Quality Analysis. *Sensors, 18*(6), 1837.

Erena, M., Atenza, J. F., García-Galiano, S., Domínguez, J. A., & Bernabé, J. M. (2019). Use of Drones for the Topo-Bathymetric Monitoring of the Reservoirs of the Segura River Basin. *Water, 11*(3), 445.

Esakki, B., Ganesan, S., Mathiyazhagan, S., Ramasubramanian, K., Gnanasekaran, B., Son, B., . . . Choi, J. S. (2018). Design of Amphibious Vehicle for Unmanned Mission in Water Quality Monitoring Using Internet of Things. *Sensors, 18*(10), 3318.

Friedrichs, A., Busch, J. A., Van der Woerd, H. J., & Zielinski, O. (2017). SmartFluo: A Method and Affordable Adapter to Measure Chlorophyll a Fluorescence with Smartphones. *Sensors, 17*(4), 678.

Garg, V., Senthil Kumar, A., Aggarwal, S. P., Kumar, V., Dhote, P. R., Thakur, P. K., . . . Rastogi, G. (2017). Spectral similarity approach for mapping turbidity of an inland waterbody. *Journal of Hydrology, 550*, 527-537. doi:https://doi.org/10.1016/j.jhydrol.2017.05.039

Glasgow, H. B., Burkholder, J. M., Reed, R. E., Lewitus, A. J., & Kleinman, J. E. (2004). Real-time remote monitoring of water quality: a review of current applications, and advancements in sensor, telemetry, and computing technologies. *Journal of Experimental Marine Biology and Ecology, 300*(1), 409-448. doi:https://doi.org/10.1016/j.jembe.2004.02.022

Hawthorne, J. (2018). Critical facts about waterborne diseases in the United States and abroad. Retrieved from https://businessconnectworld.com/2018/02/15/critical-facts-waterborne-diseases-us/

Higgins, J., & Detweiler, C. (2016, 9-14 Oct. 2016). *The waterbug sub-surface sampler: Design, control and analysis.* Paper presented at the 2016 IEEE/RSJ International Conference on Intelligent Robots and Systems (IROS).

Kaizu, Y., Iio, M., Yamada, H., & Noguchi, N. (2011). Development of unmanned airboat for water-quality mapping. *Biosystems Engineering, 109*(4), 338-347. doi:https://doi.org/10.1016/j.biosystemseng.2011.04.013

Kellner, K., Ettenauer, J., Zuser, K., Posnicek, T., & Brandl, M. (2016). An automated, Robotic Biosensor for the Electrochemical Detection of E. Coli in Water. *Procedia Engineering, 168*, 594-597. doi:https://doi.org/10.1016/j.proeng.2016.11.222

Kislik, C., Dronova, I., & Kelly, M. (2018). UAVs in Support of Algal Bloom Research: A Review of Current Applications and Future Opportunities. *Drones, 2*(4), 35.

Koparan, C., Koc, A., Privette, C., & Sawyer, C. (2018). In Situ Water Quality Measurements Using an Unmanned Aerial Vehicle (UAV) System. *Water, 10*(3), 264.

Koparan, C., Koc, A., Privette, C., Sawyer, C., & Sharp, J. (2018). Evaluation of a UAV-Assisted Autonomous Water Sampling. *Water, 10*(5), 655.

Koparan, C., Koc, A. B., Privette, C. V., & Sawyer, C. B. (2019). Autonomous In Situ Measurements of Noncontaminant Water Quality Indicators and Sample Collection with a UAV. *Water, 11*(3), 604.

Kozyra, A., Skrzypczyk, K., Stebel, K., Rolnik, A., Rolnik, P., & Kućma, M. (2017). Remote controlled water craft for water measurement. *Measurement, 111*, 105-113. doi:https://doi.org/10.1016/j.measurement.2017.07.018

Kumar, M., & Puri, A. (2012). A review of permissible limits of drinking water. *Indian journal of occupational and environmental medicine, 16*(1), 40-44. doi:10.4103/0019-5278.99696

Lally, H. T., O'Connor, I., Jensen, O. P., & Graham, C. T. (2019). Can drones be used to conduct water sampling in aquatic environments? A review. *Science of The Total Environment, 670*, 569-575. doi:https://doi.org/10.1016/j.scitotenv.2019.03.252

Lawler, D. M. (2016). Turbidity, Turbidimetry, and Nephelometry☆. In P. Worsfold, C. Poole, A. Townshend, & M. Miró (Eds.), *Encyclopedia of Analytical Science (Third Edition)* (pp. 152-163). Oxford: Academic Press.

Leeuw, T., Boss, E. S., & Wright, D. L. (2013). In situ Measurements of Phytoplankton Fluorescence Using Low Cost Electronics. *Sensors, 13*(6), 7872-7883.

Lewitus, A. J., Schmidt, L. B., Mason, L. J., Kempton, J. W., Wilde, S. B., Wolny, J. L., . . . Ringwood, A. H. (2003). Harmful Algal Blooms in South Carolina Residential and Golf Course Ponds. *Population and Environment, 24*(5), 387-413. doi:10.1023/a:1023642908116

Li, D., & Liu, S. (2019a). Chapter 1 - Sensors in Water Quality Monitoring. In D. Li & S. Liu (Eds.), *Water Quality Monitoring and Management* (pp. 1-54): Academic Press.

Li, D., & Liu, S. (2019b). Chapter 2 - Wireless Sensor Networks in Water Quality Monitoring. In D. Li & S. Liu (Eds.), *Water Quality Monitoring and Management* (pp. 55-100): Academic Press.

Li, D., & Liu, S. (2019c). Chapter 8 - Water Quality Detection for Lakes. In D. Li & S. Liu (Eds.), *Water Quality Monitoring and Management* (pp. 221-231): Academic Press.

Liu, Y., Noguchi, N., & Yusa, T. (2014). Development of an Unmanned Surface Vehicle Platform for Autonomous Navigation in Paddy Field. *IFAC Proceedings Volumes, 47*(3), 11553-11558. doi:https://doi.org/10.3182/20140824-6-ZA-1003.00616

Mayer, C. C., & Ali, K. A. (2017). Field Spectroscopy as a Tool for Enhancing Water Quality Monitoring in the ACE Basin, SC. *Journal of South Carolina Water Resources, 4*(1). doi:https://tigerprints.clemson.edu/jscwr/vol4/iss1/5

Melo, M., Mota, F., Albuquerque, V., & Alexandria, A. (2019). Development of a Robotic Airboat for Online Water Quality Monitoring in Lakes. *Robotics, 8*(1), 19.

Nagchaudhuri, A., Diab, A. H., Hartman, C. E., Zhang, L., Mitra, M., Pachepsky, Y., & Joshi, R. (2016). *STRIDER: Semi-Autonomous Tracking Robot with Instrumentation for Data-Acquisition and Environmental Research*. Paper presented at the ASEE Annual Conference & Exposition, New Orleans, Louisiana. https://peer.asee.org/25891

Ore, J.-P., & Detweiler, C. (2018a). *Sensing water properties at precise depths from the air*. Paper presented at the Field and Service Robotics.

Ore, J.-P., & Detweiler, C. (2018b). Sensing water properties at precise depths from the air. *Journal of Field Robotics, 35*(8), 1205-1221. doi:doi:10.1002/rob.21807

Ore, J.-P., Elbaum, S., Burgin, A., & Detweiler, C. (2015). Autonomous Aerial Water Sampling. *Journal of Field Robotics, 32*(8), 1095-1113. doi:10.1002/rob.21591

Pearse, J. (1984). Phytoplankton-nutrient relationships in South Carolina reservoirs: Implications for management strategies. *Lake and Reservoir Management, 1*(1), 193-197.

Peters, C. B., Zhan, Y., Schwartz, M. W., Godoy, L., & Ballard, H. L. (2017). Trusting land to volunteers: How and why land trusts involve volunteers in ecological monitoring. *Biological Conservation, 208*, 48-54. doi:https://doi.org/10.1016/j.biocon.2016.08.029

Pilgrim, C. M., Mikhailova, E. A., Post, C. J., & Hains, J. J. (2014). Spatial and temporal analysis of land cover changes and water quality in the Lake Issaqueena watershed, South

Carolina. *Environmental Monitoring and Assessment, 186*(11), 7617-7630. doi:10.1007/s10661-014-3953-9

Pule, M., Yahya, A., & Chuma, J. (2017). Wireless sensor networks: A survey on monitoring water quality. *Journal of Applied Research and Technology, 15*(6), 562-570. doi:https://doi.org/10.1016/j.jart.2017.07.004

Py, F., Ryan, J., Rajan, K., Sherman, A., Bird, L., Fox, M., & Long, D. (2007). *Adaptive Water Sampling based on Unsupervised Clustering*.

Rabta, B., Wankmüller, C., & Reiner, G. (2018). A drone fleet model for last-mile distribution in disaster relief operations. *International Journal of Disaster Risk Reduction, 28*, 107-112. doi:https://doi.org/10.1016/j.ijdrr.2018.02.020

Rodrigues, P., Marques, F., Pinto, E., Pombeiro, R., Lourenço, A., Mendonça, R., . . . Barata, J. (2015). *An open-source watertight unmanned aerial vehicle for water quality monitoring.* Paper presented at the OCEANS'15 MTS/IEEE Washington.

Saiki, K., Kaneko, K., Ohba, T., Ntchantcho, R., Fouepe, A., Kusakabe, M., . . . Hell, J. V. (2019). Vertical change in transparency of water at Lake Nyos, a possible indicator for the depth of chemocline. *Journal of African Earth Sciences, 152*, 122-127. doi:https://doi.org/10.1016/j.jafrearsci.2019.02.008

Schaeffer, B. A., Schaeffer, K. G., Keith, D., Lunetta, R. S., Conmy, R., & Gould, R. W. (2013). Barriers to adopting satellite remote sensing for water quality management. *International Journal of Remote Sensing, 34*(21), 7534-7544. doi:10.1080/01431161.2013.823524

Shoda, M. E., Sprague, L. A., Murphy, J. C., & Riskin, M. L. (2019). Water-quality trends in U.S. rivers, 2002 to 2012: Relations to levels of concern. *Science of The Total Environment, 650*, 2314-2324. doi:https://doi.org/10.1016/j.scitotenv.2018.09.377

South Carolina Department of Health and Environmental Control (SCDHEC). (2018). *State of South Carolina Monitoring Strategy for Calender Year 2018.* Retrieved from https://scdhec.gov/sites/default/files/docs/HomeAndEnvironment/Docs/Strategy.pdf (retrieved on June 3, 2019).

Stauber, C., Miller, C., Cantrell, B., & Kroell, K. (2014). Evaluation of the compartment bag test for the detection of Escherichia coli in water. *Journal of Microbiological Methods, 99*(Supplement C), 66-70. doi:https://doi.org/10.1016/j.mimet.2014.02.008

Stone, N. M., & Thomforde, H. K. *Understanding your fish pond water analysis report*.

Thomas, K. V., Hurst, M. R., Matthiessen, P., Sheahan, D., & Williams, R. J. (2001). Toxicity characterisation of organic contaminants in stormwaters from an agricultural headwater stream in South East England. *Water Research, 35*(10), 2411-2416. doi:https://doi.org/10.1016/S0043-1354(00)00535-2

United States Centers for Disease Control and Prevention (CDC). (2016). Global water, sanitation, and hygiene: fast facts.

Valada, A., Velagapudi, P., Kannan, B., Tomaszewski, C., Kantor, G., & Scerri, P. (2014). *Development of a low cost multi-robot autonomous marine surface platform.* Paper presented at the Field and service robotics.

Winkelbauer, A., Fuiko, R., Krampe, J., & Winkler, S. (2014). Crucial elements and technical implementation of intelligent monitoring networks. *Water Science and Technology, 70*(12), 1926-1933. doi:10.2166/wst.2014.415

Winkler, S., Zessner, M., Saracevic, E., & Fleischmann, N. (2008). Intelligent monitoring networks – transformation of data into information for water management. *Water Science and Technology, 58*(2), 317-322. doi:10.2166/wst.2008.672

World Health Organization (WHO). (2018). Developing drinking-water quality regulations and standards: General guidance with a special focus on countries with limited resources.

World Water Assesment Programme. (2017). *The United Nations world water development report 2017: wastewater: the untapped resource; facts and figures*. Retrieved from https://unesdoc.unesco.org/ark:/48223/pf0000247553

Xu, Z., Dong, Q., Otieno, B., Liu, Y., Williams, I., Cai, D., . . . Li, B. (2016). Real-time in situ sensing of multiple water quality related parameters using micro-electrode array (MEA) fabricated by inkjet-printing technology (IPT). *Sensors and Actuators B: Chemical, 237*, 1108-1119. doi:https://doi.org/10.1016/j.snb.2016.09.040

Yang, K., Yu, Z., Luo, Y., Yang, Y., Zhao, L., & Zhou, X. (2018). Spatial and temporal variations in the relationship between lake water surface temperatures and water quality - A case study of Dianchi Lake. *Science of The Total Environment, 624*, 859-871. doi:https://doi.org/10.1016/j.scitotenv.2017.12.119

Zeng, C., Richardson, M., & King, D. J. (2017). The impacts of environmental variables on water reflectance measured using a lightweight unmanned aerial vehicle (UAV)-based spectrometer system. *ISPRS Journal of Photogrammetry and Remote Sensing, 130*, 217-230. doi:https://doi.org/10.1016/j.isprsjprs.2017.06.004

Zhang, L., Thomas, S., & Mitsch, W. J. (2017). Design of real-time and long-term hydrologic and water quality wetland monitoring stations in South Florida, USA. *Ecological Engineering, 108*, 446-455. doi:https://doi.org/10.1016/j.ecoleng.2017.06.021

Zhuang, Y., Zhang, L., Du, Y., Yang, W., Lihui, W., & Cai, X. (2016). *Identification of critical source areas for nonpoint source pollution in the Danjiangkou Reservoir Basin, China*.

CHAPTER FIVE

SUMMARY AND CONCLUSION

UAV-assisted water quality monitoring systems have been developed and tested. The UAV-assisted water quality monitoring systems have been tested for in situ water quality measurement, water sample collection, and adaptive water sampling based on in situ water quality measurements. In order to carry the required payloads, two UAVs with small and large payload capacities were developed. The small UAV was used to carry the 0.7 kg of sensor node payload and the large UAV was used to carry the 2.1 kg of payload that was the combination of both the sensor node and the triple cartridge water collection mechanism. The UAVs that were used to carry water sampling subsystems were custom-built hexacopters with autonomous flight capability. The UAVs were equipped with floatation attachments that enabled landing on the water surface for in situ water quality measurement and water sample collection. Landing on the water surface unlike other methods, such as hovering above water surface greatly reduced battery usage. Therefore, the number of locations where the UAVs can be sent for water sampling with the same battery power was increased as well as secure flight conditions were established.

The in situ water quality measurement system was lightweight and capable of autonomous navigation for collecting georeferenced dissolved oxygen (DO), pH, electrical conductivity (EC), and temperature data from a 1.1 ha agricultural pond. The UAV-assisted in situ water quality measurement system performed successful flight missions for water quality monitoring and demonstrated capabilities that can be utilized for collecting water quality data after natural disasters such as flooding and hurricanes. On the other hand, the data collection with the system can be used to improve the quality of satellite-based water quality evaluations by providing precise ground truth data. The major limitation with the system was its limited battery

power that disabled flight distance. Because of limited battery power, the endurance and travel distance of the UAV for in situ measurement was kept at maximum 300 m.

The combination of the sensor node and the water sampling cartridge mechanism greatly increased the payload. Therefore, the UAV with 6.4 kg takeoff capacity with 10 min endurance was used to test instantaneous in situ measurement and water sample collection from pre-determined locations and depth. Both the sensor node and the water sampling cartridges were integrated with the UAV's flight controller. Both systems were successfully activated when the UAV reached pre-determined locations. The unique design of the water sampling cartridge allowed water collection at a depth of 3 m without collecting water at other depths. The field tests demonstrated the system was able to navigate autonomously to predefined locations and perform measurement and water collection tasks instantaneously. The water sampling cartridges were able to collect three 130 ml water samples at a single flight. The UAV was able to navigate to 6 predefined locations that were approximately 80 m apart from each other. The system provided rapid water sampling and in situ measurement capability that facilitated analysis at two depths of 0.5 m and 3 m. Precise timing and accuracy would provide better data comparison between in situ measurements and lab analysis results from collected samples.

Adaptive water sample collection based on in situ water quality measurements proved to be an effective water quality evaluation method. The adaptive water sampling system made in situ measurements of DO, pH, EC, temperature, turbidity, and sampling depth and successfully activated water sampling cartridges. The activation of the water sampling cartridges were achieved when the measurements exceeded the allowable limits of water quality parameters. The pH, EC, and temperature measurements were lower than the allowable limits at all the experimental sampling locations. Making in situ water quality measurements at precise depths

and locations where changes in water quality parameters are not visible by human eye achieved successfully. Water sample collection when only these parameters exceeded the allowable limits reduced unnecessary water sample collection and pinpoint the problematic areas in a waterbody. The problematic areas then can be further sampled and analyzed to identify the potential cause of the problem. Water sampling at multiple locations rather than water sampling from the shore increases the precision of water quality data and enable georeferenced water quality mapping.

APPENDICES

Appendix A

Technical drawings of the water sampling cartridge

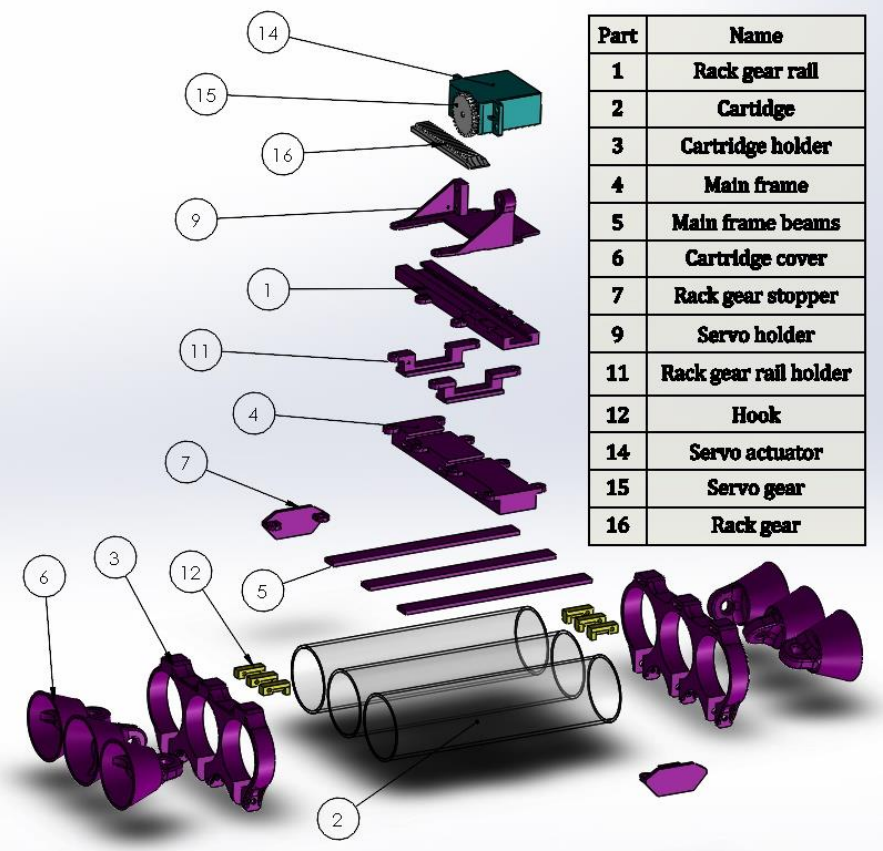

Part	Name
1	Rack gear rail
2	Cartidge
3	Cartridge holder
4	Main frame
5	Main frame beams
6	Cartridge cover
7	Rack gear stopper
9	Servo holder
11	Rack gear rail holder
12	Hook
14	Servo actuator
15	Servo gear
16	Rack gear

Figure A-1. Exploited view of the water sampling cartridge components.

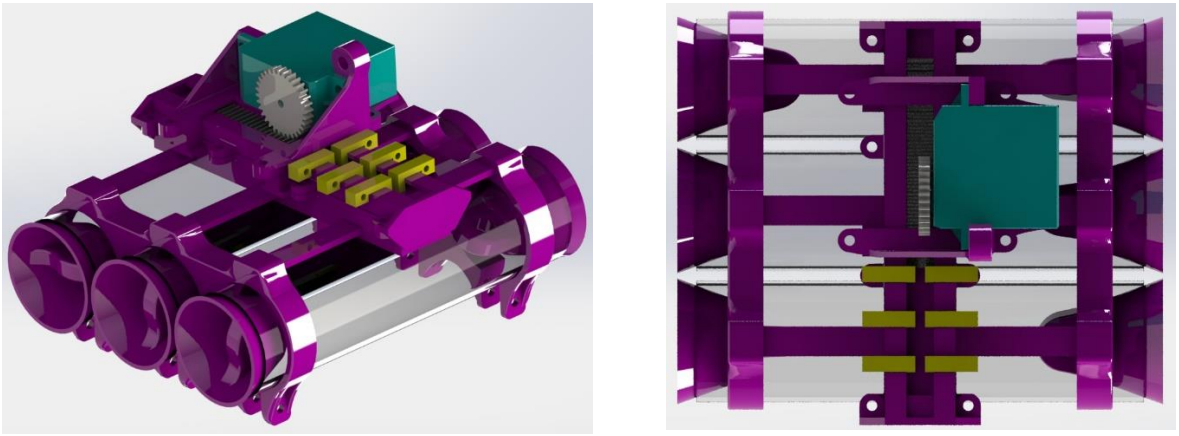

Figure A-2. SolidWorks assembled water sampling cartridge; a) perspective view and b) top view.

Appendix B

LabVIEW program of UAV performance test station

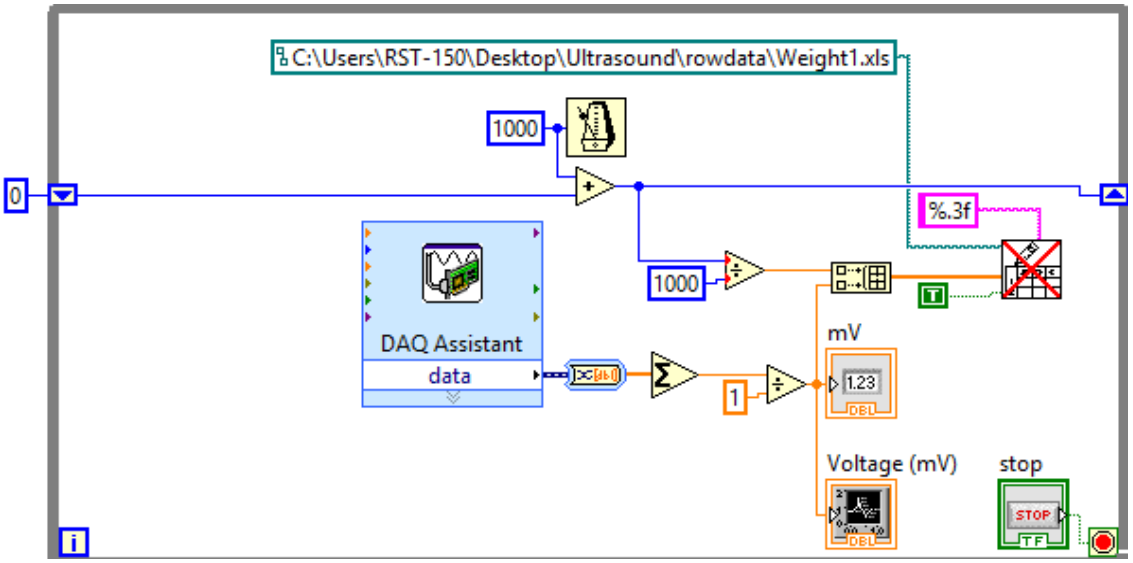

Figure B-1. LabVIEW® program for load cell calibration.

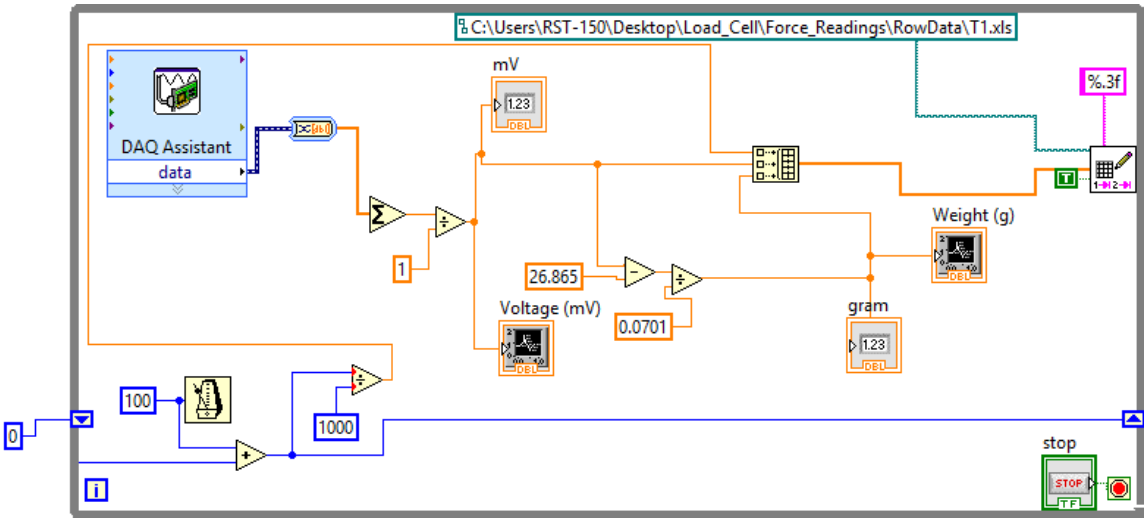

Figure B-2. LabVIEW® program for load measurements with load cell.

Appendix C

UAV performance test station close up view

Figure C-1. The image taken during UAV thrust and endurance measurements inside the UAV performance test station.

Appendix D

Water Sampling Device (WSD) components and connection

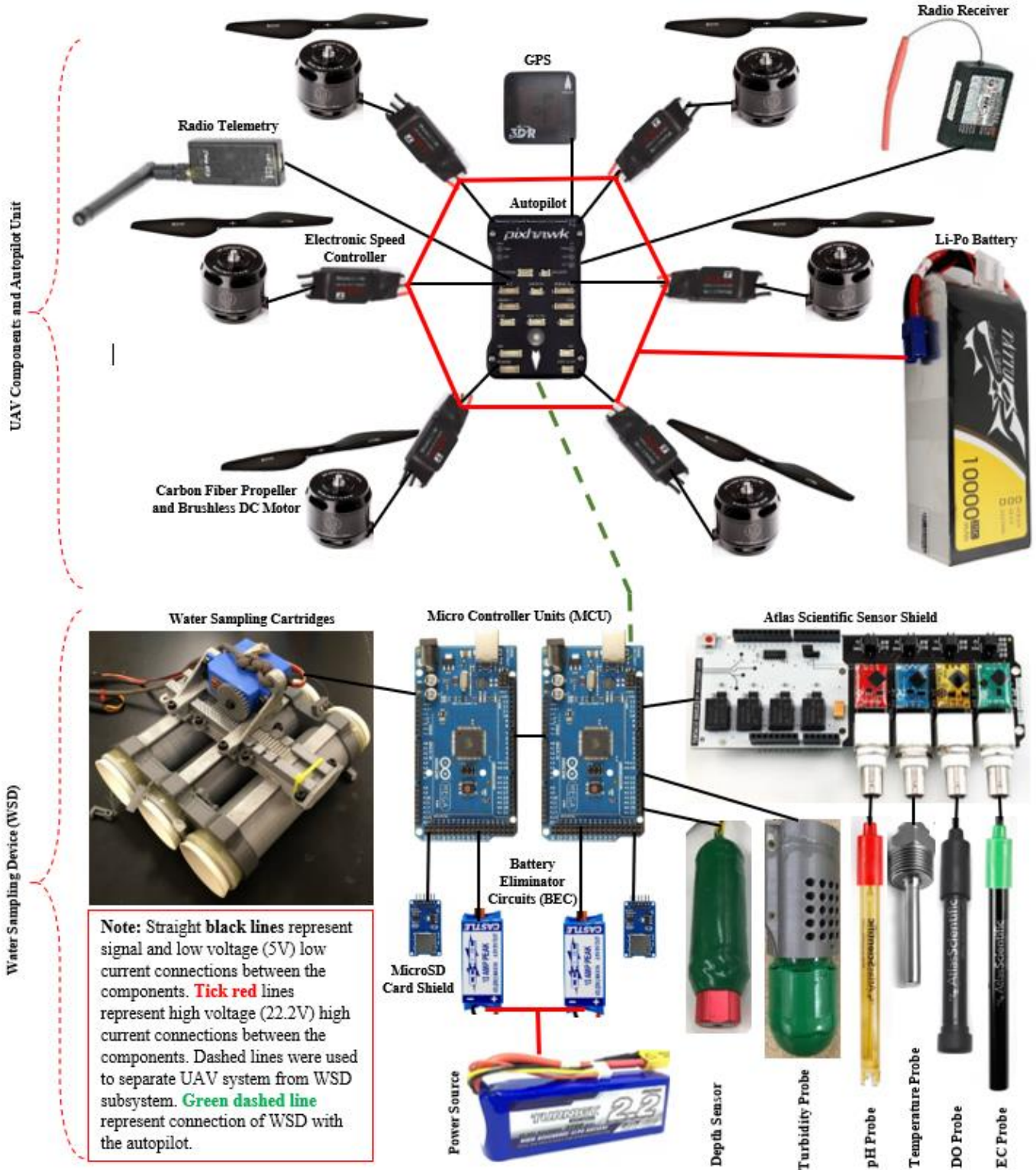

Figure D-1. Water Sampling Device (WSD) components and its wire connection diagram.

Appendix E

C++ code of the adaptive water sampling

```
//  Created Author: Harrison Eggers
//  Date: 8/7/2017
//
//  Revised Author: Cengiz Koparan
//  Date: 4/22/2019
//
//  Last Author: Cengiz Koparan
//  Last Edit: 5/20/2019
//
//  Purpose
//  This program id designed to interface with the pixhawk system to record data to an SD card from
//  various sensors.
//
//  Requirements
//  This program must perform the following tasks:
//
//  1.  Wait for Pixhawk to request a data sample
//  2.  Read Data from sensor via the following interfaces:
//    a.  I2C
//    b.  Analog Pins
//  3.  Take a water sample if data is outside expected range
//  4.  Record Data to an SD card
//
//  Bugs that addressed
//  1.  The current sampler servo doesn't work. Proper wiring and power distribution solved the issue.
//  2.  If more than one sensor returns an invalid value, then the last one to error will get recorded,
//      instead of all of them. No recording if there is an invalid value solved the data recording glitch issue.
//

// Includes
#include <SD.h>     // Used for writing to the SD card
#include <Wire.h>   // Used for I2C communication
#include <Servo.h>  // Used for taking samples

// Defined Constants - The preprocessor replaces every occurence of the thing on the left with the thing on the right
before the program is compiled (Makes much faster runtime)

// Pins
#define LED_PIN 13
#define SERVO_PIN 9
#define PIXHAWK_PIN 4
#define TURBIDITY_PIN 0
#define NULL_PIN -1

// Comms
```

```
#define BAUD_RATE 9600
#define I2C_DELAY 900         // Milliseconds
#define I2C_BUFFER_LENGTH 20  // Bytes
#define DO_I2C_ADDR 97
#define PH_I2C_ADDR 99
#define EC_I2C_ADDR 100
#define SG_I2C_ADDR 102
#define NULL_I2C_ADDR -1

// Storage
#define CHIP_SELECT 53
#define FILE_NAME "UAVdata.csv"
#define SENSOR_COUNT 5
#define MAX_VALS_PER_SENSOR 4 // The largest number of data values from any of the sensors


// Struct definitions - Blueprint for objects of the type "struct [StructName]"
//"struct DataStream" contains everything associated with reading data from an arbitrary sensor
  struct DataStream {
  String Header;
  int I2CChannel;
  int AnalogPin;
  int (* GetData)(int, double*);
  int DataBounds[MAX_VALS_PER_SENSOR][2];
};


// Global Variables - Can be accessed by any function in the program and retains its value
// throughout the course of the program. Rather dangerous. Use sparingly.
int giWaypointID;
struct DataStream Sensor[SENSOR_COUNT];

// Functions

//  Function Header
//  Name: AtlasScientificI2C
//  Purpose: Handle the reading of any AtlasScientific sensor over an I2C interface
//  Inputs: Integer Index for Sensor to read
//          Double Array to read values into
//  Output: Integer Count of values read (Return)
//          Double Array of values (Argument)
//  Extern Memory: Reads Sensor.I2CChannel
//

int AtlasScientificI2C(int iIndex, double* daSensorValues) {

  // Declare Variables
  char cExitCode;
  char cI2CByte;
  char caI2CByteArray[I2C_BUFFER_LENGTH];

  int iByteCounter = 0;
  int iDataCounter = 0;

  // Make sure there is a channel to communicate with
  if (Sensor[iIndex].I2CChannel == -1) {
```

```
  Serial.println("NO I2C CHANNEL FOUND");
  return -1;
}

// Tell sensor to take reading from the indicated channel
Wire.beginTransmission(Sensor[iIndex].I2CChannel);
Wire.write('r');
Wire.endTransmission();

// Wait for reading
delay(I2C_DELAY);

// Receive reading
Wire.requestFrom(Sensor[iIndex].I2CChannel, I2C_BUFFER_LENGTH, 1);

// Read the exit code
cExitCode = Wire.read();

// If it didn't read the data, exit the function with an error
if (cExitCode != 1) {
  Serial.println(cExitCode);
  return -2;
}

// Parse the buffer to read the data
while (Wire.available()) {

  // Receive a byte
  cI2CByte = Wire.read();
  caI2CByteArray[iByteCounter] = cI2CByte;

  // Check for separator values
  if (cI2CByte == ',' || cI2CByte == 0) {

    // If there are more datapoints than spaces in the array, exit the function with error
    if (iDataCounter > MAX_VALS_PER_SENSOR) {
      Serial.print("ERROR READING SENSOR");
      return -3;
    }

    // Record the value and prepare to read another one
    daSensorValues[iDataCounter] = atof(caI2CByteArray);
    iByteCounter = 0;
    iDataCounter ++;
  }

  // If we get an EOT, end the transmission and exit the loop
  if (cI2CByte == 0) {
    Wire.endTransmission();
    break;
  }

  // Increment the byte counter
  iByteCounter ++;
}
```

```
  // Return number of datapoints read
  return iDataCounter;
}

//  Function Header
//  Name: Analog
//  Purpose:  Handle the reading of any Analog port-mounted sensor
//  Inputs: Integer Index for Sensor to read
//          Double Array to read values into
//  Output: Integer Count of values read (Return)
//          Double Array of values (Argument)
//  Extern Memory: Reads Sensor.AnalogPin
//

int Analog(int Index, double* daSensorValue) {

  // Declare Variables
  int iAnalogValue;
  float dVoltage;

  // Make sure an analog pin has been specified
  if (Sensor[Index].AnalogPin == -1) {
    Serial.println("ERROR: NO PIN SPECIFIED");
    return -1;
  }

  // Get Reading from sensor
  iAnalogValue = analogRead(Sensor[Index].AnalogPin);

  // If appropriate, interpret the data for the Turbidity sensor
  if (Sensor[Index].AnalogPin == TURBIDITY_PIN) {
    // Perform Conversion from the analog Value to Voltage
    dVoltage = iAnalogValue * (5.0 / 1024.0);

    // Perform calibration (620 is the correction factor at 0 FNU)
    daSensorValue[0] = ((dVoltage - 1.9723) / -0.0005)+620;
  }

  return 1;
}

//  Function Header
//  Name: TakeSample
//  Purpose:  Take a water sample when requested
//  Inputs: Integer indicating which sample to take
//  Output: Integer indicating a successful sample (Return)
//  Extern Memory: NONE
//  Notes: Must be called with an incrementing iSample value (1,2,3)
//  BUGS: Servo currently doesn't work properly
<<<<<<<<<<<<<<<<<<<<<<<<<<<<<<<<<<<<<<<<<<<<<<<<<<<<<<<<<<<<<<<<<<<

int TakeSample(int iSample) {

  // Declare Variables
  int iServoPosition;
  Servo SServo1;
```

```
 // Attach the servo and move to initial position
 SServo1.attach(SERVO_PIN);
 SServo1.writeMicroseconds(2100);
 delay(200);

 // Select the proper position depending on the argument value (0 to reset)
 switch (iSample) {
   case 0:
     iServoPosition = 2100;
     break;
   case 1:
     iServoPosition = 1400;
     break;
   case 2:
     iServoPosition = 1050;
     break;
   case 3:
     iServoPosition = 700;
     break;
   default:
     // exit with error
     Serial.println("ERR: INVALID SERVO POSITION");
     return -1;
 }

 // Move to that position
 SServo1.writeMicroseconds(iServoPosition);

 Serial.println(SServo1.read());

 // Wait for it to move there
 delay(2000);

 // Move it back to the holding position
 SServo1.writeMicroseconds(2100);
 delay(2000);

 // free the servo (to keep it from burning itself out)
 SServo1.detach();

 // return error free
 return 1;
}

//  Function Header
//  Name: setup
//  Purpose:  Initialize all interfaces and values required to start the program
//  Inputs: None
//  Output: None
//  Extern Memory: Writes to all values of Sensor
//                 Reads Sensor.Header
//  Note: To add new Sensor, this function must be edited
//

void setup() {
  // Declare Variables
```

```
int iHeaderCounter;
int iSensorCounter;
int iReturnValue;
double daReturnBuffer[MAX_VALS_PER_SENSOR];

File FDataFile;

// Initialize Sensor Struct Arrays
Sensor[0].Header = String("DO");
Sensor[0].GetData = AtlasScientificI2C;
Sensor[0].I2CChannel = DO_I2C_ADDR;
Sensor[0].AnalogPin = NULL_PIN;
Sensor[0].DataBounds[0][0] = ;
Sensor[0].DataBounds[0][1] = 12;

Sensor[1].Header = String("pH");
Sensor[1].GetData = AtlasScientificI2C;
Sensor[1].I2CChannel = PH_I2C_ADDR;
Sensor[1].AnalogPin = NULL_PIN;
Sensor[1].DataBounds[0][0] = 6.5;
Sensor[1].DataBounds[0][1] = 9.5;

Sensor[2].Header = String("EC");
Sensor[2].GetData = AtlasScientificI2C;
Sensor[2].I2CChannel = EC_I2C_ADDR;
Sensor[2].AnalogPin = NULL_PIN;
Sensor[2].DataBounds[0][0] = 100;
Sensor[2].DataBounds[0][1] = 2000;

Sensor[3].Header = String("Tmp");
Sensor[3].GetData = AtlasScientificI2C;
Sensor[3].I2CChannel = SG_I2C_ADDR;
Sensor[3].AnalogPin = NULL_PIN;
Sensor[3].DataBounds[0][0] = 20;
Sensor[3].DataBounds[0][1] = 35

Sensor[4].Header = String("Tur");
Sensor[4].GetData = Analog;
Sensor[4].I2CChannel = NULL_I2C_ADDR;
Sensor[4].AnalogPin = TURBIDITY_PIN;
Sensor[4].DataBounds[0][0] = -10000;
Sensor[4].DataBounds[0][1] = 10000;

// Set up interfaces
// Set up the Serial Communication
Serial.begin(BAUD_RATE);

// Set up the I2C Communication
Wire.begin();

// Set the LED pin
pinMode(LED_PIN, OUTPUT);

// Set the PixHawk Comm pin
pinMode(PIXHAWK_PIN, INPUT);
```

```
  // Initialize SD card
  if (!SD.begin(CHIP_SELECT)) {
    Serial.println("Card failed, or not present");
    return;
  }

  // Set up data file
  // Open the Data File
  FDataFile = SD.open(FILE_NAME, FILE_WRITE);

  // Write Data File Headers
  FDataFile.print("WayPoint");
  for (iHeaderCounter = 0; iHeaderCounter < SENSOR_COUNT; iHeaderCounter++) {
    FDataFile.print(",");
    FDataFile.print(Sensor[iHeaderCounter].Header);
  }
  FDataFile.print(",ERR/NOTE");
  FDataFile.println();

  // Close the data file
  FDataFile.close();

  // Initialize Waypoint counter
  giWaypointID = 0;

  // Loop through the Sensors and perform one initialization reading (tmp reads wrong on the first try):
  for (iSensorCounter = 0; iSensorCounter < SENSOR_COUNT; iSensorCounter++) {

    // Read from the sensor
    iReturnValue = Sensor[iSensorCounter].GetData(iSensorCounter, daReturnBuffer);
  }

  // Set barometer parameters


}

//  Function Header
//  Name: loop
//  Purpose:  Run the program
//  Inputs: None
//  Output: None
//  Extern Memory: Calls Sensor.GetData
//                 Reads Sensor.DataBounds
//                 Reads Sensor.Header
//

void loop() {

  // Declare Variables
  static int iSampleCounter = 0;
  static int iTakeSample;
  static int iPHState = LOW;
  static int iLastPHState;

  int iSensorCounter;
```

```
int iReturnValue;
int iReturnCounter;
int iSampleReturn;

double daReturnBuffer[MAX_VALS_PER_SENSOR];

File FDataFile;

String sSensorWithError;

// write the depth and temperature measurements from pressure sensor

// Read the current state of the Pixhawk Pin
iLastPHState = iPHState;
iPHState = digitalRead(PIXHAWK_PIN); //Defaults to HIGH if nothing is connected

// If HIGH, take a reading
if (iPHState == HIGH) {

 // Open the Data File
 FDataFile = SD.open(FILE_NAME, FILE_WRITE);

 // If first time HIGH, indicate a new waypoint
 if (iPHState != iLastPHState) {

  // Indicate WayPoint
  FDataFile.print(giWaypointID);
  giWaypointID ++;
 }

 // Loop through the sensors
 for (iSensorCounter = 0; iSensorCounter < SENSOR_COUNT; iSensorCounter++) {

  // Read from the sensor
  iReturnValue = Sensor[iSensorCounter].GetData(iSensorCounter, daReturnBuffer);

  // Loop through the return values
  for (iReturnCounter = 0; iReturnCounter < iReturnValue; iReturnCounter++) {

   // Make sure data is within range
   if (daReturnBuffer[iReturnCounter] < Sensor[iSensorCounter].DataBounds[iReturnCounter][0]) {
    // Too Low
    iTakeSample = 1;
    sSensorWithError = Sensor[iSensorCounter].Header;
   }
   if (daReturnBuffer[iReturnCounter] > Sensor[iSensorCounter].DataBounds[iReturnCounter][1]) {
    // Too High
    iTakeSample = 2;
    sSensorWithError = Sensor[iSensorCounter].Header;
   }

   // Write Data to output
   FDataFile.print(" , ");
   FDataFile.print(daReturnBuffer[iReturnCounter]);
  }
 }
```

```
    // If indicated, record a sample requested and why
    if (iTakeSample != 0) {

      FDataFile.print(",Sample ");
      FDataFile.print(iSampleCounter);
      FDataFile.print(" - "); sSensorWithError.replace(",", " ");
      Serial.println(sSensorWithError);
      FDataFile.print(sSensorWithError);
      if (iTakeSample == 1) {
        FDataFile.print(" Too Low");
      }
      if (iTakeSample == 2) {
        FDataFile.print(" Too High");
      }


    }

    FDataFile.println();
    FDataFile.close();
  }

  // First time the pin goes low, check for sample requests
  if (iPHState == LOW) {
    if (iPHState != iLastPHState) {

      // Take sample if requested
      if (iTakeSample > 0) {

        // Attempt to take sample
        iSampleReturn = TakeSample(iSampleCounter);

        // If all went well, increment the sample counter, other report error
        if (iSampleReturn > 0) {
          iSampleCounter ++;
        }
        else {
          FDataFile = SD.open(FILE_NAME, FILE_WRITE);
          FDataFile.println("ERR: SAMPLE NOT TAKEN");
          FDataFile.close();
        }

        // Reset the Sample flag
        iTakeSample = 0;

      }
    }
  }
}
```

Appendix F

C++ code of the turbidity and depth sensor integration with the microcontroller unit

```
#include <Wire.h>
#include "MS5837.h"
#include <SPI.h>
#include <SD.h>

MS5837 barsensor;

char* fileName = "Depth.csv";   //create a csv file for sd card
File dataFile;

const int chipSelect = 53;
int button = 11;          // choose the input pin (ch13(aux5) on Pixhawk)
int val = 0;              // variable for reading the pin status
int led = 13;             // choose the output pin for led
int traveltime = 0;       // travel time between sample locations (time difference between sensro activation)
boolean active = true;
boolean inactive = false;

void setup() {

  Serial.begin(9600);
  Serial.println("Waiting for activation code");
  Wire.begin();
  pinMode(button, INPUT);   //declare pushbutton as input
  pinMode(led, OUTPUT);     //declare led as output

  barsensor.setModel(MS5837::MS5837_02BA);    // set barometric sensor models (from company specs)
  barsensor.init();                           //initiation code for barometric sensor
  barsensor.setFluidDensity(997); // kg/m^3 (997 freshwater, 1029 for seawater)   //parameter set for fluid density

  // see if the card is present and can be initialized:
  if (!SD.begin(chipSelect))
  {
    Serial.println("Card failed, or not present");
    // don't do anything more:
    return;
  }
  Serial.println("card initialized.");

  dataFile = SD.open(fileName, FILE_WRITE);
  dataFile.println("Travel(s), Depth(m), Temp(C), Press(mbar), Altitude(m)");
  dataFile.close();
  }

void loop() {

    barsensor.read();       //request sensor reading from barometric sensor

    bool active = (val == HIGH);      //define names for if conditios for pin (or pushbutton)
    bool inactive = (val == LOW);
```

```
val = digitalRead(button);         //read command for sensor input value
if(active){                        //if high, take reading

digitalWrite(led, HIGH);               //turn on the led

dataFile = SD.open(fileName, FILE_WRITE);       //open the SD card file

dataFile.print(traveltime);                    //print sensor outputs
dataFile.print(",");
dataFile.print(barsensor.depth());
dataFile.print(",");
dataFile.print(barsensor.temperature());
dataFile.print(",");
dataFile.print(barsensor.pressure());
dataFile.print(",");
dataFile.println(barsensor.altitude());
dataFile.close();

}

while (inactive){        //while loop to increment values, so we can differentiate sample locations
traveltime++;
digitalWrite(led, LOW);
break;
}

delay(1000);
```